ABSTRACT

Title of Document: **PLUVIAL FLOOD RISK ESTIMATION PROCEDURE FOR SMALL URBAN WATERSHEDS**

John Trevor Cone, Master of Science, 2012

Directed By: Dr. Richard H. McCuen
Department of Civil and Environmental Engineering

Pluvial flooding, when runoff causes flooding before it reaches a body of water, is a type of flooding that often is overlooked in flood risk studies. This study outlines a general procedure that can be used to model urban pluvial flood scenarios, estimate damages, and quantify pluvial flood risk for microwatersheds (watersheds of a few square miles or less). The model development was accomplished using EPA's SWMM in combination with GIS datasets and analyses. Sensitivity analyses were performed on many model inputs including runoff surface slope, imperviousness, infiltration parameters, and pipe roughness. The overall procedure was tested on a 215-acre sewershed in Washington, DC. The results indicate that pluvial flooding can have serious consequences, even in areas that are not close to existing bodies of water and are at relatively high elevations. The 10-, 100-, and 200-yr rainfall events modeled produced damage estimates of approximately $430,000, $904,000, and $1,093,000, respectively.

PLUVIAL FLOOD RISK ESTIMATION PROCEDURE FOR SMALL URBAN WATERSHEDS

By

John Trevor Cone

Thesis submitted to the Faculty of the Graduate School of the
University of Maryland, College Park, in partial fulfillment
of the requirements for the degree of
Master of Science
2012

Advisory Committee:
Professor Richard H. McCuen, Chair
Associate Professor Kaye L. Brubaker
Assistant Professor Barton Forman

TABLE OF CONTENTS

CHAPTER 1 ..... **1**
INTRODUCTION **1**
1.1 Introduction 1
1.1.1 Storm Severity 3
1.1.2 Imperviousness 4
1.1.3 Capacity and Efficiency 4
1.1.4 Drainage Slope 5
1.1.5 Infiltration 5
1.1.6 Pluvial Flood Damages 6
1.1.7 Pluvial Flood Risk 6
1.1.8 Summary 7
1.2 Goals and Objectives 7
1.3 Implications 8
CHAPTER 2 ..... **9**
LITERATURE REVIEW **9**
2.1 Model Structure 9
2.2 GIS Modeling 10
2.3 Surface Runoff Modeling 12
2.4 Flood Damage Assessment 14
2.4.1 Army Corps of Engineers 16
2.5 SWMM Simulation Options 17
2.5.1 Process Model Options 18
2.5.1.1 Rainfall/Runoff 18
2.5.1.2 Flow Routing 20
2.5.2 Infiltration Model Options 21
CHAPTER 3 ..... **23**
SWMM MODEL SETUP PROCEDURE **23**
3.1 Introduction 23
3.1.1 Ponding Option 24
3.1.2 Routing Model Options 26
3.2 Dual Drainage System 29
3.3 Building a SWMM model 33
3.3.1 Select a Study Site 33
3.3.2 Obtain Site-specific Model Input Data 34

3.3.2.1 Site-specific Elevation Data 35
3.3.2.2 Site-specific Aerial Imagery 36
3.3.2.3 Site-specific Rainfall Data 37
3.3.2.4 Site-specific Stormwater Drainage Network 40
3.3.2.5 Site-specific Roadway Geometry 41
3.3.3 Modeling the Pipe Network 41
3.3.3.1 Required Pipe Sizes 43
3.3.3.2 Pipe Sizing Iterations 45
3.3.3.3 Pipe Design Example 46
3.3.4 Adding Street Channels 47
3.3.4.1 Assessment of Flow Depth Rationality 52
3.4 Sensitivity Analyses 53
3.4.1 Sensitivity of 24-hr Rainfall Time Increment 53
3.4.2 Sensitivity of Watershed Slope 56
3.4.3 Sensitivity of Infiltration Parameters 58
3.4.4 Sensitivity of Imperviousness 60
3.4.5 Sensitivity of Depression Storage 62
3.4.6 Sensitivity of Overland Flow Width 63
3.4.7 Sensitivity of Roughness Coefficients 64
3.4.7.1 Roughness Coefficient of Impervious Areas 65
3.4.7.2 Roughness Coefficient of Pervious Areas 65
3.4.7.3 Roughness Coefficient of Pipes 68
3.4.7.4 Roughness Coefficient of Street Channels 69
3.4.8 Pluvial Flooding on 8 December 2011 71
3.4.8.1 Potential Inefficient Drainage Problems 72
3.4.8.2 Partial Clogging of Inlets 75
3.5 Summary 80
CHAPTER 4 82
PLUVIAL FLOOD DAMAGE ESTIMATION 82
4.1 Introduction 82
4.2 Depth-Damage Curve Selection 83
4.3 Estimation of damages 88
4.3.1 Individual Property Damages 89
4.3.2 City Block Damages 92
4.3.3 Microwatershed Damages 93
4.4 Summary 94

CHAPTER 5 ..... **96**
PLUVIAL FLOOD RISK ESTIMATION **96**
5.1 Flood Frequency Analyses 96
5.1.1 Assume a Probability Density Function 97
5.1.2 Estimate Population Parameters from Known Flood Magnitudes 98
5.1.3 Construct a Frequency Curve 99
5.1.4 Flood Frequency Curve for Flood Damages 102
CHAPTER 6 ..... **105**
CASE STUDY – CAPITOL HILL SEWERSHED **105**
6.1 Introduction 105
6.2 Site Selection 105
6.3 Site Specific Data 108
6.4 Modeling the Pipe Network 109
6.5 Modeling the Street Channels 111
6.6 Simulation Results 113
CHAPTER 7 ..... **120**
CONCLUSIONS **120**
APPENDIX **125**
Appendix A 125
REFERENCES **128**

LIST OF FIGURES

Figure 2-1. Conceptual view of the rainfall/runoff model used in SWMM. 19
Figure 3-1. Layout of simple SWMM model used to evaluate ponding option 25
Figure 3-2. Layout of a simple SWMM model used to demonstrate how dual drainage modeling can be accomplished with SWMM. 26
Figure 3-3. Flow rates for pipes C90 and C92 and street channel C91 for a 2-yr, 2-hour storm. 30
Figure 3-4. Flow rates for pipes C90 and C92 and street channel C91 for a 10-yr, 2 hour storm. 31
Figure 3-5. Water depths reported at inlet J61 for a 10-yr, 2-hour storm. 32
Figure 3-6. Flow rates for pipes C90 and C92 and street channel C91 for a 100-yr, 2-hour storm. 32
Figure 3-7. Extent of study area used for SWMM model setup. The study area is part of Capitol Hill in Washington, DC. 34
Figure 3-8. NOAA's 24-hr depth-duration-frequency curves for Washington, DC. 37
Figure 3-9. NRCS Type II cumulative rainfall distributions for a 24-hr storm for the 2-, 10-, 100-, and 200-yr return periods in Washington, DC. 40
Figure 3-10. Pipe network with labeled inlets for SWMM model of 16 square blocks on Capitol Hill. 42
Figure 3-11. Pipe network with labeled pipes for SWMM model of 16 square blocks on Capitol Hill. 45
Figure 3-12. Pipe and street channel layout of pipe design example SWMM model. 47
Figure 3-13. Cross-section geometry for an urban residential street in Washington, DC. 48
Figure 3-14. Peak flows in each pipe and street channel for various return period rainfall events. 49
Figure 3-15. Flow depth in street channels during the central 2 hours of a 24-hr, 200-yr storm. 50
Figure 3-16. Alternate street channel cross-section with artificial barrier at edge of sidewalk used to keep track of water volume. 51
Figure 3-17. Flow depth in street channels for central 2 hours of a 200-yr, 24-hr storm using alternate street channel cross-sections. 51
Figure 3-18. Water elevation profile for street channels C41 and C43 during the peak of a 200-yr event with an outlet. 52
Figure 3-19. Water elevation profile for street channels C41 and C43 during the peak of a 200-yr event without an outlet. 53
Figure 3-20. Peak flows in each pipe for the NRCS Type II, 24-hr, 10-yr storm event defined at 30-, 15-, and 2-min time increments. 55
Figure 3-21. Peak flows for each conduit and each storm frequency for an average watershed slope of 1%. 56
Figure 3-22. Peak flows for each conduit and each storm frequency for an average watershed slope of 2%. 57

Figure 3-23. Flow depths in street channel C43 during a 200-yr rainfall with minimum and maximum infiltration rates representing sandy, loam, and clay soils. 60
Figure 3-24. Flow depths of street channel C43 during a 200-yr event with various degrees of imperviousness. 61
Figure 3-25. Flow depths in street channel C43 during a 200-yr, 24-hr storm for various average overland flow widths. 64
Figure 3-26. Flow depths in street channel C43 for a 200-yr, 24-hr event with impervious area roughness coefficients of 0.011, 0.013, and 0.015. 66
Figure 3-27. Flow depths of street channel C43 for a 200-yr, 24-hr storm with pervious area roughness coefficients of 0.05, 0.17, 0.29, and 0.41. 67
Figure 3-28. Flow depths of street channel C43 for a 200-yr, 24-hr storm with the roughness coefficient for the pipes set to 0.011, 0.014, and 0.017. 69
Figure 3-29. Localized flooding on the morning of 8 December 2011 along Massachusetts Avenue between 1st and 2nd Streets in northeast Washington, DC. 72
Figure 3-30. Flow depths in street channel C43 during a 24-hr storm for 2-, 10-, 100-, and 200-yr return periods with a local depression at inlet J25. 73
Figure 3-31. Flow depths in street channel C43 for a 2-, 10-, 100-, and 200-yr storm of 24-hrs with the outlet completely inundated, eliminating watershed outflow. 74
Figure 3-32. Flow depths in street channels (C41, C42, and C43) for a 10-yr storm when primary inlets J19 and J24 are half-clogged. 77
Figure 3-33. Flow depths in street channels (C41, C42, and C43) for a 100-yr storm when primary inlets J19 and J24 are half-clogged. 79
Figure 3-34. Flow depths in street channels (C41, C42, and C43) for a 200-yr storm when primary inlets J19 and J24 are half-clogged. 79
Figure 4-1. Example study site flow depths during the peak of a 200-yr, 24-hr storm and typical residential townhomes of the site. 84
Figure 4-2. Depth-damage curves for 3-story, single-family, residential buildings with basements obtained from HAZUS-MH. 85
Figure 4-3. HAZUS building and contents depth-damage curves fitted with composite models. 87
Figure 4-4. Cross-section for street channel C43 (3rd St NE, Washington, DC) adjusted to reflect building setback distance. 90
Figure 4-5. Flood depth profile along street channel C43, from inlet J20 to J25, for 200-yr, 24-hr storm with adjusted street channel cross-section. 92
Figure 5-1. Comparison of log-normal and log-Pearson III distribution curves fitted to flood depths of a selected property within the watershed. 100
Figure 5-2. Flood frequency curves plotted of logarithmic scale for log-normal and log-Pearson III distributions. 104
Figure 5-3. Final flood frequency curve using log-Pearson III distribution with logarithms converted back to dollar values. 104
Figure 6-1. Delineated sewersheds in Washington, DC, with selected study site highlighted. FEMA's 500-yr floodplain is also shown. 107

Figure 6-2. Exported GIS image to be imported as SWMM backdrop. Pipe segments are in yellow and catchbasins are in red. 109
Figure 6-3. Capitol Hill sewershed SWMM model layout with pipes and subcatchments. 111
Figure 6-4. Capitol Hill sewershed SWMM model layout with pipes, subcatchments, and street channels included. 112
Figure 6-5. Flood frequency analysis of flood depths of a selected building in the sewershed..... 115
Figure 6-6. Flood frequency analysis of peak average flood depths along the street channel of the selected building..... 116
Figure 6-7. Flood frequency analysis of estimated damages of the selected building..... 117
Figure 6-8. Flood frequency analysis of estimated damages of the block on which the selected building is located. 117
Figure 6-9. Flood frequency analysis of estimated damages of the full sewershed..... 118

LIST OF TABLES

Table 3-1. Summary of effect of ponding with outlet pipes of 0.01 and 1.0 ft. 26
Table 3-2. Maximum flow (ft^3/s), velocity (ft/s), and depth (ft) along conduit C91 and at inlet J61 for 2-, 10-, and 100-yr storm events 29
Table 3-3. Inputs and results of IDF curve equations for 24-hr storms of various return periods for Baltimore, MD. 39
Table 3-4. Total rainfall depths for 24-hr storm from various estimation methods and data sources. 40
Table 3-5. Elevations of junctions in Capitol Hill example SWMM model. 43
Table 3-6. Summary of required pipe size calculations based on the simulation of a 10-yr rainfall event. 44
Table 3-7. Commercially available concrete drainage pipe sizes. 47
Table 3-8. Pipe sizing calculations for each iteration. 47
Table 3-9. The peak flows for each pipe and each time increment are reported. The errors and relative errors were determined by comparing the 15- and 30-min peak flows against the 2-min peak flows. 55
Table 3-10. Peak flows for each conduit for average watershed slopes of 0.5, 1, and 2%. Differences and relative differences for 1 and 2% slopes from 0.5% slope are reported. 58
Table 3-11. Varied values of Horton's infiltration parameters with the maximum depth of street channel C43 for each simulation reported 59
Table 3-12. Peak depths in street channel C43 for simulations of a 200-yr event with imperviousness ranging from 70 to 75 percent. 62
Table 3-13. Absolute and relative sensitivities of peak flood depths along street channel C43 for the 200-yr, 24-hr storm to several types of roughness coefficients 71
Table 4-1. Summary of goodness-of-fit statistics for each component of the composite models for the building and contents depth-damage curves. 87
Table 4-2. Summary of goodness-of-fit statistics for full composite models of the building and contents depth-damage curves. 88
Table 4-3. Summary of significant inputs and results of the damage estimate for a 200-yr rainfall event for a selected individual property with a flood depth of 0.57ft in Washington, DC. 91
Table 4-4. Summary of significant inputs and results of the damage estimate for a 200-yr rainfall event for a selected city block with an average flood depth of 0.49ft in Washington, DC. 93
Table 4-5. Summary of significant inputs and results of the damage estimate for a 200-yr rainfall event for a selected microwatershed in Washington, DC. 94
Table 4-6. Summary of damage estimates for three levels of analysis. 95
Table 5-1. Various return period flood depths along street channel C43 which were used in flood frequency analyses. 97

Table 5-2. Flood frequency curve calculations for log-normal and log-Pearson III distributions based on flood depth of a selected property within the watershed. 100
Table 5-3. Summary of errors using the log-normal and log-Pearson III distributions to predict flood depths along street channel C43 for various return periods. 101
Table 5-4. Damage estimates of a selected building within the watershed for various return periods. 103
Table 6-1. Summary of input parameters that remained constant across the sewershed and for each return period. 114
Table 6-2. Errors and relative errors of log-Pearson III distribution functions and estimated damages for various return periods of each spatial scale. 119

CHAPTER 1

INTRODUCTION

1.1 INTRODUCTION

Effective water resources planning and management can be best accomplished when the available data for a region can be incorporated into a model that can provide reliable predictions of future problems. With respect to flood events, the more that can be understood about the risks involved the better those risks can be managed appropriately. When equipped with the insight that a watershed model can provide, strategic plans can be adopted to reduce flood risks to acceptable levels.

The issue of concern in this study is that of pluvial flooding in urban areas. Perhaps more familiar, fluvial flooding refers to flooding that occurs when the water surface of a river, stream, or other tributary exceeds its natural channel and inundates the adjacent land. Alternately, pluvial flooding refers to flooding that results from rainfall-generated overland flow and is usually a result of high intensity rainfall events. A pluvial flood is a flood that occurs before storm runoff reaches a river, stream, or other tributary. Therefore, pluvial flooding is not confined to areas in close proximity to existing water bodies and can theoretically occur anywhere.

While significant resources and extensive studies have contributed to a much better understanding of fluvial flood risks, pluvial flood risks remain relatively unknown and

unaddressed. For example, the Federal Emergency Management Agency (FEMA) has conducted thorough Flood Insurance Studies (FIS) and produced detailed Flood Insurance Rate Maps (FIRM) for nearly all communities in the United States. These resources assist the National Flood Insurance Program (NFIP) to set flood insurance premiums based on estimated levels of fluvial (riverine and coastal) flood risk. Pluvial flooding is not considered in the FIS or FIRM, and therefore, pluvial flood risk is not a factor in setting NFIP flood insurance premiums.

Pluvial flooding is more difficult to predict than fluvial flooding, not only because it can happen virtually anywhere, but also because less historical data are generally available at any particular location. Additionally, in the case of fluvial flooding, river storage attenuates the discharge rates, which reduce storm-to-storm variations. Urban streets offer little storage, thus producing greater storm-to-storm variation. When the same location along a river is flooded a number of times over a specific time period, the frequency and magnitude of the historical floods can be used to estimate the probably that flooding of a specific magnitude will occur at that same location in any given year. Pluvial flood studies do not have the luxury of long records of flow data from which such frequency analyses can be conducted. Therefore, specific projections of flood probabilities with defined boundaries, such as the 1% chance annual flood (100-yr flood), do not apply to pluvial flooding.

Pluvial flood risk, though not commonly understood, can still be significant, as evidenced by the flooding of the Federal Triangle in Washington, DC, in June of 2006. Though the area where flooding occurred in this instance was in the 100-yr floodplain associated with fluvial flooding, a detailed study coordinated by the National Capital

Planning Commission (NCPC) found that all of the $10 million in damages were attributable to pluvial flooding. Pluvial flood risk can be estimated on a site-by-site basis with a site specific pluvial flood model. If the pluvial flood model contains reasonable representations of the major physical processes at work during a pluvial flood event, then simulations of various scenarios can provide enough data to estimate the pluvial flood risk at a certain location. Pluvial flood risk determined in this manner should be considered distinct from, and in addition to, the fluvial flood risk of the same location.

The Environmental Protection Agency (EPA) has developed free software, referred to as the Stormwater Management Model (SWMM), which is capable of modeling urban stormwater drainage systems. The occurrence and extent of pluvial flooding are highly influenced by several important factors: the severity of the rainfall event, the imperviousness of the runoff surface, the capacity and efficiency of the stormwater drainage system, the slope of the runoff surface and the stormwater pipes, and the infiltration rate of the pervious areas. The SWMM software was selected for this study because it is capable of modeling each of these factors.

1.1.1 Storm Severity

A common conclusion of many contemporary climate change studies has been that major storms are likely to become more frequent and more severe. This seems to be consistent with local experience as several record breaking storms have occurred in just the past few years in the Washington, DC, area. This trend poses many challenges for effective stormwater management. Rainfall frequency analyses will have to be revised often and estimated return periods will not remain constant. The term that is used to describe the effects of changing climate conditions is nonstationarity. Nonstationarity

implies that if a 10-yr rainfall event was used 30 years ago to design a stormwater drainage system, that same rainfall event may only be considered an 8- or even 5-yr rainfall today. This translates into more frequent overloading of the drainage system, with more frequent and severe pluvial flooding as a result.

1.1.2 Imperviousness

The percentage of impervious area in a watershed significantly influences runoff patterns. An impervious surface is a barrier to infiltration, meaning that almost 100% of rain that falls on an impervious surface becomes runoff. Depression storage does capture a fraction of the rainfall; however, that fraction is typically small, especially when considering severe storms. Impervious surfaces also generally have low roughness coefficients, allowing rainfall to run off rapidly. Urbanization is continually increasing as population increases and more people move to urban centers, both within the U.S. and around the globe. As urbanization increases in a particular location, so too does imperviousness. With greater imperviousness, stormwater infrastructure inevitably becomes strained because it is required to drain larger volumes of runoff in shorter amounts of time. Therefore, this study focused primarily on highly developed urban areas where a greater threat of pluvial flooding exists due to large concentrated areas of imperviousness.

1.1.3 Capacity and Efficiency

Aging stormwater infrastructure often leads to reduced capacity. Over time, mineral deposits have a tendency to build up along the interior circumference of drainage pipes, effectively reducing pipe diameters and increasing pipe roughness. Both effects

contribute to reduced flow capacity. Inefficiencies can also arise in several other forms. One that was explored in this study was the partial clogging of inlets. When an inlet is clogged, the maximum inflow into the pipe network is reduced, also reducing the efficiency of the system because the full capacity of the pipe network is not utilized. This is an issue common to many urban areas that could be resolved with a strict maintenance schedule in which inlets are cleaned frequently, though such a maintenance schedule is not always followed.

1.1.4 Drainage Slope

The slope of the runoff surface heavily influences the rate at which runoff arrives at a site and the slope of the stormwater pipes heavily influences the rate at which the runoff can be drained from the site. Often construction and roadway design codes limit the allowable slope used in order to help control runoff. Stormwater pipes generally, but not always, run several feet below ground and parallel to the slope of the ground surface. Design may require slopes different from the ground surface slope to be used to control flow.

1.1.5 Infiltration

As areas become more urbanized with more impervious surfaces, infiltration has less opportunity to influence runoff patterns. This has been recognized as a problem and one solution to counter this effect has been the implementation of green roofs. Green roofs and other Low Impact Development (LID) ideas attempt ensure that pervious surfaces are not completely eliminated. With more pervious surfaces, subsurface soils will be able to capture and store more rainfall, reducing the overall runoff. This strategy can make a

difference for small storms; however, it may not be enough to significantly mitigate pluvial flooding from major storms.

1.1.6 Pluvial Flood Damages

In order to make meaningful flood damage estimates, it is necessary to develop stage-damage curves that accurately represent local conditions. Stage-damage curves are used to translate the depth, duration, and sometimes the velocity of flooding into potential losses. Losses are often expressed in terms of property damages (monetary losses), though loss of life can be considered as well. Stage-damage curves vary according to land use and building type across different regions. In determining the damages to a building, both the damage to the structure and the contents must be considered. In addition to the direct damages just described, indirect damages, such as disruption to transportation and commercial activity, may be significant. Accurate estimates of the total damage must include both direct and indirect damages. Though considerable uncertainty in flood damage estimates will always remain, such estimates can provide planners, insurance companies, and citizens of a community a reasonable idea of what expect and prepare for.

1.1.7 Pluvial Flood Risk

When measuring risk, the probability of pluvial flooding must be combined with the potential losses caused by the flooding. Therefore, the risks associated with flooding of any kind in urban areas are generally much greater than in other areas due to the high density and value of property, and of course, the high density of population. These risks are only increasing as the intensity of storms is expected to increase as a result of climate

change, population is continuing to rise, and the infrastructure designed to route stormwater away from urban centers is aging, and in many cases, beyond its design life. Aging pipes that are partially clogged with debris or mineral deposits do not have the same capacity as when they were designed and installed. Each of these factors is leading to increased pluvial flood risk.

1.1.8 Summary

While this study focuses on the set up of a model of a small urban watershed, the same set up procedure could be applied to less urbanized areas as well. Urban areas do, however, have the conditions in place that create higher pluvial flood risk. The increasing frequency and severity of storms, the greater extent of imperviousness, the aging stormwater infrastructure, and the lower infiltration capacities factor into the overall pluvial flood risk. Each of these factors can be adjusted within a SWMM model. This study outlines the steps necessary to build a SWMM model of a small pluvial flood site and use the model to evaluate pluvial flood risk.

1.2 GOALS AND OBJECTIVES

The goal of this research was to develop a procedure to quantify pluvial flood risk for small urban watersheds. An understanding of pluvial flood risk, in addition to other flood risks, can assist in the design of adequate stormwater drainage systems. This goal was achieved through the following objectives:

1. Develop a procedure for using SWMM to model pluvial flooding in highly urbanized watersheds.
2. Develop a procedure for using the model to evaluate localized flooding.

3. Develop/select flood damage function(s) applicable to selected site for damage estimation.
4. Quantify risk by combining flood probabilities and potential consequences.

1.3 IMPLICATIONS

Pluvial flood risk is generally not considered, and certainly not quantified, by FEMA in creating flood risk maps (FIRMs) that dictate flood insurance premiums throughout the country. Many communities create flood mitigation plans based on these maps as a requirement to participate in the NFIP. With a better understanding of pluvial flood risk, communities can better plan and prepare for potential flooding that could occur outside of the designated "100-yr floodplain." With effective communication and outreach, this would lead to a more accurate perception of overall flood risk and encourage many communities and individuals to make necessary preparations to more fully mitigate that risk. Local governments, floodplain managers, developers, emergency management agencies, the NFIP, and individual citizens alike, would benefit from an increased understanding of pluvial flood risk.

CHAPTER 2

LITERATURE REVIEW

2.1 MODEL STRUCTURE

Dawdy and O'Donnell (1965) discussed two schools of thought for hydrologic modeling: over-all catchment models and component models. Over-all models use a lumped form for the catchment components and are largely empirically based. Several subjective decisions are required, for instance, in specifying behavioral relationships and in the choosing of processes to include. Component models are more physically based and allow for more objectivity, but they also tend to be more complex. Both approaches can provide accurate models of catchment behavior. They showed that parameter optimization can be performed objectively with computers, even for complex models.

Madramootoo and Broughton (1987) developed a model to simulate surface and subsurface flows from agricultural fields in humid regions. This model was developed based on the most important physical hydrologic and hydraulic processes occurring both above and below the ground during the growing season. The processes considered were rainfall, interception and depression storage, infiltration, drainage, evapotranspiration, and overland flow. The interaction between surface and subsurface flows can be important in influencing potential flooding, especially downstream from agricultural areas. The model was only applicable to agricultural fields of up to 20 ha. Comparing

one such field entirely subsurface drained and another entirely surface drained, it was shown that peak flows were much lower and times to peak were longer for the subsurface drained field.

2.2 GIS MODELING

Maidment and Olivera (1999) developed a spatially distributed, GIS-based model that produces runoff at an outlet from rainfall over a watershed. A digital elevation model (DEM) was used to obtain surface elevations from which a stream network was derived. Routing water from one cell to the next was accomplished using the first-passage time response function derived from the advection dispersion equation. The watershed response was determined by the sum of the flow path response functions from each cell. The paper presented an attempt to generalize the unit hydrograph method for runoff response on a spatially distributed basis in which the runoff responses from subareas are considered separately rather than being spatially averaged.

Melesse and Shih (2002) used remotely-sensed data and GIS tools to predict changes in runoff response for three watersheds in Florida. The study aimed to show the effect of changes in land-cover on storm runoff response. Land-use information was obtained for the years 1984, 1990, 1995, and 2000 to capture land-use changes and their effects. The spatially distributed runoff was estimated using the NRCS curve number method, and GIS was used to compute hydrologic parameters from DEMs. The slope, flow accumulation, flow direction, drainage area delineation, and stream network were all determined from 30-m resolution DEMs and were later used to develop spatially distributed direct runoff hydrographs. This was done using a previously developed routing model (Melesse and Graham 2003) based on travel time, without relying on unit

hydrograph theory. The Thiessen method was used to determine the weighting coefficients for the spatial distribution of rainfall based on three rain-gage stations. Using land-cover information, a spatial distribution of Manning's roughness coefficient was determined for each year. The results showed that the changes in land-cover during the years of study increased the impervious area and, consequently, the predicted runoff depth.

Kalin et al. (2003) evaluated the effect of geomorphologic resolution on runoff hydrographs for small watersheds. They indicated that accepted guidelines for determining an appropriate resolution of inputs are not available. This suggests that the extraction of channel networks and delineation of watersheds are really subjective processes because they are heavily dependent on input resolution. Analyses were performed for two small USDA experimental watersheds (83 and 107 acres) using the KINEROS model with a GIS interface. Results showed that the optimum spatial resolution can vary depending on the quantity of interest. The criteria for determining the optimal resolution were maximum accuracy of output with minimum computation time. The optimal resolution was relatively fine when considering peak runoff and relatively coarse when considering total sediment load. It was found that runoff hydrographs were less sensitive to spatial resolution during large rainfall events than small rainfall events. The study also suggested that geometric simplification of a watershed may be appropriate depending on the watershed properties and size of rainfall events to be used.

Jain et al. (2004) developed a grid based rainfall-runoff model capable of handling spatially distributed data to be applied to isolated storm events. The model requires distributed information such as slope, flow direction, soil type, and drainage path to be

specified for each cell. This data can generally be derived from DEMs and digital analysis of satellite data using GIS. The results indicate the model reasonably predicts temporal variation of the spatial distribution of flow depth and runoff over the catchment. The model does have the limitation that it requires some parameters to be calibrated.

Du et al. (2009) developed a GIS based runoff routing method based on travel time used to simulate storm runoff response accounting for spatial and temporal variability of runoff generation. This was accomplished by discretizing the watershed into grid cells that were designated as overland or channel cells based on the delineation from the DEM using GIS. The travel time for each overland cell was estimated by combining the steady state kinematic wave approximation with Manning's equation, while the travel time for each channel cell was estimated by combining Manning's equation with the steady state continuity equation. The total travel time from each cell to the outlet was determined as the sum of travel times of all cells along the flow path. Direct runoff flow was determined as the sum of flow rates from all contributing cells at each respective travel time for all time intervals. The results showed that good accuracy could be obtained with a grid size of less than 200 m.

2.3 SURFACE RUNOFF MODELING

Butler (1977) conducted a study of the influence of Reynold's Number on overland-flow travel time in the case of uniform excess rainfall on a strip of uniform width. The analysis was limited this type of "strip flow", a condition generally occurring at airports, parking lots, roofs, etc. In this case, the factors that contributed to the time of concentration are the rainfall excess, friction, slope, and length of the "strip". The time of concentration formula developed allowed for possible flow regime changes within the

reach of study. Although the correlation between the experimental and theoretical values for time of concentration showed good agreement, the model was positively biased, which signified consistent overprediction.

Akan (1985) developed a set of equations that combine kinematic wave theory with the Rational method to predict peak runoff for various basin types. The purpose was to be able to determine design discharge rates explicitly using physically based equations. According to Akan, one advantage of physically based equations is that their applicability is not restricted to a specific location or specific flow conditions. Major assumptions applied in this study included: (1) a spatially and temporally uniform rainfall distribution, (2) a rainfall duration that is equal to the equilibrium time, (3) losses occur at a uniform rate, and (4) the friction slope is equal to bed slope.

Wong and Chen (1997) derived a physically-based time of concentration formula for sheet flow by coupling the kinematic-wave equations and the Darcy-Weisbach friction formula. Being physically based, this formula is more suited for general use than previous empirically derived models. The time of concentration formula is suitable for laminar, transitional, and turbulent flow regimes, and is limited to conditions of uniform rainfall excess, constant upstream flow, and a single flow regime that covers the entire plane. This formula was applied to runoff surfaces of a single flow regime and compared against formulas that attempt to predict runoff over surfaces of varying flow regimes. The results showed that the time of concentration was shorter when considering a single flow regime over the runoff surface than when multiple flow regimes were considered.

Woods and Sivapalan (1999) developed a method of relating the variability of catchment-averaged storm runoff rates in terms of the space and time variability of

hydrological inputs and landscape properties. Models of rainfall runoff and linear routing were combined in order to quantify the effect of multiple inputs on the variability of catchment averaged storm runoff rates. The combined model was able to synthesize space and time variability in order to make the runoff predictions. The subsequent equations can help identify the major sources of storm runoff variability from one catchment to another. The method was applied to a 10-hour storm over a 420km^2 catchment in Australia.

Myers (2002) developed a model for two-dimensional laminar flow over a rough surface. Formulae used to predict the height and average and maximum velocities were developed. Predictions from these formulae showed good agreement with previous experiments. It was noted that the Manning, Chezy, and Darcy-Weisbach equations all overpredict the velocity for laminar flow. The inundation ratio, which is the maximum roughness height over the film height, was illustrated to be an important parameter in characterizing laminar flow.

2.4 FLOOD DAMAGE ASSESSMENT

Smith (1994) discussed methods and challenges of constructing stage-damage curves for use in flood damage estimation. One method is to use data from an actual flood event to develop the relationship between depth of flooding and damages incurred. A damage curve developed in this manner may have limited applicability in other locations due to differences in building type, contents, warning time, and prior flood experience. The other method Smith identified produces synthetic stage-damage curves of which there are two types: one is based on existing databases; the other is based on surveys by valuers and loss adjusters. Both cases require the buildings in consideration to be subdivided into

categories. Although only direct damages were addressed in this study, Smith recommended that indirect losses should also be considered in shaping flood policy, as they can be significant.

Merz et al. (2003) discussed methods to quantify the various sources of uncertainty in flood damage estimation. Four thousand damage records were analyzed covering nine flood events in Germany from 1978 to 1994. The analysis illustrated the high level of variability in flood damages, which contributes to the high level of uncertainty. Damage estimates are most problematic for small areas, i.e., a single building, because of higher uncertainty. Additionally, buildings that represent highly variable economic sectors (i.e. manufacturing) can introduce further uncertainties.

Dutta et al. (2003) developed an integrated model to simulate flood inundation and estimate flood losses in a river basin. The hydrologic component of the model was based on the governing physical equations of the water cycle, while the loss estimation component of the model was based on stage-damage relationships. The two components were dynamically linked to allow for a spatial distribution of flood losses at any time during a flood event. Application of this model was demonstrated on a mid-size river in Japan. Simulated discharges and inundation levels showed good agreement with observations from previous flood events. The greatest errors were associated with the peak values. Simulated urban flood losses also provided reasonable agreement with post-flood survey estimates. It is suggested that more detailed regional and local stage-damage functions are needed to increase the accuracy of loss estimation. Indirect losses were not considered in this study.

Jonkman et al. (2007) developed an integrated hydrodynamic model to estimate damages caused by floods. This model predicts direct and indirect economic losses, as well as loss of life. The model was used to estimate flood damages in South Holland under low probability-high impact conditions. Much of the analysis was aided by the use of GIS. Land use data, economic data, flood characteristics, and stage-damage functions were utilized in estimating direct and indirect losses. Inputs of flood characteristics, exposed population, evacuation possibilities, and an approximate mortality rate among those exposed were needed for loss of life estimations. Predictions of indirect damages beyond the affected area were not reliable due to lack of necessary data.

2.4.1 Army Corps of Engineers

The US Army Corps of Engineers (USACE) operates their own Hydrologic Engineering Center (HEC) that is devoted to developing software for various purposes related to hydrologic studies. Their Flood Damage Analysis software (HEC-FDA) allows users to perform an integrated hydrologic engineering and economic analysis that can assist in developing policy and making decisions relating to flood risk management (USACE 2008). As part of the economic analysis, HEC-FDA computes expected annual damages (EAD) for a given location. In order for an EAD to be computed, certain stage-damage curves must be utilized.

Generic stage-damage curves have been developed by USACE (2003) to aid in various types of economic analysis. Separate damage curves have been developed for damages to structure, contents, vehicles, etc. Several different curves may be suitable for residential buildings, depending on how many stories there are, and whether or not there are basements. Generic damage curves for vehicles are dependent on different vehicle

types (sedan, minivan, SUV, etc.). The Flood Damage Data Collection Program was initiated by USACE for the specific purpose of providing the data necessary to develop these standardized relationships between flood depth and damage.

Developing generic damage curves for commercial, industrial, or public buildings is much more difficult. While generic curves may still be applicable for structural damage by incorporating factors based on building type, the value and location of contents is highly variable. Therefore, estimating the damage to contents in these types of buildings requires more detailed information. For residential buildings, USACE relates content values to structure values as a percentage. Based on information from the Flood Damage Data Collection Program, the content damage-structure value ratio is relatively stable for residential structures of certain categories. Thus, treating the ratio as a constant for use in a generic content-damage curve is reasonable and can be expected to produce meaningful damage estimates. The content damage-structure value ratio is not nearly as stable for other building types. Obtaining accurate damage estimates for other building types, therefore, usually requires the development of site-specific damage curves.

Regression analysis was used by USACE to develop the damage curves. Depth of flooding is the most important variable in any flood damage estimation curve. While other variables were also examined, such as flood duration and warning time, it was found that the models best able to explain the variation in damages were quadratic and cubic forms with depth as the only independent variable.

2.5 SWMM SIMULATION OPTIONS

SWMM has a simulation options menu that offers control of model functions. Before beginning the formulation of a model, these options should be reviewed and

selected to match the purposes for which the model is being used. Only the options relevant to the modeling of pluvial flooding are discussed herein.

2.5.1 Process Model Options

SWMM has the capability of combining several process models into a single simulation (EPA 2004). These process models include; rainfall/runoff, snow melt, groundwater, flow routing, and water quality. If input data are available, any combination of these process models may be selected for a given simulation. Only the rainfall/runoff and flow routing process models are relevant to this study; therefore, these are the only two process model options that were selected for the SWMM simulations throughout this study.

2.5.1.1 *Rainfall/Runoff*

The rainfall/runoff process model component is the hydrologic modeling component of SWMM that will be used for this study. It converts rainfall inputs for a subcatchment into runoff that drains to an inlet or another subcatchment. An illustration of the general conceptual rainfall/runoff process model used by SWMM is shown in Figure 2-1. Snowmelt was not considered for the analyses of this study. Additionally, evaporation can be ignored for modeling single-events based on the assumption that evaporation does not occur while rain is still falling. Therefore, removing snowmelt and evaporation from Figure 2-1, the rainfall/runoff model is simplified to include rainfall, depression storage, and infiltration as the processes, and runoff as the output.

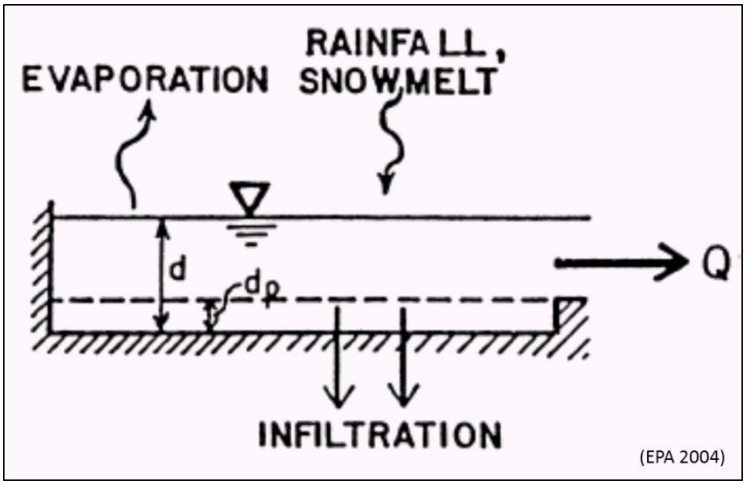

Figure 2-1. Conceptual view of the rainfall/runoff model used in SWMM.

In the rainfall/runoff process model, each subcatchment acts like a reservoir where runoff only occurs when the storage capacity is exceeded. The rainfall inflow enters the storage element from which water is allowed to infiltrate according to the infiltration model selected. Rainfall inflow arriving faster than the infiltration rate or after the soil becomes saturated begins to fill the depression storage. Once the capacity of the depression storage is reached, additional rainfall becomes runoff. The flowrate of the runoff is given by Manning's equation:

$$Q = W\frac{1.49}{n}(d - d_p)^{5/3}S^{1/2} \tag{2.1}$$

where Q is the runoff (cfs), W is the characteristic width (or average width of the longest flow path) of the subcatchment (ft), n is Manning's roughness coefficient, d is the average water depth (ft), d_p is the depression storage depth (ft), and S is the average slope (ft/ft) of the subcatchment. The average water depth (d) is updated within SWMM

at each time step by numerically solving a water balance equation. The other inputs (i.e., *W*, *n*, d_p, and *S*) are user defined.

2.5.1.2 *Flow Routing*

The flow routing process model is the hydraulic modeling component of SWMM that will be used to develop a pluvial flood model. This process model dictates how the water is routed through a system of open channels and closed conduits based on the conservation of mass and conservation of momentum equations. These conservation equations applied to gradually varied, unsteady flow become the St.Venant equations:

$$\frac{\partial A}{\partial t} + \frac{\partial Q}{\partial x} = 0 \tag{2.2}$$

$$\frac{1}{g}\frac{\partial V}{\partial t} + \frac{V}{g}\frac{\partial V}{\partial x} + \frac{\partial h}{\partial x} + \left(S_f - S_0\right) = 0 \tag{2.3}$$

where *A* is the cross-sectional area of the conduit (ft^2), *Q* is the discharge (cfs), *V* is the velocity (fps), *h* is the depth of flow (ft), S_f and S_0 are the friction and bed slopes, respectively (ft/ft), *g* is the gravitational constant (32.2 fps), and t and x are the time and distance along the conduit, respectively (McCuen 2005). When Equation above is integrated along the length of a conduit, it becomes the more familiar conservation of mass equation:

$$Q_{in} = Q_{out} \pm \frac{\partial S}{\partial t} \tag{2.4}$$

where Q_{in} and Q_{out} are the inflow and outflow (cfs), respectively, S is the storage volume (ft^3), and t is time (sec). Three levels of sophistication are available for solving the St. Venant equations (Equations 2.2 and 2.3); steady flow, kinematic wave, and dynamic wave, each of which will be discussed further in section 3.1.2 Routing Model Options. It should be noted that each of these routing methods utilizes Manning's equation to relate flowrate, flow depth, and friction slope for each conduit.

2.5.2 Infiltration Model Options

The following three infiltration model options are available for use with pervious areas in SWMM: Horton, Green-Ampt, and Curve Number. The Horton infiltration model is the default option and was used for this study; however, with proper justification the Green-Ampt or Curve Number models could be more suitable when considering local conditions and overall modeling goals. The Horton equation defines the infiltration rate at any point in time:

$$f_t = f_c + (f_0 - f_c)e^{-Kt} \tag{2.5}$$

where f_t is the infiltration rate at time t (in./hr), f_c is the infiltration capacity after a long period of rainfall, the final, or ultimate, infiltration rate (in./hr), f_o is the initial infiltration rate (in./hr), K is the infiltration rate decay constant specific to soil type (hr^{-1}), and t is the elapsed time from the beginning of the rainfall (hrs) (Wanielista et al. 1997). This equation is also known as Horton's Infiltration-Capacity Curve, which when integrated provides the total volume of infiltration:

$$F_t = f_c t + \frac{(f_0 - f_c)}{K}(1 - e^{-Kt}) \quad (2.6)$$

where F_t is the total volume of infiltration at time t (in.) (Wanielista et al. 1997). This equation allows the total infiltration to be reported at any time step in the modeling process making it possible to accurately evaluate a water balance equation.

CHAPTER 3

SWMM MODEL SET UP PROCEDURE

3.1 INTRODUCTION

After some preliminary research was conducted, it became apparent that EPA's Storm Water Management Model (SWMM) software would be suitable for achieving the first two objectives of this study: (1) to set up a model of a potential urban pluvial flood site, and (2) to use the model to identify conditions under which pluvial flooding of various magnitudes would occur. While numerous modeling software packages exist, the procedure developed herein is intended to be as broadly applicable as possible. The SWMM software package is public domain and is available for download free of charge on EPA's website. Because of accessibility, as well as relative simplicity compared with other models, SWMM is widely used.

SWMM was first developed by the EPA in 1971 and has continued to evolve with the growth of computing technology. The most recent version is SWMM 5.0. SWMM was designed specifically for urban stormwater studies, but it can also be used outside the urban environment. It is a dynamic simulation model that combines hydrologic and hydraulic components to track the flow of water from rainfall to runoff and through the stormwater system (EPA 2004).

Before adopting SWMM, it was important to confirm that it would be able to offer the needed features and flexibility to accurately model conditions that lead to pluvial flooding in small urban watersheds. To ensure this, several simple SWMM models were set up to highlight the important processes involved in pluvial flooding situations. This procedure also provided justifications for formulating full-scale models.

3.1.1 Ponding Option

Pluvial flood modeling requires accounting for the full volume of water in the system at each time step. SWMM has a ponding option that allows overflow at an inlet to be accumulated above the inlet until it can be routed appropriately through the system. This option was valuable for this research because the third research objective was to estimate the damages associated with pluvial flooding of certain depths. If the ponding option were not available, then the flood locations could be observed, but the depth of flooding would not be part of the output. As the flood depth is the key input for any stage-damage function, the ponding option was turned on for all simulations in this study.

A simple SWMM model was formulated to evaluate the effects of the ponding option. The layout of this model is show in Figure 3-1. The 5-acre subcatchment is 100% impervious and drains to J1. An allowable ponding area can be input when the ponding option is on. In this case, 0.1 acre (4,356 ft^2) was chosen as the ponding area. The only conduit, C1, was a pipe of 0.01-ft diameter. While an outlet is required to simulate a model in SWMM, reducing pipe C1 to a near-zero diameter effectively eliminated the outlet. This model was used to force all of the volume of rainfall from a 100-yr, 2-hour storm to pond above inlet J1. The maximum ponded depth reported when this model was simulated was 14.88 ft. Hand calculations confirmed this value to

correspond with 1.49 ac-ft, or 3.57 in. across the watershed. This is accurate because the total precipitation was 3.67 in. with 0.1 in. captured in depression storage.

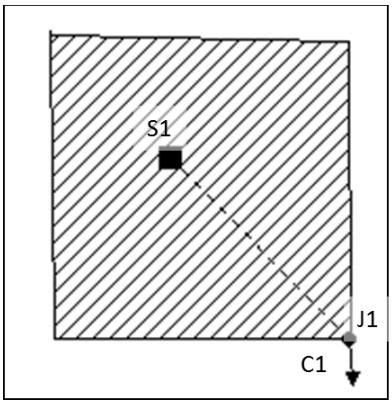

Figure 3-1. Layout of simple SWMM model used to evaluate ponding option.

Additional simulations of this layout were made with the ponding option not used and with pipe C1 having a 1.0-ft diameter to provide a comparison how this can influence various model results. Table 3-1 gives a summary of several output quantities for each simulation. When the ponding option is not active and the inlet is flooded, the water that overflows the inlet becomes "lost" to the system. While SWMM does record the volume of flooding in this case, the flow characteristics of the rest of the system are not influenced by the flooding, as they would be at an actual flood site. Therefore, as Table 3-1 shows, the maximum flow and velocity for the simulation using the ponding and the 1-ft pipe were greatly influenced by the depth of ponded water above the inlet. The ponding at the inlet creates a pressurized flow system that greatly affects the characteristics of flow. Without the ponding option, these effects would not be incorporated into the flow scheme. Therefore, the ponding option was used in all of the analyses of this study to more accurately represent actual flooded conditions.

Table 3-1. Summary of effect of ponding with outlet pipes of 0.01 and 1.0 ft.

	Flood Volume (10^6 gal)	Max. Ponded Depth (ft)	Max. Flow (cfs)	Max. Velocity (fps)
Ponding - 0.01-ft pipe	0.484	14.88	0.00	0.00
No ponding - 0.01-ft pipe	0.484	0.01	0.00	0.00
Ponding – 1-ft pipe	0.111	4.41	9.16	11.66
No ponding – 1-ft pipe	0.231	1.00	3.78	5.15

3.1.2 Routing Model Options

Three flow routing model options are available in SWMM: steady flow, kinematic wave, and dynamic wave (EPA 2004). Using the SWMM model shown in Figure 3-2, an evaluation of these wave routing methods was made. It was expected that dynamic wave routing would be the most suitable for the purposes of this study because it is equipped to deal with pressurized flow, flow reversal, and backwater effects. These conditions are undesirable in stormwater management; however, they are representative of the extreme conditions under which pluvial flooding is likely to occur and must be modeled with accuracy to ensure meaningful results.

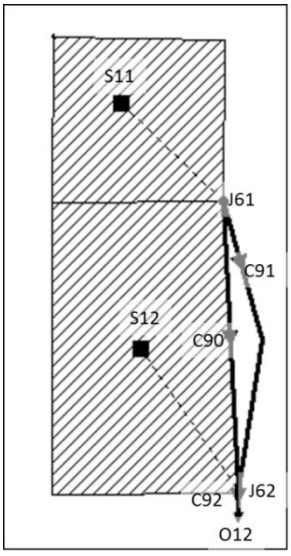

Figure 3-2. Layout of a simple SWMM model used to evaluate various flow routing methods available in SWMM. Conduit C90 represents a stormsewer pipe and conduit C91 represents a street channel connected by the same inlets.

Steady-flow routing is the simplest available routing method. The main assumption applied is that flow is steady and uniform in all conduits during each computational time step. In other words, the flow and depth at the downstream end of each conduit is the same as at the upstream end. This transition occurs immediately; therefore, conduit storage is not possible. Flow reversal and pressurized flow are similarly not possible using the steady-flow option.

Kinematic wave routing combines the continuity equation with a simplified form of the momentum equation. This method allows a maximum flow equal to the computed capacity of each conduit. The ponding option may be used with kinematic wave routing; however, this method cannot account for pressurized flow, reverse flow, or backwater effects. Therefore, while using kinematic wave routing, the ponding option would not fully represent the actual effects of flooding at one location on the flow characteristics of the rest of the drainage system. An advantage of using the kinematic wave routing method is that it can maintain numerical stability for relatively large time steps. This translates to shorter simulation run times.

The dynamic wave routing method is the most advanced and accurate method available in SWMM. This method numerically solves the full one-dimensional St. Venant equations at each time step. It does generally require smaller time steps to be used (one minute or less) in order to maintain numerical stability. For large systems or continuous simulations, this can significantly increase the simulation run time. This method can accommodate more complex pipe networks that are not strictly dendritic. It can also account for pressurized flows, which is important when modeling pluvial flooding.

For direct comparison, simulations were attempted with each of these three routing methods. It was found that SWMM was unable to successfully run the model with the steady flow or kinematic wave routing options. The reason cited in the SWMM output report was that more than one link was connected to J61. In other words, these routing methods are not capable of splitting flow between two different conduits connected to the same junction. Therefore, SWMM cannot run a dual drainage model with any other routing method than the dynamic wave method.

The differences in numerical results of the three routing methods can still be explored if the street channel (C91) is removed from the system (see Figure 3-2). A summary of these comparisons for the 2-, 10-, and 100-yr storms is given in Table 3-2. For the 2-yr storm, all of the values are very similar for each routing method. This is because the capacity of C90 has not yet been exceeded. Significant differences begin to appear in the maximum velocities in the 10-yr storm. The maximum flow and velocity for the 10- and 100-yr storms were identical under steady-flow routing, which is unreasonable. Under kinematic wave routing, the maximum flow remained the same from the 10-yr to the 100-yr storms, while the maximum velocity increased significantly. This does not make physical sense as the continuity equation, $Q = VA$, is not satisfied. Additionally, both the steady-flow and kinematic wave routing methods cannot account for any water beyond the depth of the conduit. In other words, the effects of surcharging and flooding cannot be represented with steady-flow and kinematic wave routing methods because water volumes that surcharge and flood are essentially removed from the system. The dynamic wave routing method allows such water volumes to accumulate and continue to influence the rest of the system.

Table 3-2. Maximum flow (ft^3/s), velocity (ft/s), and depth (ft) along conduit C90 and at inlet J61 for 2-, 10-, and 100-yr storm events.

	(2-yr)		
	Max. Flow	**Max. Velocity**	**Max. Depth**
Steady Flow	3.07	4.74	0.77
Kinematic Wave	2.93	4.81	0.77
Dynamic Wave	2.94	4.52	0.74

	(10-yr)		
	Max. Flow	**Max. Velocity**	**Max. Depth**
Steady Flow	3.28	4.76	1.00
Kinematic Wave	3.54	6.42	1.00
Dynamic Wave	3.66	5.01	1.36

	(100-yr)		
	Max. Flow	**Max. Velocity**	**Max. Depth**
Steady Flow	3.28	4.76	1.00
Kinematic Wave	3.54	8.86	1.00
Dynamic Wave	4.36	5.57	3.42

In summary, dynamic wave routing is the only routing option in SWMM that can be successfully used to model surface and subsurface flow in a dual drainage system. Even after removing the street flow channel (C90) to allow steady flow and kinematic wave routing to operate, each revealed significant errors once the capacity of the pipe was exceeded. This was expected because steady flow and kinematic wave methods are not equipped to deal with pressurized flow, a condition that presupposes pluvial flooding in urban environments. Therefore, dynamic wave routing was the chosen routing method for all simulations in this study.

3.2 DUAL DRAINAGE SYSTEM

A simple SWMM case study was designed to evaluate how accurately SWMM can represent a dual drainage system, specifically, above-ground gutter flow combined with below ground pipe flow. The same simple watershed shown in Figure 3-2 was used for

this analysis. Two subcatchments, labeled S11 and S22, drain into inlets J61 and J62, respectively. Runoff entering the system at J61 flows to J62 through a dual drainage system consisting of conduit C90 which is a below ground stormwater pipe, and conduit C91 which is an above ground street channel. The street channel C91 does not appear straight on the map because this was more convenient for visualization. However, both conduits, C90 and C91, are defined as the same length and connect the same inlets. Because SWMM does not allow more than one conduit to be directly connected to an outfall, C92 was created, a short pipe that carries all of the runoff from this system to the outfall O12. The results of the first simulation using this model and the 2-yr, 2-hr storm are shown in Figure 3-3. The bump in the figure at 2-hrs indicated the end of the rainfall, though residual runoff continued to drain from the system.

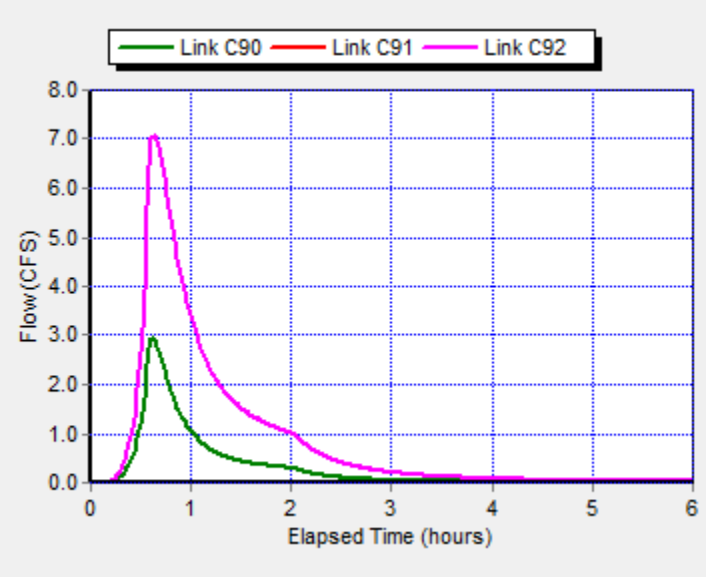

Figure 3-3. Flow rates for pipes C90 and C92 and street channel C91 for a 2-yr, 2-hour storm.

Simulations of this model were made for 2-hr storms of various return periods. For the 2-yr storm, none of the pipes reached capacity and flow did not appear in street channel C91. However, during the 10-yr storm, the capacity of pipe C90 was exceeded

and water began to flow in street channel C91. The capacity of each drainage pipe was determined using Manning's equation under gravity flow conditions. This capacity was only exceeded when the flow became pressurized, which occurred when an inlet was submerged. Because the cross-sectional area is constant in a closed conduit, an increase in flow rate beyond the natural capacity can only be accounted for by an increase in velocity caused by an increase in pressure. In the example case study, the inlet for pipe C90 became submerged about 30 minutes into the 10-yr storm simulation (see Figure 3-4). Due to the pressurized condition, the flow began to exceed the gravity flow capacity of 3.28 cfs. As the depth of submergence increased, so did the pressure, and consequently, the flow through pipe C90. Figure 3-5 shows the depth at J61 sharply increased until it reached 3 ft, which is the depth at which the water began to overflow into street channel C91. This occurred at the same time that the flow through C90 plateaued at 4.17 cfs (see Figure 3-4).

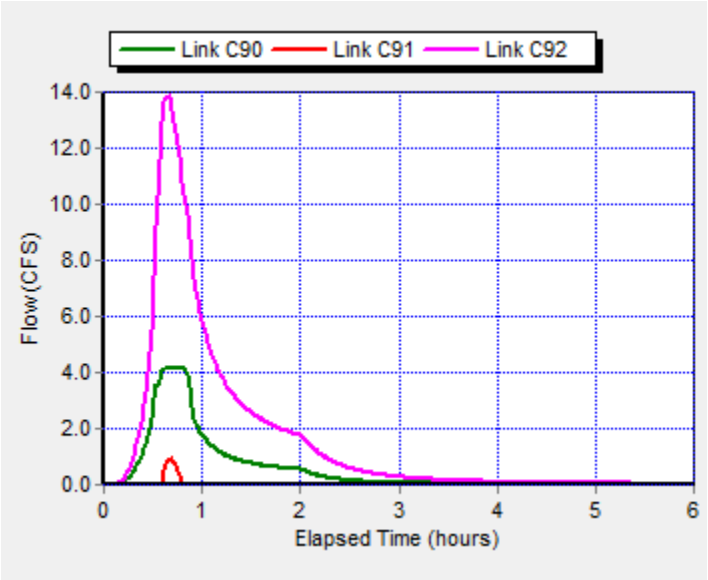

Figure 3-4. Flow rates for pipes C90 and C92 and street channel C91 for a 10-yr, 2 hour storm.

Finally, the results for the 100-yr storm are shown in Figure 3-6. In this case, the flow in street channel C91 exceeded the flow in pipe C90 for a time, reaching a peak discharge of 10.73 cfs. In each simulation, the shape of the flow curve for the pipe leading to the outlet (C92) was the same. This means that for this short duration storm over this small area, the timing of the flow to the outlet was not influenced significantly by either the return period or the flow path, but the backup at the inlet was significant.

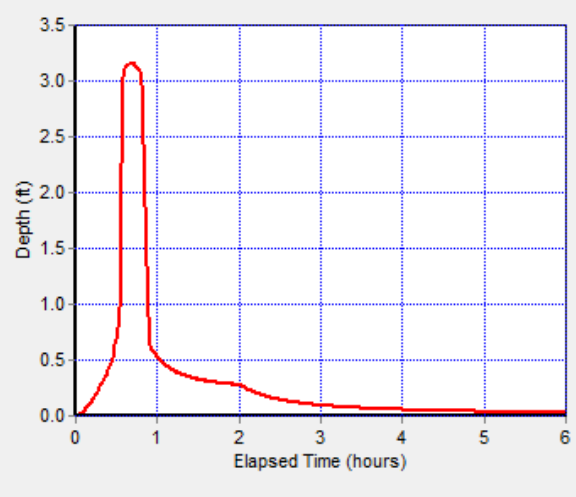

Figure 3-5. Water depths reported at inlet J61 for a 10-yr, 2-hour storm.

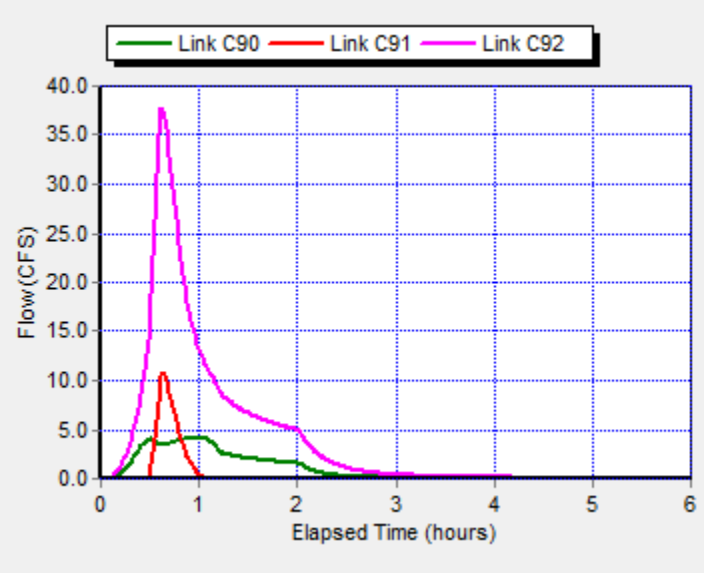

Figure 3-6. Flow rates for pipes C90 and C92 and street channel C91 for a 100-yr, 2-hour storm.

3.3 BUILDING A SWMM MODEL

Another model was structured for a situation that is somewhat more realistic in characteristics and scale than the previous case studies. This allows the process of building a pluvial flood model in SWMM to be shown. The basic steps are outlined. Some of the assumptions and decision justifications may vary depending on the intended use of the model. Below is a list of the steps that were used:

1. Select a potential pluvial flood site.
2. Obtain site-specific model input data.
3. Model the pipe network.
4. Model the street channels.

3.3.1 Select a Study Site

A site can be modeled for any one of a number of reasons. First, the site of interest could be a site that has previously been subjected to pluvial flooding and an analysis is required to identify reasonable measures that could be taken to prevent future flooding under similar conditions. Second, the site of interest may not have experienced flooding, but is selected because the characteristics of the site indicate that it has potential to experience pluvial flooding. Third, a pluvial flood model would be useful in the planning of local renovation of an existing pipe system. Fourth, the model could be used in the design of a new system, such as, in the building of a large tech center. Other possible reasons for selecting a particular site could be the accessibility of relevant data, close proximity that would allow site visits, or some other special interest.

The models for the previous analyses were used to determine the functionality of certain components of SWMM. The following example model of a portion of

Washington, DC, is intended to emphasize the applicability of SWMM to an actual dual drainage system. The study site chosen for this example model was a 4 block-by-4 block section of the Capitol Hill area. This area was chosen for the convenience of setting up the SWMM model due to the simple layout in that section of the city. The extent of the study area can be seen in Figure 3-7.

Figure 3-7. Extent of study area used for SWMM model setup. The study area is part of Capitol Hill in Washington, DC.

3.3.2 Obtain Site-specific Model Input Data

The ability to obtain site-specific data is important for any hydrologic analysis. It does not matter how accurate a model is able to represent the actual physical processes involved in urban runoff if the input data are poor or too generic. Therefore, it is valuable to understand the types of data that exist and their accessibility.

3.3.2.1 *Site-specific Elevation Data*

One of the limiting factors in a flood study of a small-scale watershed is the availability of data at the appropriate resolution. For example, an elevation dataset is a key factor in calculating runoff timing and routing because it will determine the slopes that dictate where and how quickly runoff will flow. Several forms of elevation data exist for which several levels of resolution are possible. This discussion should assist the user in determining which form of elevation data would be best suited for a particular pluvial flood risk study.

The USGS maintains the National Elevation Dataset (NED). The NED is in the public domain and is updated on a bi-monthly basis to incorporate any newly available or improved elevation data provided by local sources (USGS 2006). From the NED, elevation data are readily available for most areas of the U.S. at 30m and 10m resolutions in the form of Digital Elevation Models (DEMs). These would be excellent for regional or primary watershed scale hydrologic models. Certain locations have produced DEMs of 3m resolution to facilitate more detailed analysis. This resolution would be appropriate for hydrologic models the size of a large city. None of these resolutions would be sufficiently detailed for a study site of a few hundred acres or less, as was the intent for this research.

Light Detection and Ranging (LiDAR) is another form of elevation data that may be available at some locations. This remote sensing technology is able to produce elevation data at very high resolutions of 1m or less. While the high resolution of data that LiDAR can provide has advantages, legitimate concerns about the quality and accuracy of this data in certain circumstances do exist (Barber and Shortridge 2005). LiDAR data are

often produced and maintained by the local jurisdictions. Due to the expense of producing and maintaining this data, part of that cost is usually passed on to the user in the form of a fee for accessing the data.

For microwatersheds, even the high resolution elevation data that LiDAR can provide is often limiting. This is particularly true of urban environments where many structural constraints exist, such as tunnels and bridge overpasses, which may not be accurately represented in the LiDAR data. Topographic contour lines can assist in mapping elevations in locations that have particularly steep slopes.

3.3.2.2 *Site-specific Aerial Imagery*

Aerial imagery can be helpful in developing a SWMM model, though it is not essential. One benefit of having an aerial image of the study site is that it can be set as a backdrop image in the SWMM display window. This can assist in the placement of important SWMM features that will represent the system. Additionally, the SWMM display window can be manually scaled so that the image represents real-life dimensions. Set up in this way, and with the Auto-Length setting on, all features drawn to match the image will automatically be dimensioned correctly. An example of the pipe drainage network having been drawn to fit an aerial photo was shown in Figure 3-7. The alternative is to have default lengths and areas for new features (not associated with the visual scale on the map) that have to be manually edited in order to match the system. This can be a cumbersome process that is multiplied by the number of features represented in the model.

3.3.2.3 *Site-specific Rainfall Data*

Quality rainfall data are the first essential input required for a pluvial flood model. Both the total rainfall depth and the temporal distribution of rainfall are necessary. The depth determines the amount of water potentially available for runoff while the temporal distribution of rainfall influences the temporal distribution of runoff. For small watersheds, it can generally be assumed that rainfall does not vary spatially, but rather, is constant across the watershed (McCuen 2005). NOAA's National Weather Service has developed intensity-duration-frequency (IDF) and depth-duration-frequency (DDF) curves specific to different areas of the U.S. based on weather patterns and climatic trends. Graphs of these curves are accessible on NOAA's website (NOAA 2012). The NOAA DDF curves for Washington, DC, for 24-hr storms were used to graphically estimate the total rainfall depths for the 2-, 10-, 100-, and 200-yr storms as 3.0, 5.0, 8.5, and 10.0 inches, respectively (see Figure 3-8).

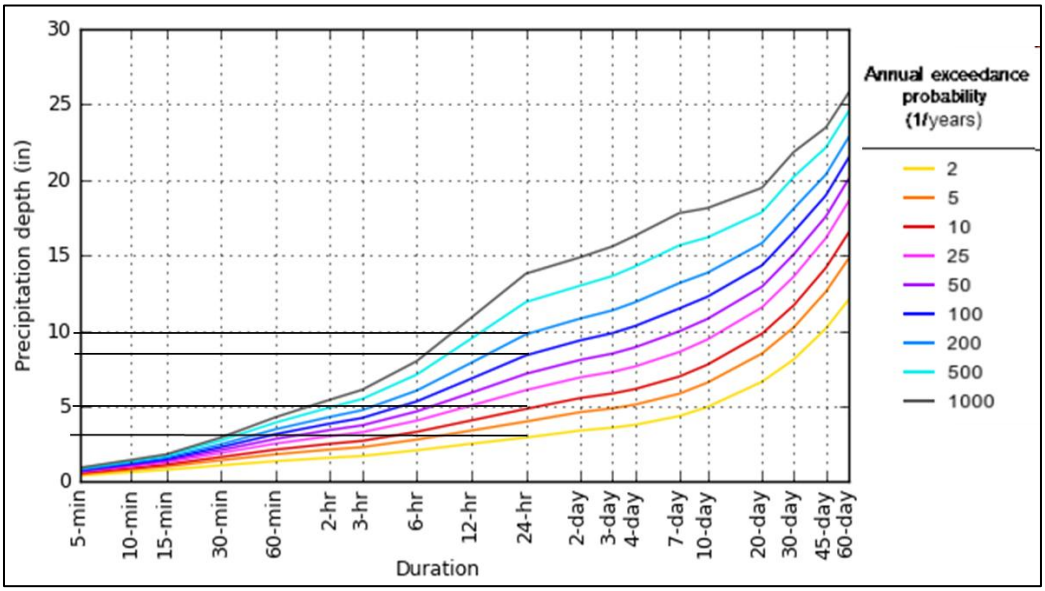

Figure 3-8. NOAA's 24-hr depth-duration-frequency curves for Washington, DC.

Equations for the various IDF curves representing Baltimore, MD, were also utilized to ensure that the total rainfall depths obtained from NOAA's DDF curves were reasonable. The general form of the IDF curve equation used is:

$$i = cD^d \quad \text{for D} > 2 \text{ hr} \tag{3.1}$$

where i is the average intensity over the duration of an event (in./hr), D is the duration (hrs), and c and d are coefficients that vary with frequency (McCuen 2005). Once the average intensity was determined, it was multiplied by the duration (24-hrs) to obtain the total rainfall depth. The inputs and results of using this equation for 24-hr storms of various return periods for Baltimore, MD, are given in Table 3-3. The equations resulted in total rainfall depths of 3.03, 5.05, and 7.45 and 9.10 in. for the 2-, 10-, 100- and 200-yr storms.

The depths for the 2- and 10-yr return periods were very similar when graphically estimated from NOAA's DDF curves for Washington, DC, and when derived from IDF curve equations specific to Baltimore, MD. However, using the two different sources the depths for the 100- and 200-yr storms were significantly different (8.5 and 10 in. for Washington and 7.45 and 9.10 in. for Baltimore). Washington and Baltimore are only about 40 miles apart and share a nearly identical climate, both having Mid-Atlantic, tidally influenced weather patterns. Therefore, it is unlikely that the difference in location can account for the difference in depths for the 100- and 200-yr storms. The difference is more likely due to a difference in the periods of record. For example, using rainfall records from the first half of the 20th century could lead to significantly different

rainfall depths for a given return period than using rainfall records from the second half of the 20th century. Additionally, the longer that the period of record used is, the more reliable the rainfall depth estimates will be, especially for large return period events.

Table 3-3. Inputs and results of IDF curve equations for 24-hr storms of various return periods for Baltimore, MD.

Return Period (years)	*c*	*d*	*i* (in./hr)	Total depth (in.)
2	1.367	-0.75	0.126	3.03
10	2.280	-0.75	0.210	5.05
100	3.364	-0.75	0.310	7.45
200	4.110	-0.75	0.379	9.10

The most accurate rainfall depths would theoretically derive from a rainfall frequency analysis based rainfall records specific to Washington, DC. A recent study conducted at the University of the District of Columbia (UDC) performed this analysis from rainfall records at Washington Reagan Airport from 1948 to 2009 (Behera 2011). Rainfall depths obtained from this study, along with the depths determined by the two methods described above, are provided in Table 3-4. The graphical estimation method provided similar results to the frequency analysis. This suggests that, if more detailed data are not available for a particular location, estimating rainfall depths from NOAA's DDF curves could provide reasonable values. However, in this case the results from the frequency analysis using DC data (Behera 2011) were selected and used throughout the remainder of this study.

Once the depths for each frequency were obtained, then the temporal distribution of rainfall for a 24-hr storm event needed to be determined. The Natural Resources Conservation Service (NRCS) has developed normalized 24-hr rainfall distributions for four different types of storms typical to different regions of the U.S. Washington, DC, is

in the Type II region (McCuen 2005). Therefore, in order to determine the 24-hr rainfall distributions for the various frequencies being considered, the total rainfall depths obtained from the DDF curves were multiplied by the NRCS Type II 24-hr rainfall distribution values. The result is the four rainfall distributions shown in Figure 3-9.

Table 3-4. Total rainfall depths for 24-hr storm from various estimation methods and data sources.

	Total Estimated Rainfall Depths (in.)		
Return Period (yrs)	Graphical method, DC data	IDF equations, Baltimore data	Frequency analysis, DC data
2	3.0	3.03	2.88
10	5.0	5.05	5.05
100	8.5	7.45	8.61
200	10.0	9.10	9.83

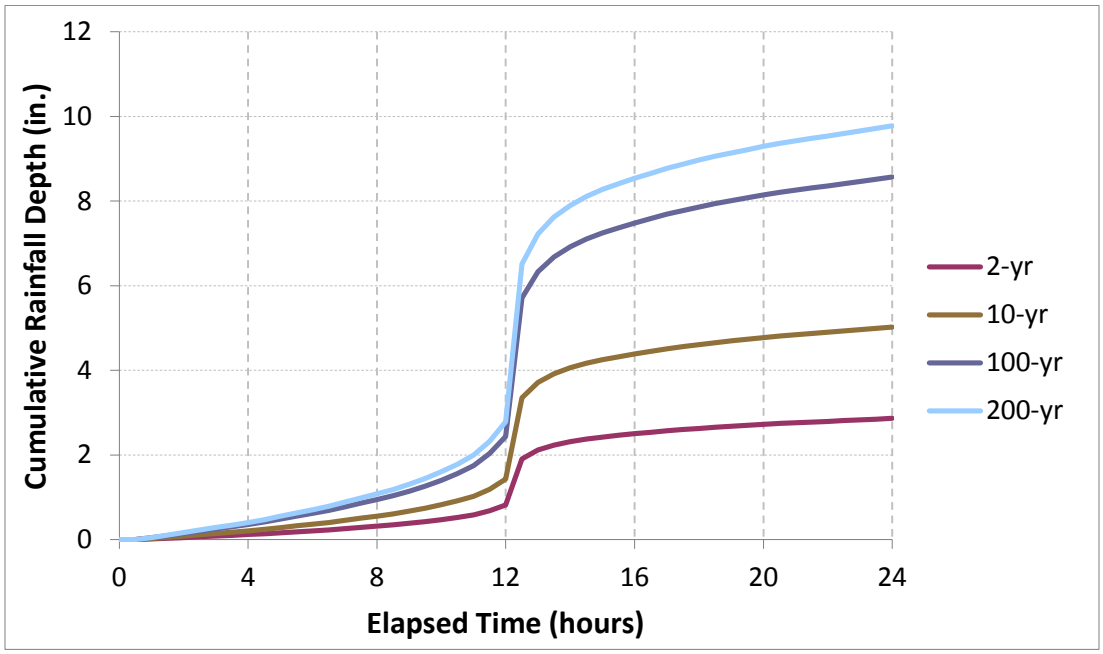

Figure 3-9. NRCS Type II cumulative rainfall distributions for a 24-hr storm for the 2-, 10-, 100-, and 200-yr return periods in Washington, DC.

3.3.2.4 *Site-specific Stormwater Drainage Network*

The layout of the stormwater drainage network may be accessible in some locations. The data are typically maintained by the local water and sewer authority. In some cases,

the information is inaccessible for security reasons because it can be considered critical infrastructure. If the data are available, it will improve the accuracy of model outputs because the actual site conditions will be able to be represented more accurately. If such data are unavailable, a pipe design method can be used to create a network with the capacity to drain a specific design storm. In such a case, modeling results should only be used to estimate the potential magnitude of flood problems in the area. Discussing the flooding of specific buildings or intersections when a hypothetical drainage network is in place is not meaningful or reasonable. Therefore, it is valuable to consider the level of detail of desired results before formulating a pluvial flood model. This will largely determine the types and resolutions of data inputs required.

3.3.2.5 *Site-specific Roadway Geometry*

The geometry of the roadways that will convey the water that exceeds the capacity of the stormwater drainage network is necessary to accurately model pluvial flood scenarios. If the existing data are available or can be obtained by surveying the site, then the resulting model will more accurately represent the system. However, due to financial, geographical, or time constraints, it may not be feasible to perform a detailed survey of the site. If the data cannot be obtained, then local department of transportation design manuals can be referenced in order to generate this data to meet local design criteria.

3.3.3 Modeling the Pipe Network

A stormwater drainage model requires accurate measurements of conduit lengths and subcatchment areas as they greatly influence the volume and timing of runoff. For this case study, a high resolution orthographic image was imported into ArcGIS and projected

to provide the correct scaling of the image. This scaling was then manually input into SWMM so that, when the backdrop image was imported, it would maintain the true geometry. With the backdrop image scaled and the SWMM Auto-Length option activated, the elements of the map were laid out and automatically sized. Inlets were placed at each intersection, pipes that connect the inlets were drawn, and subcatchments, with each covering a city block, were delineated. This basic setup is shown in Figure 3-10.

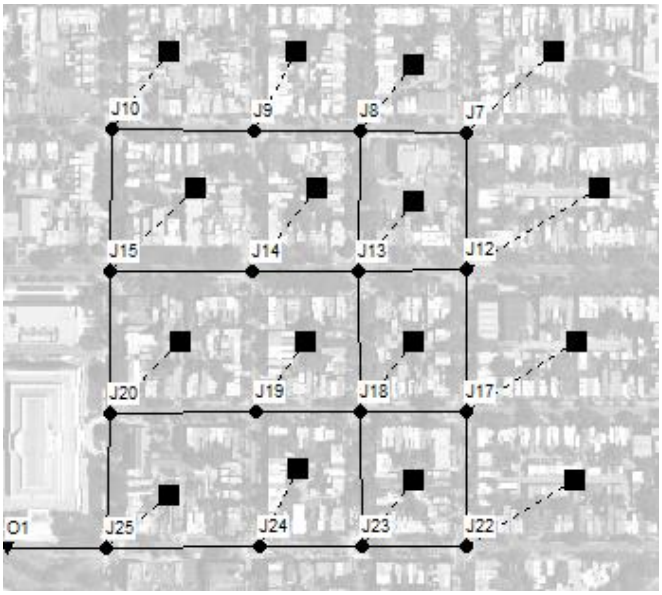

Figure 3-10. Pipe network with labeled inlets for SWMM model of 16 square blocks on Capitol Hill.

Though the model depicted in Figure 3-10 was based on a real location, several simplifications were necessary. First, the boundary of the 16 square blocks was treated as the extent of the watershed. Second, external inflows were not introduced and only a single outfall location was used. Third, the average slope, from top right to bottom left in Figure 3-10, was assumed to be 0.5%. This assumption was made to be consistent with a previous assumption that the average slope in each subcatchment was 0.5%. A zero elevation datum at the outfall was selected and all other elevations were established from

that point in order to maintain the assumed 0.5% slope across the watershed. This resulted in a slope of roughly 0.35% along the streets and pipes in both north-south and east-west directions. The elevations for each node are reported in Table 3-5.

Table 3-5. Elevations of junctions (inverts) in Capitol Hill example SWMM model.

Junction	Elevation (ft)
J7	9.31
J8	8.23
J9	7.20
J10	5.69
J12	7.90
J13	6.82
J14	5.78
J15	4.27
J17	6.44
J18	5.36
J19	4.33
J20	2.82
J22	5.13
J23	4.05
J24	3.01
J25	1.50
O1	0.00

3.3.3.1 *Required Pipe Sizes*

Once the pipe layout and pipe slopes were determined, Manning's equation assuming a full-flowing circular pipe was used to compute the required pipe diameter:

$$D = 1.333(Qn)^{3/8}S^{-3/16} \tag{3.2}$$

where D is the required pipe diameter (ft), Q is the expected peak flowrate (cfs), n is Manning's roughness coefficient, and S is the slope (ft/ft) (McCuen 2005). The initial

pipe sizes needed to be estimated in order to model the runoff of the 10-yr rainfall event and determine the peak flows for each pipe. From the initial estimated pipe diameters, Table 3-6 provides a summary of the calculations of required pipe diameters for the pipe network shown in Figure 3-11. Pipe C35 drains the entire watershed and, according to these calculations, requires a diameter of at least 3.05 ft to adequately drain a 10-yr rainfall event. These results were not final, however, because the new required pipe diameters needed to be updated in the model, which would affect the peak flows, and again influence the required pipe sizes. Therefore, the design process was iterated until the required pipe diameters converged to constant values.

Table 3-6. Summary of required pipe size calculations based on the simulation of a 10-yr rainfall event.

Pipe ID	Initial pipe diameter (ft)	Peak flow (cfs)	Slope (%)	Required pipe diameter (ft)
C6	2.0	4.32	0.3456	1.23
C7	2.5	4.09	0.3364	1.21
C8	3.0	7.39	0.3671	1.49
C10	2.0	4.33	0.3412	1.23
C11	2.5	5.18	0.3364	1.32
C12	3.0	8.57	0.3636	1.58
C14	2.0	4.34	0.3501	1.23
C15	2.5	6.44	0.3409	1.43
C16	3.0	9.80	0.3567	1.66
C18	2.0	4.23	0.3501	1.22
C19	3.0	14.84	0.3501	1.95
C20	3.0	18.01	0.3501	2.10
C28	2.0	3.54	0.3466	1.14
C29	3.0	6.06	0.3569	1.39
C30	3.0	7.30	0.3358	1.51
C32	3.0	11.03	0.3432	1.75
C33	3.5	23.33	0.3535	2.31
C34	4.0	36.91	0.3358	2.77
C35	5.0	58.67	0.5001	3.05

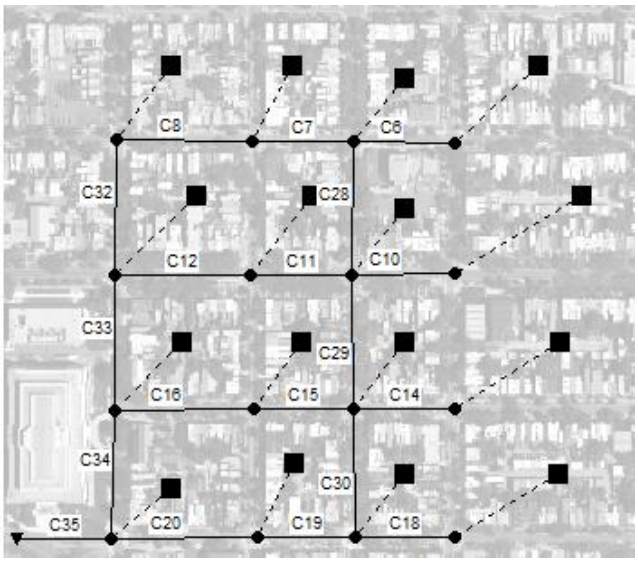

Figure 3-11. Pipe network with labeled pipes for SWMM model of 16 square blocks on Capitol Hill.

3.3.3.2 *Pipe Sizing Iterations*

The pipe sizing process described above must be iterated several times to develop accurate sizing for all the pipes in the system for the 10-yr rainfall event. The required pipe sizes indicated in Table 3-6 were based on peak flows in each pipe that were determined from initial estimates of the pipe sizes. In cases where the required pipe size calculated was smaller than the initial estimate, the capacity and possibly the peak flow will become smaller as well, which may further decrease the required pipe size. The opposite is also true, that as these pipes are increased in size, and therefore capacity, they will experience higher peak flows which may require a further increase in size. Additionally, each pipe influences the whole network. So even when only a few pipes are adjusted in size, this can affect the flow patterns of the entire network, thus requiring other pipes to be adjusted that were initially under or over capacity.

3.3.3.3 *Pipe Design Example*

A simple pipe network for a small section of the watershed was used for the purpose of demonstrating the pipe design method (see Figure 3-12). The pipes are assumed to be parallel to the streets. Once configured spatially, the pipes needed to be sized to adequately pass the NRCS Type II, 10-yr, 24-hr rainfall event without causing ponding at the inlet. Pipe sizing is typically an iterative process and for this simple case three iterations were required. The process of sizing the pipes in a pipe network can be described as follows:

1. Assume initial pipe sizes.
2. Simulate NRCS 10-yr, 24-hr rainfall over subwatershed in SWMM model.
3. Record peak flows in each pipe.
4. Calculate required pipe size from peak flow using Equation 3.2 ($D = 1.333(Qn)^{3/8}S^{-3/16}$).
5. Round calculated pipe sizes to next largest commercially available pipe size.
6. Repeat steps 2 through 5 until the process converges to the pipe sizes.

The process outlined above was used to size the pipes for the example SWMM model shown in Figure 3-12. The commercially available pipe sizes used for this design process are indicated in Table 3-7 (ACPA, 1974). The pipe diameters were determined using Equation 3.2 and implementing a minimum pipe size requirement of 1.5-ft (DDOT 2009). Three iterations were required for the pipe sizes to converge (see Table 3-8). This same process can be followed to design pipe sizes for larger pipe networks, but a larger number of iterations may generally be required.

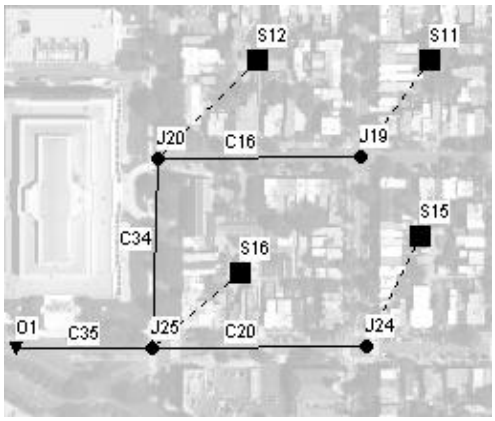

Figure 3-12. Pipe and street channel layout of pipe design example SWMM model.

Table 3-7. Commercially available concrete drainage pipe sizes.

feet	inches	feet	inches	feet	inches
1.50	18	4.00	48	8.00	96
1.75	21	4.50	54	8.50	102
2.00	24	5.00	60	9.00	108
2.25	27	5.50	66	9.50	114
2.50	30	6.00	72	10.00	120
2.75	33	6.50	78	10.50	126
3.00	36	7.00	84	11.00	132
3.50	42	7.50	90	11.50	138
				12.00	144

Table 3-8. Pipe sizing calculations for each iteration.

		Iteration 1			Iteration 2			Iteration 3		
Pipe IDs	Initial D (ft)	Peak flow (cfs)	Req D (ft)	New D (ft)	Peak flow (cfs)	Req D (ft)	New D (ft)	Peak flow (cfs)	Req D (ft)	New D (ft)
C16	1.5	8.56	1.59	1.75	10.7	1.73	1.75	12.43	1.83	2.00
C20	1.5	7.37	1.50	1.75	9.45	1.65	1.75	9.72	1.66	1.75
C34	2	18.06	2.10	2.25	23.88	2.33	2.50	27.12	2.45	2.50
C35	2.5	37.01	2.57	2.75	47.14	2.81	3.00	50.05	2.88	3.00

3.3.4 Adding Street Channels

In the design of stormwater drainage systems, street channels are often treated as part of the expected conveyance system to drain runoff. Roadways are often inundated during storms of return periods higher than those used for designing the pipe system. In fact,

roadways are designed according to specific criteria of roadway width, curb height, cross-slope, etc., all of which influence the way that runoff will flow along a section of roadway. For Washington, DC, these design criteria are determined and maintained by the District Department of Transportation, or DDOT. The policies that specify the design criteria can differ depending on state and local requirements. Regional or local restrictions also govern the level of flow through street channels that is acceptable. Therefore, in order to adequately represent the system, street channels needed to be added to the SWMM model, resulting in a dual drainage system.

Representing a street channel in SWMM requires the dimensions of the cross-section of the roadway. For the small watershed being modeled in this example, all of the street channels were treated as having the same cross-sectional geometry, as they are all urban residential streets. If the roadway types were not uniform, it would be necessary to define specific cross-sections to represent each roadway. For the analysis herein, the roadway cross-section shown in Figure 3-13 was used.

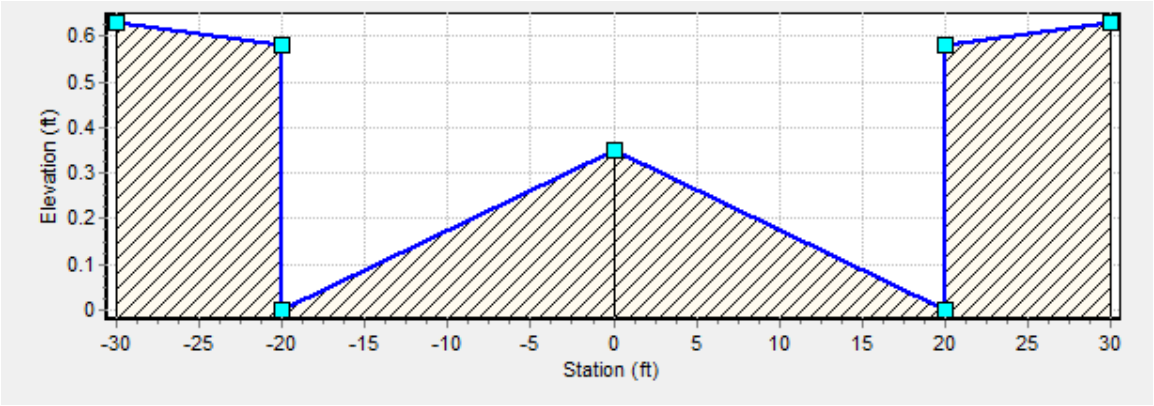

Figure 3-13. Cross-section geometry for an urban residential street in Washington, DC.

The street channels were then added to the SWMM model and simulations were performed for the 2-, 10-, 100-, and 200-yr rainfall events. It should be noted that on the

map (see Figure 3-12) the street channels (C41, C42, and C43) are not drawn as straight lines in order to visually distinguish them from the pipe segments that are on the same path. They do, however, have the same lengths as the corresponding pipe segments. The peak flows that result from these analyses for each pipe and street channel are indicated in Figure 3-14. The results show that flow in the street channels did not occur for the 2- and 10-yr storms. This was expected as the pipes were designed with capacity to pass the 10-yr storm. However, for the 100- and 200-yr storms, the pipe system alone was not adequate to carry the total discharge.

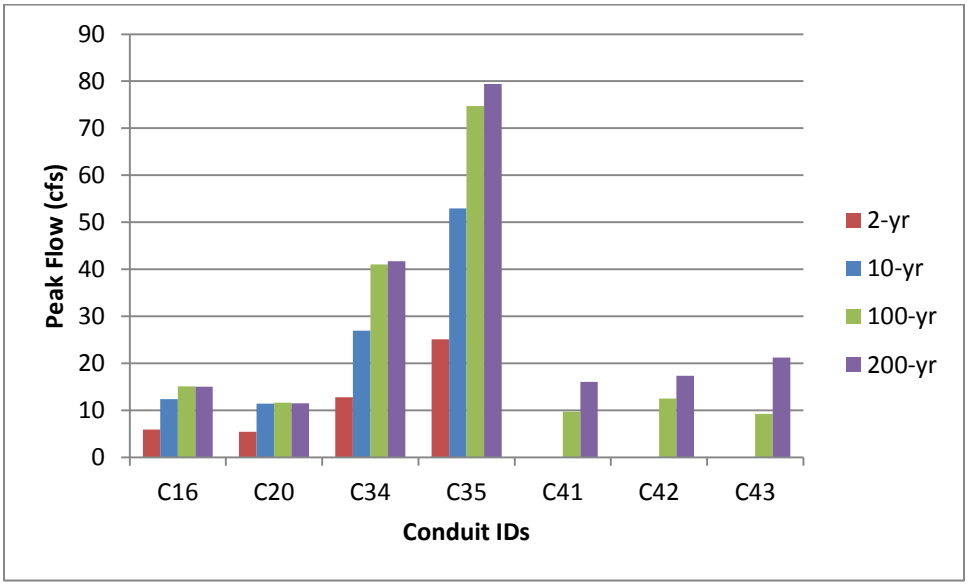

Figure 3-14. Peak flows in each pipe and street channel for various return period rainfall events.

In addition to the flowrates in the street channels, it is important to know the maximum depth of ponded water in the street. The depth will indicate when a roadway is not passable for transportation or when the adjacent buildings can expect to be flooded. The depths of flow in the street channels for the 24-hr, 200-yr storm are indicated in Figure 3-15. For all three street channels (link C41, C42, and C43) the water depth exceeded the crown of the street (0.35 ft) at the peak of the storm. However, only in the

case of C43 did the water reach a depth of 0.58 ft and overtop the curb. The depth at which C43 plateaus coincides with the maximum depth of the street channel, or the edge of the sidewalk. Flooding at this level would cause the roadway to be closed to traffic and flooding of adjacent buildings, resulting in potentially significant economic damages.

The plateaued peak depth of street channel C43 in Figure 3-15 indicates the times when the street and sidewalk were submerged, though it does not record any depth beyond that level of 0.63-ft for which the street channel was defined. Therefore, a new street cross section was defined with an artificial barrier rising vertically at the boundary of the sidewalk. This was to allow the volume of water beyond the edge of the sidewalk to be recorded so that the effect of that volume of water without the artificial barrier could later be assessed. This alternate street cross-section is shown in Figure 3-16, and the resulting flow depths from using this street cross-section and the same 200-yr storm

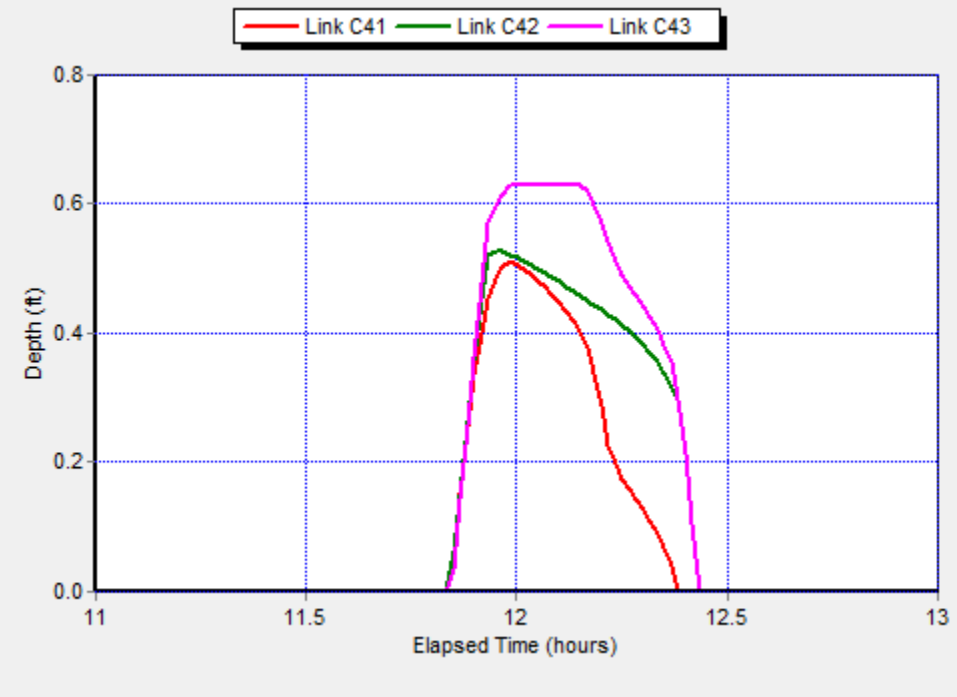

Figure 3-15. Flow depth in street channels during the central 2 hours of a 24-hr, 200-yr storm.

are shown in Figure 3-17. With the flow restricted to the dimensions of this alternate street cross-section, the maximum flow depths of C42 and C43 increased from 0.52 and 0.63 ft to 1.05 and 1.14 ft respectively. Any depth above the sidewalk (0.63 ft) can be considered flooding volume. This flooding volume will be important to determine the flood depth and damages associated with structures adjacent to the sidewalk.

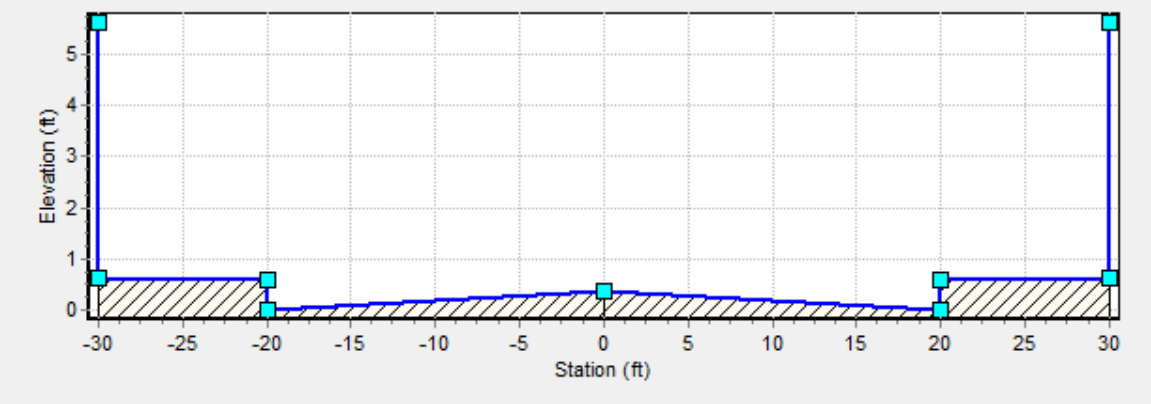

Figure 3-16. Alternate street channel cross-section with artificial barrier at edge of sidewalk used to keep track of water volume.

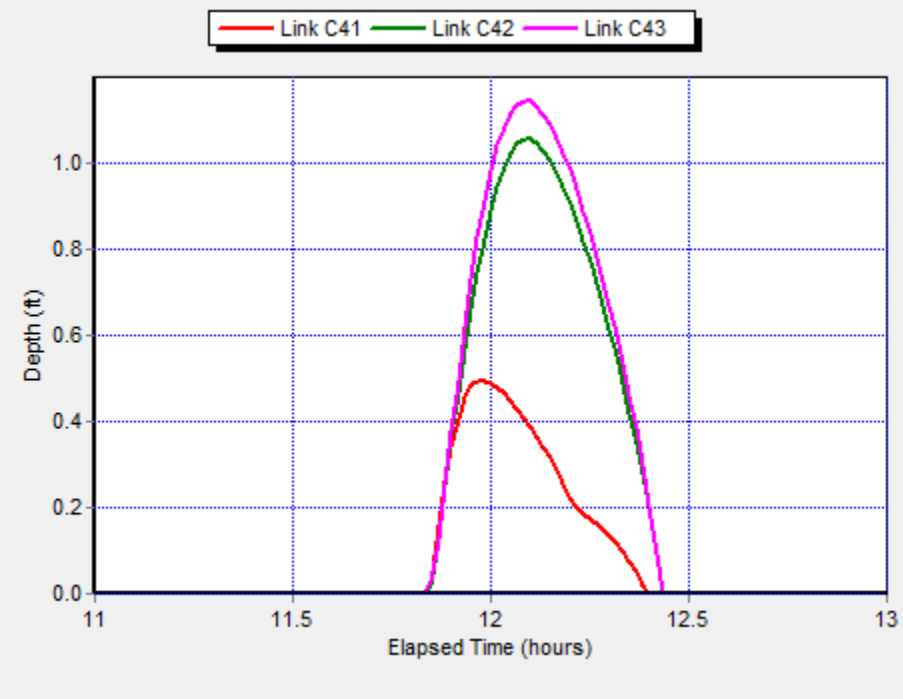

Figure 3-17. Flow depth in street channels for central 2 hours of a 200-yr, 24-hr storm using alternate street channel cross-sections.

3.3.4.1 *Assessment of Flow Depth Rationality*

In any modeling scenario, it is good practice to regularly assess the rationality of the outputs. In this case, it was unclear where along the length of each conduit the reported maximum depths of the SWMM output were located. For further clarification, a water elevation profile for a 200-yr storm from inlet J19 to inlet J25 by way of street channels C41 and C43 was created, as shown in Figure 3-18. This profile indicates that the water depth is neither constant along the length of the street channels, nor does it form a flat, constant elevation water surface that might be expected. The model did produce a constant elevation water surface when the outlet was removed and all of the runoff continued to pool at inlet J25 (see Figure 3-19). Therefore, the SWMM model did appear to operating realistically. The reason the water surface elevation was sloped in the first example is because there continued to be significant outflow from J25, comparable in magnitude to (though somewhat less than) the inflow.

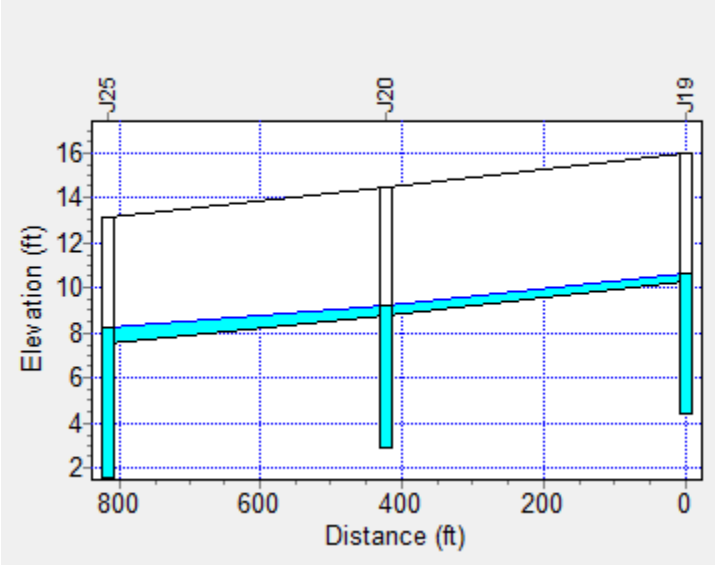

Figure 3-18. Water elevation profile for street channels C41 and C43 during the peak of a 200-yr event with an outlet.

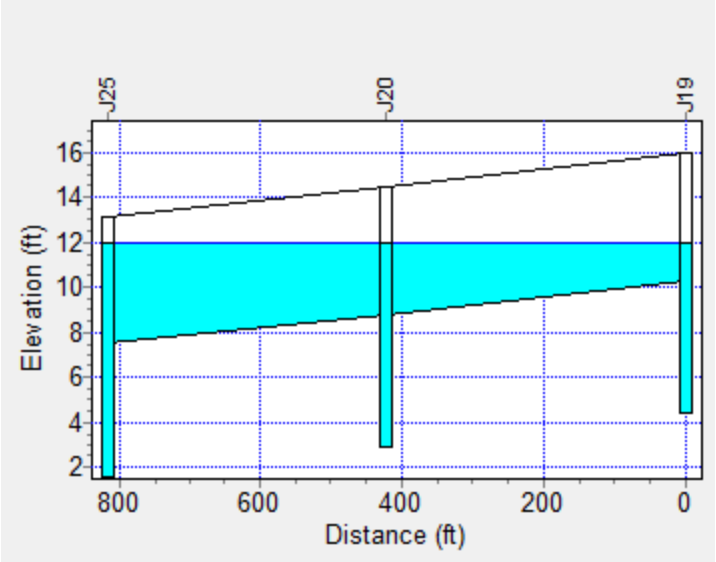

Figure 3-19. Water elevation profile for street channels C41 and C43 during the peak of a 200-yr event without an outlet.

3.4 SENSITIVITY ANALYSES

Having designed the pipe network and street channels according to local regulations, the next step was to perform sensitivity analyses of various rainfall, watershed, and pipe network characteristics. The effect of the size of time increment used to define the NRCS 24-hr rainfall was evaluated. The sensitivity of watershed characteristics were analyzed by simulating the 2-, 10-, 100-, and 200-yr storm events while varying the watershed slope, infiltration, imperviousness, depression storage, overland flow width, and Manning's n values. Manning's n values were also varied for the pipe network for each storm frequency. Various components of drainage network efficiency were also analyzed.

3.4.1 Sensitivity of 24-hr Rainfall Time Increment

If the reporting time interval of a rainfall distribution has a significant influence on computed volumes and peak runoffs for a particular storm event, then failure to recognize

this could lead to over- or under-design. The NRCS rainfall distributions are commonly reported in tables, providing the dimensionless cumulative rainfall depths at 30-min intervals. While this interval may be a convenient form of reporting the rainfall distributions, some rainfall characteristics are not evident when a large time interval is used. The duration of the peak of the rainfall event is of particular concern because using a 30-min time interval truncates the peak of the storm that would be evident for a shorter duration, e.g., 2 minutes.

To ensure that design discharges reflected rainfall characteristics of the region, the computation interval needed to be short relative to the travel time of the design flow rates. In order to evaluate the effect of the time interval on runoff and pipe flow patterns, a simple SWMM model was developed that used the NRCS Type II, 10-yr, 24-hr storm reported at 30-, 15-, and 2-min time intervals (the storm ordinates are given in Appendix A). The resulting peak flows for each pipe are shown in Figure 3-20. The resulting peak discharge increases with decreasing time interval. Use of a large interval (e.g., 30-min) averages the intensities of shorter durations. This reduces the corresponding peaks. The 2-min time interval storm introduces a higher peak intensity of rainfall into the system, resulting in somewhat higher peak flows in each pipe.

Recognizing that the different time increments used produced somewhat different results, it was important to evaluate the significance of those differences. The 2-min interval was assumed to be the most precise; therefore, the calculated errors and relative errors in peak flow were based on the assumption that the 2-min interval produced the "correct" peak flows (see Table 3-9). Relative error is defined as the prediction error divided by the actual value of the variable being predicted and is given as a percentage.

In this case, the relative errors in peak flow between the 2- and 15-min time intervals ranged from -1.0 to -2.5 percent. The relative errors in peak flow between the 2- and 30-min time intervals ranged from -5.5 to -9.0 percent. The negative percentages indicate the larger time intervals always produced lower peak flows. The process of designing pipe sizes is based on peak flow predictions. If using a time interval of 30-min under-predicts the peak flows by anywhere from five to ten percent, this could cause some of the pipes to be under-designed. Therefore, it is recommended that the 2-min time interval be used, as it was for all subsequent simulations in this study.

Table 3-9. The peak flows for each pipe and each time increment are reported. Assuming the 2-min interval to be the most precise, the errors and relative errors were determined by comparing the 15- and 30-min peak flows against the 2-min peak flows.

	Peak flow (cfs)			Error (cfs)		Relative Error (%)	
Pipe ID	**2-min**	**15-min**	**30-min**	**15-min**	**30-min**	**15-min**	**30-min**
C16	8.56	8.35	7.84	-0.21	-0.72	-0.0245	-0.0841
C20	7.37	7.16	6.88	-0.21	-0.49	-0.0285	-0.0665
C34	18.06	17.74	17.06	-0.32	-1.00	-0.0177	-0.0554
C35	37.01	36.63	33.68	-0.38	-3.33	-0.0103	-0.0900

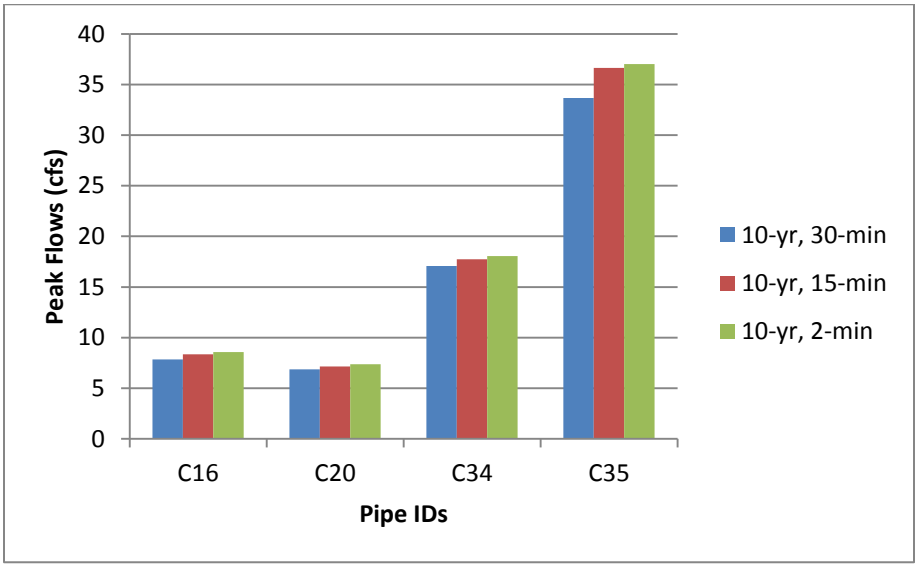

Figure 3-20. Peak flows in each pipe for the NRCS Type II, 24-hr, 10-yr storm event defined at 30-, 15-, and 2-min time increments.

3.4.2 Sensitivity of Watershed Slope

Watershed slope influences the amount and timing of runoff from a storm event, both of which are factors that may play a large role in stormwater management. The average slope of each subcatchment in the SWMM model was originally assumed to be 0.5 percent. This assumed slope was used to design the pipes and street channels. The sensitivity of the existing model was computed using changes in the average slope from 0.5 percent to 1 and 2 percent. The results for the 1 and 2 percent slopes are given in Figure 3-21 and Figure 3-22 and the differences and relative differences from the 0.5 percent slope are reported in Table 3-10.

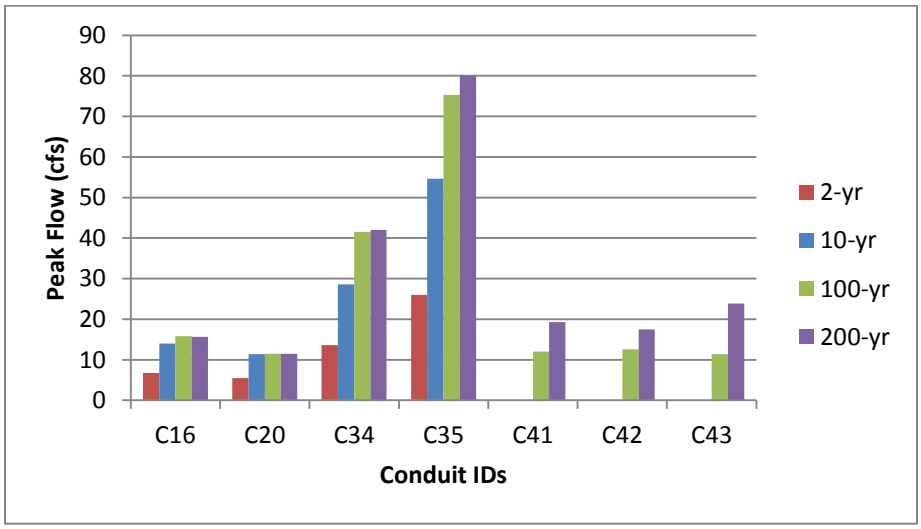

Figure 3-21. Peak flows for each conduit and each storm frequency for an average watershed slope of 1%.

Comparisons of Figure 3-20 to Figure 3-22 indicate a general trend of increasing peak flows for pipes and street channels as the watershed slope increases. This was expected because higher slopes not only cause excess rainfall from a storm event to drain run off more rapidly, but also allow less time for infiltration to occur, which increases the total volume of runoff. Both of these effects are pronounced with higher intensity rainfall

events, which explains why more dramatic differences occur for the 100- and 200-yr storms.

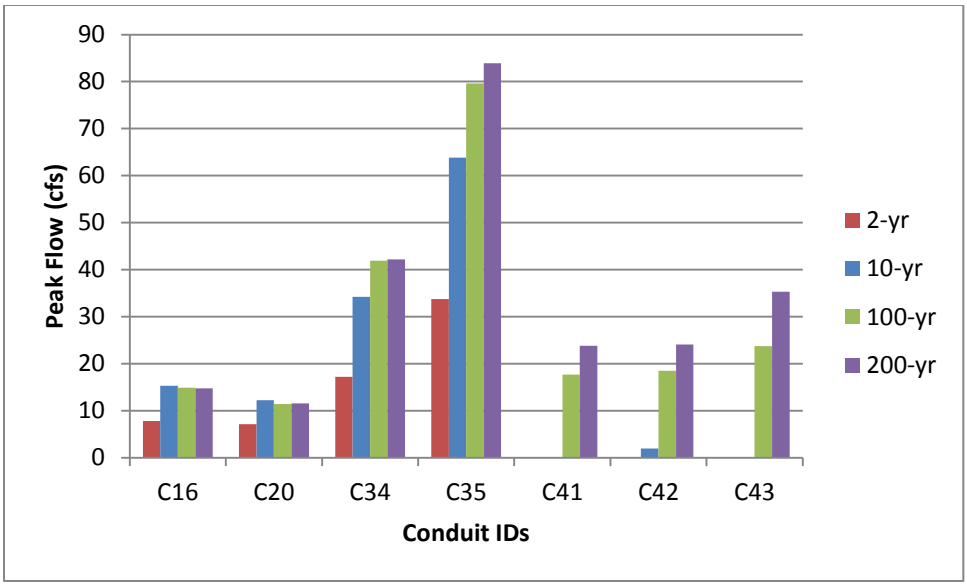

Figure 3-22. Peak flows for each conduit and each storm frequency for an average watershed slope of 2%.

A consideration of the relative differences between the peak flows of the 0.5 percent slope and those for the 1 and 2 percent slopes revealed the sensitivity of the model to watershed slope. Only the results for the 100- and 200-yr events were reported in Table 3-10 because they showed more significant differences and were the only storm frequencies where flow occurred in the street channels (C41, C42, and C43). Because the pipes are closed conduits, once their capacity is reached and flow accumulated in the streets, the peak flows changed very little even with increased runoff. However, for the 100- and 200-yr events the peak flow for street channel C43 increased with a slope change from 0.5 to 2 percent by more than 14 cfs. This corresponds to a 156 and 67 percent relative difference for the 100- and 200-yr events, respectively. The conclusion

from these results is that the model is highly sensitive to changes in watershed slope, and considerably more so for large return period storm events.

Table 3-10. Peak flows for each conduit for average watershed slopes of 0.5, 1, and 2%. Differences and relative differences for 1 and 2% slopes from 0.5% slope are reported.

	Conduit	slope = 0.5%	slope = 1%	slope = 2%	diff 1	diff 2	relative diff 1	relative diff 2
100-yr	C16	15.11	15.84	14.85	0.73	-0.26	4.8%	-1.7%
	C20	11.59	11.47	11.42	-0.12	-0.17	-1.0%	-1.5%
	C34	41.00	41.49	41.90	0.49	0.90	1.2%	2.2%
	C35	74.73	75.26	79.62	0.53	4.89	0.7%	6.5%
	C41	9.70	11.99	17.68	2.29	7.98	23.6%	82.3%
	C42	12.49	12.55	18.47	0.06	5.98	0.5%	47.9%
	C43	9.25	11.37	23.71	2.12	14.46	22.9%	156.3%
200-yr	C16	15.03	15.65	14.72	0.62	-0.31	4.1%	-2.1%
	C20	11.50	11.50	11.57	0.00	0.07	0.0%	0.6%
	C34	41.71	42.01	42.16	0.30	0.45	0.7%	1.1%
	C35	79.40	80.01	83.91	0.61	4.51	0.8%	5.7%
	C41	16.04	19.25	23.77	3.21	7.73	20.0%	48.2%
	C42	17.34	17.43	24.05	0.09	6.71	0.5%	38.7%
	C43	21.21	23.88	35.32	2.67	14.11	12.6%	66.5%

3.4.3 Sensitivity of Infiltration Parameters

Infiltration is one of the physical processes that represent a primary component of SWMM's conceptual model (see Figure 2-1). Depending on the characteristics of a watershed, infiltration parameters can have a significant bearing on the runoff process and potential for flooding. Using Horton's infiltration equation (see Equation 2.5) for non-impervious areas, the effect of various infiltration parameters on the depth of flow in the street channels was evaluated. Typical values for the initial and final infiltration rates for three general soil types (sandy, loam, and clay) were used (Rawls et al., 1982). In addition, the decay constant was varied from 2 to 7 (hr^{-1}), which is the range of typical values indicated in the SWMM reference material. Analyses were made with the 200-yr rainfall and an assumed 90 percent imperviousness in order to evaluate the potential

influence of infiltration during extreme events. The variations of the infiltration parameters for each analysis, along with the results, are given in Table 3-11.

Table 3-11. Varied values of Horton's infiltration parameters with the maximum depth of street channel C43 for each simulation reported. Soil type "default" represents the default infiltration rate value used by SWMM. These default values were used while evaluating the sensitivity of K.

Soil Type	Initial infiltration rate, f_o (in./hr)	Final infiltration rate, f_c (in./hr)	Decay constant, K (hr^{-1})	Max. depth for C43 (ft)
Default	3.00	0.50	2	0.71
Default	3.00	0.50	4	0.71
Default	3.00	0.50	7	0.71
Sandy	5.00	4.74	4	0.63
Loam	3.00	0.13	4	0.74
Clay	1.00	0.01	4	0.73

As infiltration is one of the primary physical processes involved in rainfall-runoff modeling, it is important to understand the effects of each of the infiltration parameters on the overall model output. The infiltration rate decayed from the initial to the final rate within the first two hours of the storm for all of the decay constants tested. When the final infiltration rate is high, then significant volumes of water will continue to infiltrate throughout the duration of the 24-hr storm. Due to this effect, the peak depth was reduced for the sandy soil 1.32 inches (i.e., from 0.74 to 0.63 ft, the same elevation as the sidewalk) (see Figure 3-23). It should be noted that the infiltration parameters become more important in less impervious areas. However, in highly impervious urban areas, and during large return period and long duration storms, flow depths in street channels were not significantly sensitive to changes in infiltration parameters. Within the study site the soil was identified using GIS data as predominantly of the urban land – sassafras classification, indicative of a blend of many soil types. To best represent this soil type, the infiltration parameters of loam soils were used throughout this study.

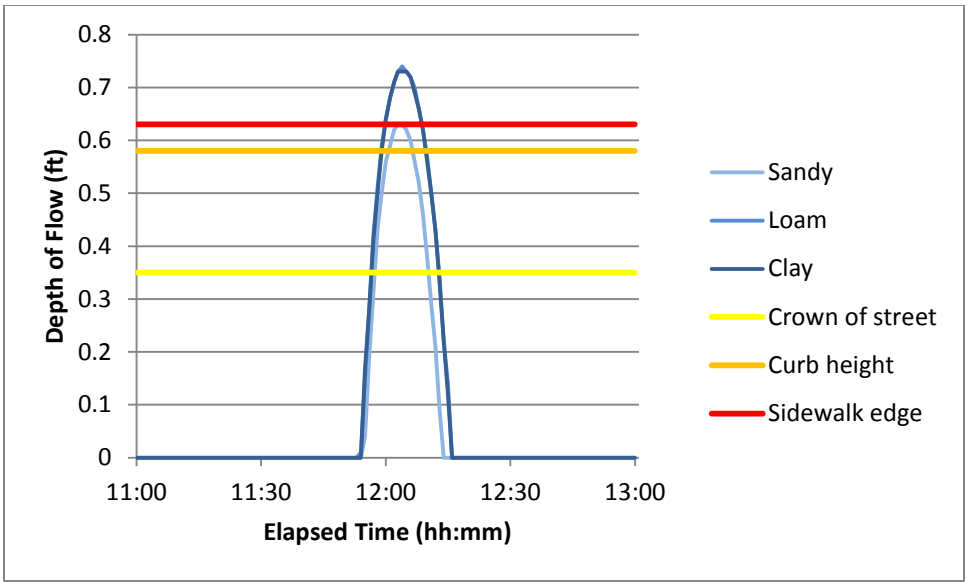

Figure 3-23. Flow depths in street channel C43 during a 200-yr rainfall with minimum and maximum infiltration rates representing sandy, loam, and clay soils.

3.4.4 Sensitivity of Imperviousness

Imperviousness has a direct influence on both the magnitude and timing of runoff from a rainfall event. The magnitude of runoff is influenced because impervious surfaces prevent water from infiltrating into the ground. Therefore, greater imperviousness leads to greater surface runoff volumes. The timing of runoff is also influenced because impervious surfaces are generally smoother than pervious surfaces, allowing water to flow across them more rapidly. Performing simulations of the runoff and routing of the same site using 50, 70, and 90 percent imperviousness, with all other inputs held constant, allowed the influence of imperviousness on this system to be quantified. The resulting flow depths for street channel C43 are shown in Figure 3-24. The peak depth with 90 percent imperviousness was 0.73 ft. Relative to this depth, the simulations with 70 and 50 percent imperviousness reduced the peak depths by 15 and 49 percent to 0.62 and 0.37-ft, respectively. When the imperviousness was changed by 20 percent increments, the difference in flow depths was significant. However, analyses for

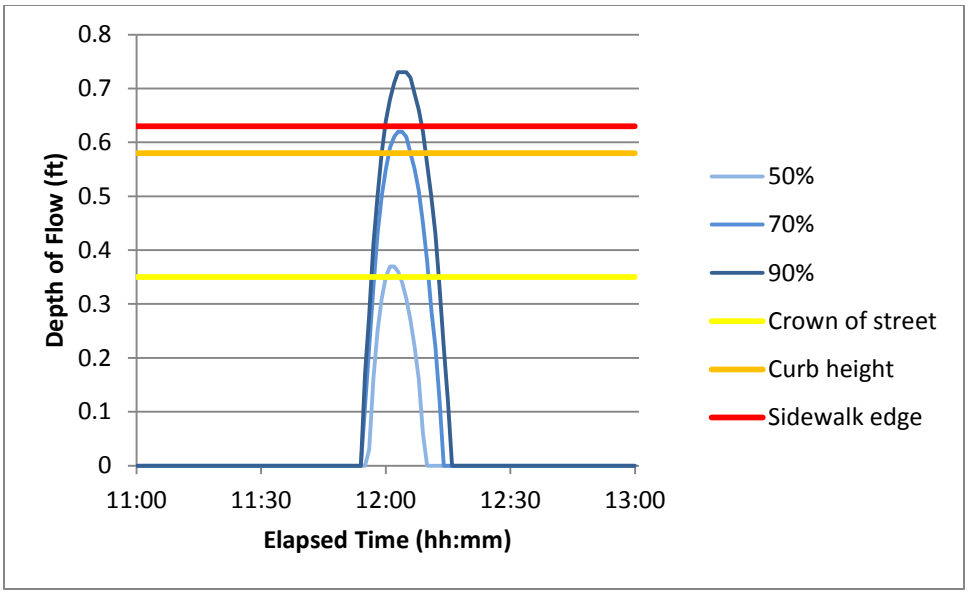

Figure 3-24. Flow depths of street channel C43 during a 200-yr event with various degrees of imperviousness.

impervious values of 71 to 75 percent were also performed to evaluate the influence of smaller incremental changes in imperviousness. These results are given in Table 3-12. The effect of a one percent increase in imperviousness under these particular conditions caused a nearly consistent 0.01-ft increase in the peak depth. A least-squares linear regression line fit to this data had a slope of 0.0094 feet of flood depth per percent imperviousness and a correlation coefficient of 0.91, indicating a strong relationship between percent imperviousness and flood depth.

The two analyses performed suggest that peak depths are moderately sensitive to changes in imperviousness. An error of 20 percent in estimating imperviousness will alter the resulting flows significantly. However, an error within five percent will not likely cause a significant difference in flood depths. If imperviousness values are not available for a particular site, care should be taken to estimate these values to within a five percent margin of error. It should be noted that imperviousness and infiltration parameters have a significant bearing on each other. For example, if the soil type dictates

very low infiltration rates, then increases in imperviousness may not significantly influence the overall hydrologic response because the difference in runoff patterns on the pervious and impervious areas in minor. The opposite is also true, i.e., with more pervious area the infiltration parameters will take on greater importance. Understanding the interaction between these inputs with each other and the overall outputs will help in determining the level of accuracy required for specific modeling purposes.

Table 3-12. Peak depths in street channel C43 for simulations of a 200-yr event with imperviousness ranging from 70 to 75 percent.

Imperviousness (%)	70	71	72	73	74	75
Peak Depth (ft)	0.62	0.63	0.62	0.64	0.65	0.67

3.4.5 Sensitivity of Depression Storage

Depression storage is an important enough factor of runoff patterns to be included in most runoff models, including SWMM. It represents the volume of water that can be stored in localized depressions on the runoff surface. Different values can be input into SWMM for impervious and pervious areas. Typical values for impervious and pervious areas range from 0.05 to 0.10 in. and 0.10 to 0.30 in., respectively (ASCE 1992). The default value in SWMM for both is 0.05 in. For these analyses, both the impervious and pervious depression storage values were varied together from 0.05 to 0.10 to 0.50 in. for the 200-yr storm. In this case, the effect on peak depths was negligible.

As with the infiltration parameters and imperviousness, the effect of depression storage would be greater for smaller and shorter storms. This is because the storage volume would represent a larger percentage of the total rainfall volume and it would be less likely to be filled before the peak of the storm. The 200-yr storm has a total depth of 9.83 in., of which the largest depression storage value used only represented about five

percent. Even a depression storage of five percent of the total rainfall depth could be significant for a shorter duration and smaller return period storm; however, for a 24-hr storm, the storage capacity was already filled well before the time of the peak of the storm. Therefore, under the conditions pertinent to pluvial flooding, peak depths have low sensitivity to depression storage. The remainder of this study used the SWMM default depression storage values of 0.05 in. for both pervious and impervious areas.

3.4.6 Sensitivity of Overland Flow Width

Overland flow width is a parameter used in SWMM to define the average width along the longest overland flow path of a subcatchment. Overland flow is defined within SWMM as the flow regime that is characterized by relatively uniform and shallow depths before channelization begins (EPA 2004). This is more commonly termed sheet flow. Instead of directly inputting the length of the longest overland flow path into SWMM, this value is implied by inputting the overland flow width. In other words, using a small overland flow width implies a longer overland flow path which would result in slower runoff. Therefore, the response time of a subcatchment can be expected to decrease when the overland flow width increases. Furthermore, shorter response times caused by increasing overland flow widths leads to a greater potential for significant drainage and flooding problems.

The sensitivity of the flood depths in street channel C43 to overland flow width was evaluated by making simulations with overland flow widths of 50, 100, and 200 ft. An overland flow width of 50 ft was used here to provide the base flood depth against which other simulation depths were compared. The results of these simulations are given in Figure 3-25. Treating the depth of 0.73-ft produced by the 50-ft overland flow width as

the base depth, the depth increased 44 percent to 1.05-ft and 77 percent to 1.29-ft for the 100 and 200-ft overland flow widths, respectively. The high sensitivity of the peak depth to the overland flow width is evident both graphically and statistically. Therefore, it is important to accurately estimate the overland flow widths in order to develop reliable flood depths. A basic method of estimating the overland flow width by using the average width of the streets within the subcatchment was used for this analysis. This approach assumes that overland flow in densely urban areas will largely follow the roadways. For this study, an overland flow width of 50 ft was used, representing the width of many of the residential streets within the study site.

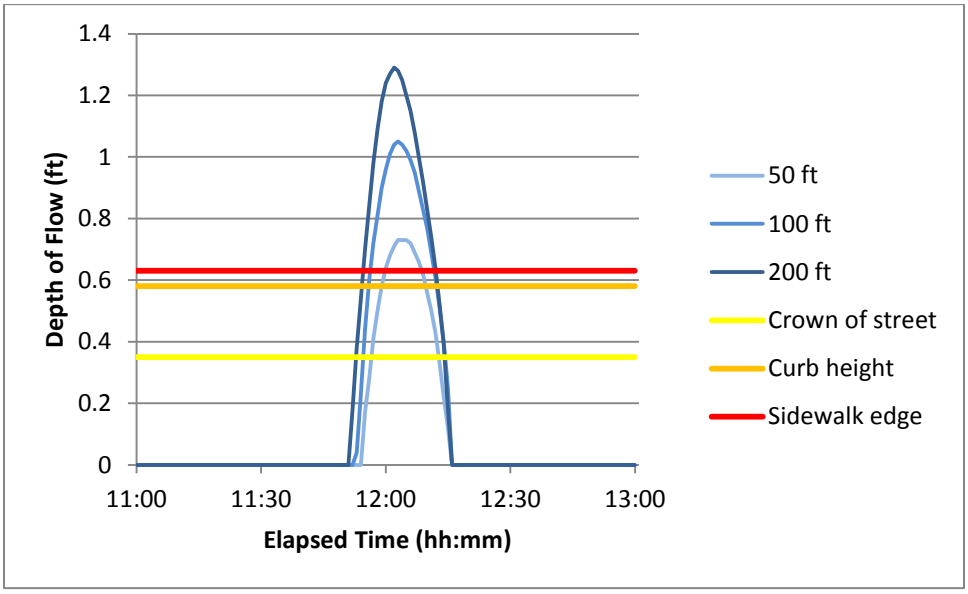

Figure 3-25. Flow depths in street channel C43 during a 200-yr, 24-hr storm for various average overland flow widths.

3.4.7 Sensitivity of Roughness Coefficients

Several forms of Manning's equation are used in SWMM for various components of the rainfall-runoff and routing processes. A roughness coefficient must be input in each case. A separate sensitivity analysis was conducted for each roughness coefficient

associated with the runoff portion of the model (pervious and impervious areas) and the routing portion of the model (pipes and street channels). An overall sensitivity to roughness inputs was then estimated from the individual analyses of the four roughness coefficients.

3.4.7.1 *Roughness Coefficient of Impervious Areas*

First, the roughness coefficient for impervious areas of the runoff portion of the model was analyzed. The roughness coefficients for typical impervious surfaces (asphalt, concrete, etc.) range from 0.011 to 0.015 (McCuen et al. 2002). In order to evaluate the flow depth sensitivity to this roughness coefficient, analyses were conducted with impervious area roughness coefficients of 0.011, 0.013, and 0.015. A 200-yr, 24-hr event was used with 90 percent imperviousness and a roughness coefficient for pervious areas of 0.05 for each simulation. The roughness coefficient of 0.05 was the lowest value of typical pervious surfaces, which represents bare soils. It was expected that increasing the impervious area roughness coefficient would reduce the peak depth by increasing the response time of the subcatchment. The results confirm this expectation and are shown in Figure 3-26. The peak depths for impervious area roughness coefficients of 0.011, 0.013, and 0.015 were 1.10, 1.01, and 0.92-ft, respectively. Each 0.002 increase in the roughness coefficient caused an eight percent decrease in peak depth, or 0.09-ft. The relative sensitivity of this roughness coefficient under these conditions is -0.45.

3.4.7.2 *Roughness Coefficient of Pervious Areas*

Next, the roughness coefficient for the pervious areas of the runoff portion of the model was analyzed. The roughness coefficient for typical pervious surfaces in urban

areas (bare soils, grass, etc.) ranges from 0.05 to 0.41 (McCuen et al. 2002). The roughness coefficients for the pervious areas were varied using 0.05, 0.17, 0.29, and 0.41 for separate simulations. Again, a 200-yr, 24-hr event was used with 90 percent imperviousness. The roughness coefficient for the impervious areas was held constant at 0.011 for each of these simulations. It was again expected that increases in the pervious area roughness coefficient would decrease the peak depths because they would slow the runoff process, allowing more time for infiltration to occur and for arriving runoff to be drained through the sewer system.

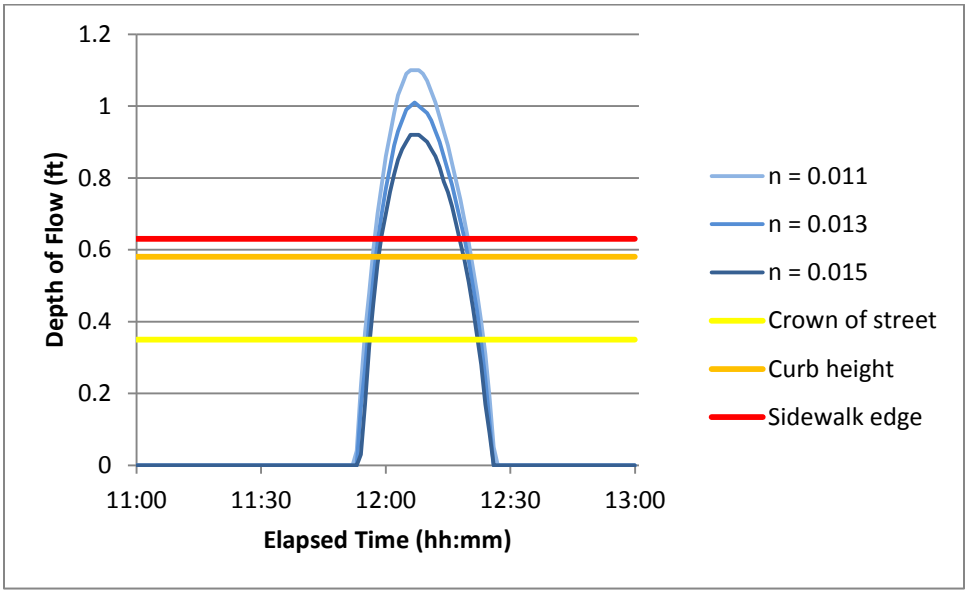

Figure 3-26. Flow depths in street channel C43 for a 200-yr, 24-hr event with impervious area roughness coefficients of 0.011, 0.013, and 0.015.

The results of the pervious area roughness coefficient simulations agreed with expectations. The simulations with roughness coefficients of 0.05, 0.17, 0.29, and 0.41 produced peak depths of 1.10, 1.04, 0.98, and 0.97-ft, respectively (see Figure 3-27). Each 0.12 increase in the roughness coefficient reduced the peak depth between 0.06 and 0.01-ft. This indicates that the peak depth has a lower sensitivity to the roughness

coefficient of the pervious areas than of the impervious areas. This is due, in part, to the higher percentage of impervious area used in this analysis. Additionally, it appears that the sensitivity of the peak depths to changes in the pervious area roughness coefficient decreases when the roughness coefficient becomes large. This is evidenced by the change of only 0.01-ft in the peak depth when the roughness coefficient was changed from 0.29 to 0.41 as compared to the change of 0.06-ft in peak depth when the roughness coefficient was changed from 0.17 to 0.29. The relative sensitivity of this roughness coefficient under these conditions is -0.02. Though still negative, this is a significantly smaller magnitude than the relative sensitivity for the impervious area roughness coefficient.

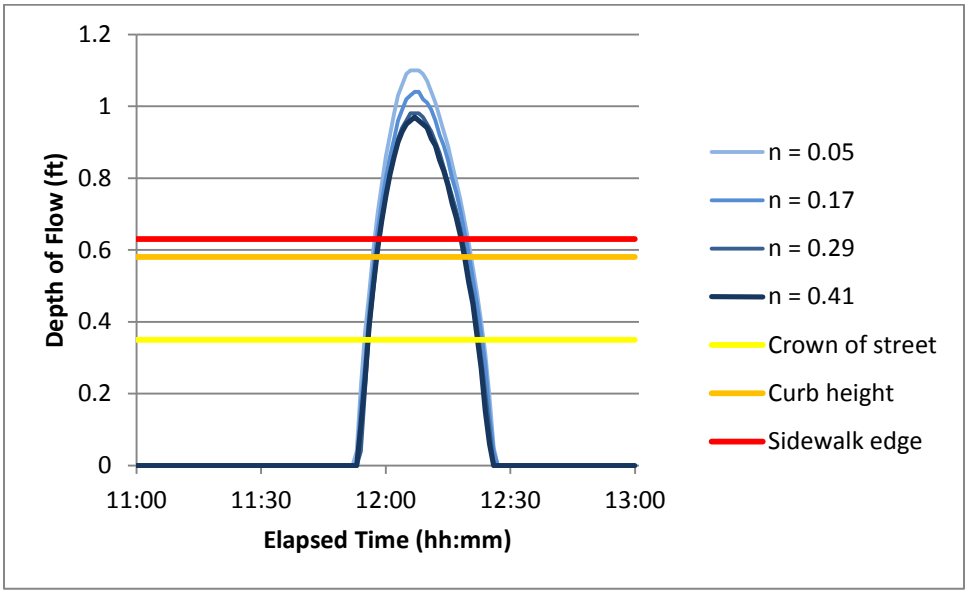

Figure 3-27. Flow depths of street channel C43 for a 200-yr, 24-hr storm with pervious area roughness coefficients of 0.05, 0.17, 0.29, and 0.41.

Roughness coefficients for both the impervious and pervious areas of each subcatchment should be selected based on local conditions. These coefficients may vary considerably across a study site. If so, this can be represented in SWMM by assigning

different roughness coefficients to each subcatchment. Depending on accuracy requirements, it may be appropriate to use an average roughness coefficient for the whole study site. The remainder of this study used impervious and pervious roughness coefficients of 0.011 and 0.15, representative of smooth asphalt and short grass, respectively.

3.4.7.3 *Roughness Coefficient of Pipes*

The next sensitivity analysis of roughness was focused on the roughness coefficients of the pipes in the routing portion of the model. Several common pipe materials (cast-iron, concrete, PVC) have been shown to have a range of roughness coefficients from 0.011 to 0.017 (ASCE 1982). To evaluate the sensitivity of this roughness coefficient, analyses were made with the coefficient set to 0.011, 0.014, and 0.017 using a 200-yr, 24-hr event with 90 percent imperviousness. The roughness coefficient for the street channels was held constant at 0.015. The results of these analyses are shown in Figure 3-28. Increasing the roughness coefficient of the pipes significantly increased the peak depths. Each 0.003 increase in the roughness coefficient increased the peak depth by about 0.27ft. Figure 3-28 also shows that increased roughness coefficients extended the duration of flooding as well. Both the increased peak depths and durations of flooding are the result of lower drainage capacities with higher roughness coefficients. The relative sensitivity of this roughness coefficient under these conditions is 1.53, which is significantly higher than the relative sensitivities of the impervious and pervious roughness coefficients.

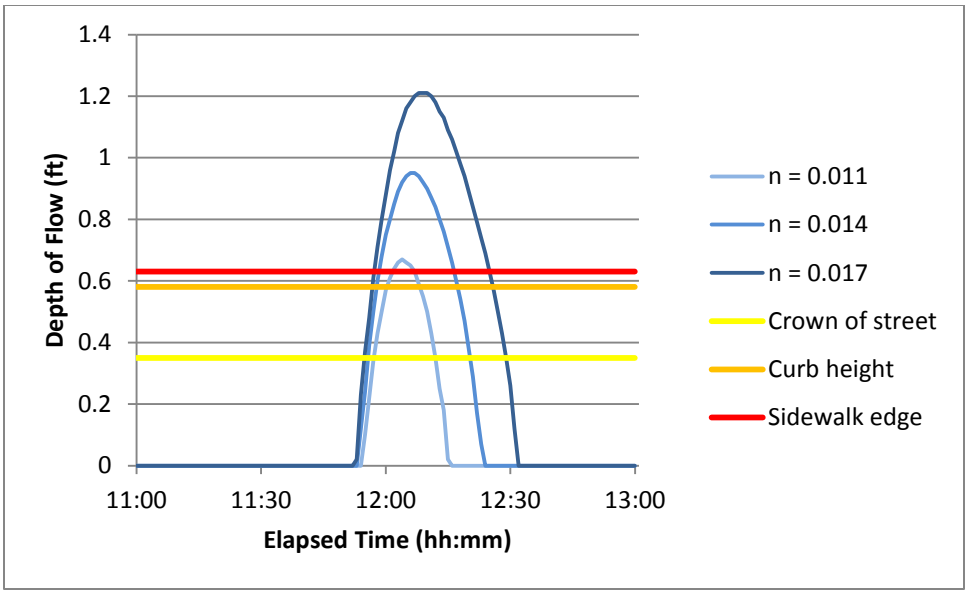

Figure 3-28. Flow depths of street channel C43 for a 200-yr, 24-hr storm with the roughness coefficient for the pipes set to 0.011, 0.014, and 0.017.

Due to the high relative sensitivity of the pipe roughness coefficient, this value should be selected carefully. Fortunately, roughness coefficients for different material pipes do not vary widely. It was assumed for this study that all pipes were either cast iron or concrete. Both materials have a reported range of roughness coefficients of 0.011 to 0.015 (ASCE 1982). The middle of this range, 0.013, was the selected roughness coefficient used throughout this study.

3.4.7.4 *Roughness Coefficient of Street Channels*

The final roughness coefficient sensitivity analysis focused on the street channel roughness coefficient. Asphalt or concrete open channel (street channel) roughness coefficients range from 0.011 to 0.020 (ASCE 1982). For this analysis the street channel roughness coefficient values of 0.011, 0.015, and 0.020 were assessed with all other inputs and parameters remaining the same. All three analyses resulted in the same peak depth of 0.9-ft. Therefore, the peak depths are not sensitive to changes in the street

channel roughness coefficients. However, this coefficient should still be selected based on local conditions. The street channel roughness coefficient selected for use throughout this study was 0.015, which is in the middle of the range of suggested values for both asphalt and concrete.

It should be noted that the impervious area of the runoff surface includes the street channels; however, the runoff over the impervious area and the flow along the street channels are modeled separately. Therefore, the roughness coefficient for the impervious area and the street channels are input separately. Because these two roughness coefficients represent similar characteristics their selected values should be similar as well.

The results of all of the analyses of roughness coefficients showed that the sensitivity of the different roughness coefficients varied significantly. The relative sensitivities of the different roughness coefficients are shown in Table 3-13. The highest sensitivities were for the pipe and impervious area roughness coefficients, while the relative sensitivities for the pervious area and street channel roughness coefficients were very low. Additionally, increasing roughness values of the pipes led to higher peak depths, which was the opposite trend observed with increasing roughness coefficients for the runoff surfaces. This occurs because higher roughness in pipes reduces the velocity and capacity of the each conduit allowing back-up and accumulation to occur more rapidly. Higher roughness coefficients on the runoff surfaces also reduce the velocity of flow, but this actually lowers the flooding potential by slowing the runoff arrival rate into the storm sewer network. This provides the storm sewer network more time to drain a

given volume of water. The worst case for stormwater management is when runoff arrives rapidly but drains slowly and is when flooding is most likely to occur.

Table 3-13. Absolute and relative sensitivities of peak flood depths along street channel C43 for the 200-yr, 24-hr storm to several types of roughness coefficients.

Type of roughness coefficient	Absolute sensitivity (ft)	Relative sensitivity
Impervious	-45.00	-0.45
Pervious	-0.50	-0.02
Pipes	93.33	1.53
Street channels	0.00	0.00

When selecting the different roughness values, a few guidelines are useful. First, when a range of values for a specific surface or material is published, it is best to use the central value of the suggested range unless the use of a different value can be adequately justified. Second, when taking into account several surfaces of different roughness, it is best to use a weighted average. Third, select roughness values carefully because flow depths can be sensitive to relatively small errors in roughness coefficients.

3.4.8 Pluvial Flooding on 8 December 2011

On the morning of December 8, 2011, following an evening of heavy rainfall, localized flooding was observed near the study region on Massachusetts Ave between 1st and 2nd St. in northwest Washington, DC (see Figure 3-29). From this event, the water level reached above the crown of the street, the curb, and the sidewalk with ponding on the lawn adjacent to the sidewalk. This may have been the result of several factors, one of which was undoubtedly a depression in the roadway, which created a low point in the middle of the block where the storm drains are located. Another factor that was contributing to the problem was that the inlets were at least partially clogged. This was

confirmed by a DC Water field technician. These observations led to an inquiry of the effect of drainage inefficiencies on the drainage network.

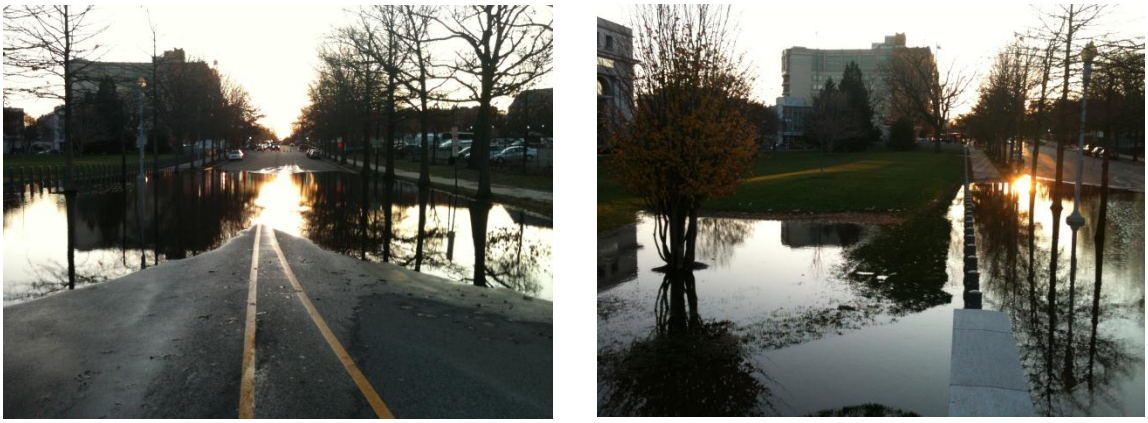

Figure 3-29. Localized flooding on the morning of 8 December 2011 along Massachusetts Avenue between 1st and 2nd Streets in northeast Washington, DC.

3.4.8.1 *Potential Inefficient Drainage Problems*

Even when a storm drainage system is designed for a certain frequency storm, if that frequency storm comes and the system is not operating at its original efficiency, then significant flooding could still occur. Three conditions representing reduced efficiency were modeled to evaluate their effects. The first condition was a localized depression, or sump condition, at an inlet. The depression would cause water to pool in the street channel when the capacity of the local pipes is exceeded. The second condition was to have an inundated outlet, causing all of the runoff to remain in the street system for the duration of the storm. The third condition would be if the inlet is clogged with trash or debris.

In order to model the first condition, the elevation of the outlet was raised creating a local depression at node J25. The elevation of the outlet invert was raised such that the slope of conduits on either side of J25 was a positive 0.5 percent. This local depression

allowed water to pool above the inlet until the pressure head was large enough to cause flow from the lower elevation inlet to the raised outlet. Hydrographs of the flow depths in the street channels for the central hours of the storm are given in Figure 3-30. Critical elevations such as the crown of the street, the height of the curb, and the edge of the sidewalk are indicated. With this condition in place, the 10-yr storm would cause overtopping of the sidewalk edges for two of the three street channels in this system. Having been designed for the 10-yr storm, under efficient conditions the depths of the 10-yr storm simulation never reached the crown of the street. However, with this local depression, even the 2-yr storm reached near the crown of the street, thus inundating most of the roadway. The 200-yr storm reached a peak depth of over 1.8-ft for street channel C43. The volume of water associated with this depth would realistically spread far beyond the edges of the sidewalk and could cause significant flood damage to surrounding buildings.

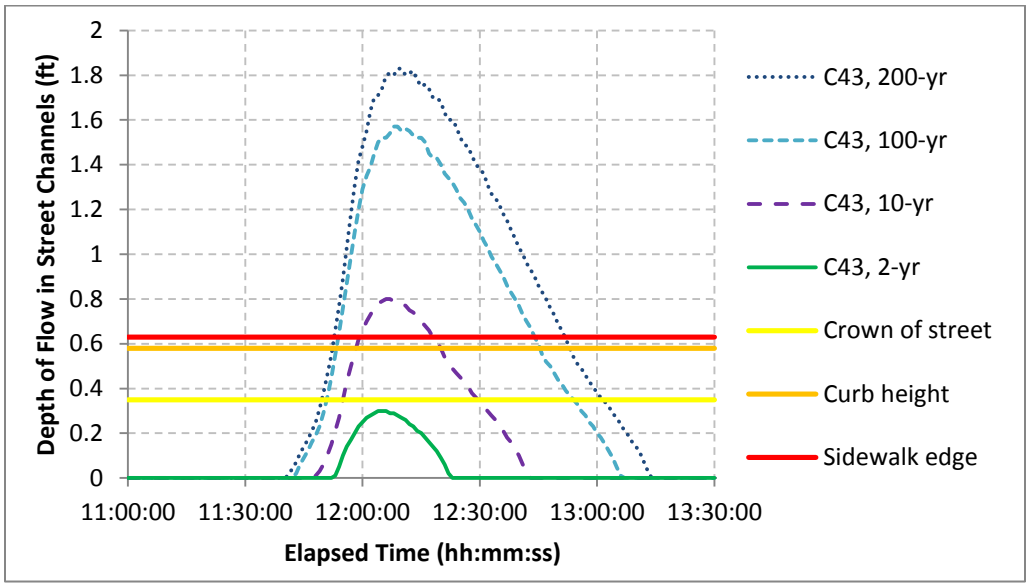

Figure 3-30. Flow depths in street channel C43 during a 24-hr storm for 2-, 10-, 100-, and 200-yr return periods with a local depression at inlet J25.

The second inefficient condition was to have an inundated outlet where water could not drain from the system for the duration of the storm. This was represented in the model by effectively zeroing out the diameter of the pipe leading to the watershed outlet. This caused all of the water to accumulate at the inlet to the outlet pipe and caused a backup at that location. Figure 3-31 shows that under this condition the sidewalk edge along street channel C43 is overtopped by all of the storm frequencies.

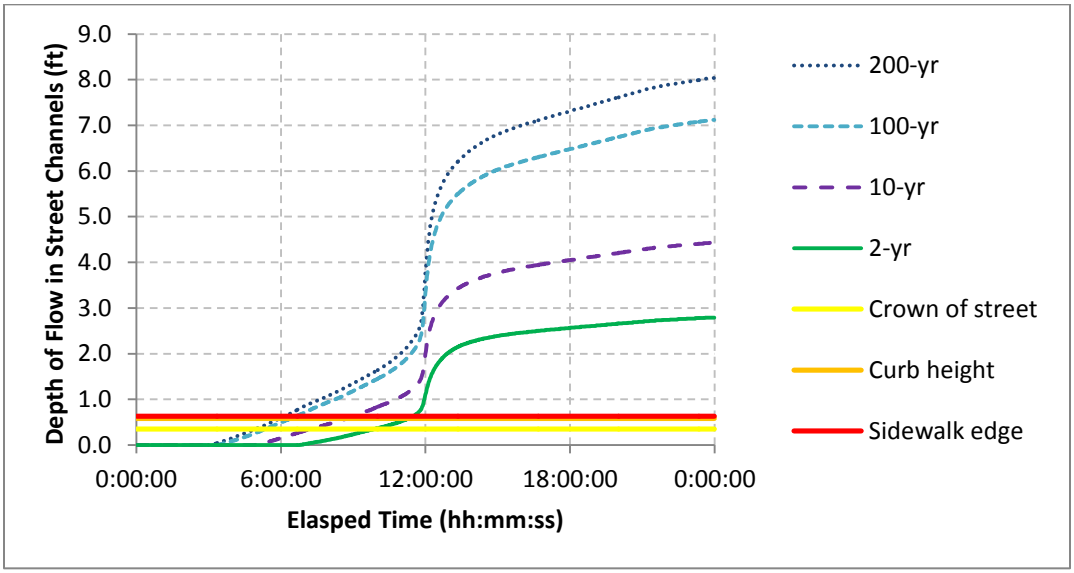

Figure 3-31. Flow depths in street channel C43 for a 2-, 10-, 100-, and 200-yr storm of 24-hrs with the outlet completely inundated, eliminating watershed outflow.

Timing and duration of flooding can be important to consider, especially with respect to potential road closures or even evacuation orders. As was expected, overtopping of the curbs and sidewalks occurred earlier for the larger return period storms. For the 200-yr event, this occurred 6 hours and 10 minutes into the storm, well before the peak rainfall intensity occurred at 12 hours. This would be extremely problematic and damaging if flooding beyond the sidewalk occurred even before the peak of the storm hit. Even the 2-yr storm, under this condition, overtops the sidewalk at the

peak of the storm. The peak depths caused by the 2-, 10-, 100-, and 200-yr storms when the watershed outlet was removed were 2.84, 4.50, 7.22, and 8.14-ft, respectively. Although the condition of having the outlet inundated at the start of a storm is not typical, it could happen if the local river or stream to which the drainage system drains is already at flood stage when the storm begins. This could occur at down-gradient locations when significant rainfall events occur over a short time frame. Though this scenario represents an extreme case, flood depths above 7ft and 8ft could have devastating consequences in any urban location.

3.4.8.2 *Partial Clogging of Inlets*

One potentially significant problem for urban stormwater drainage systems is clogged inlets. Without frequent maintenance and cleaning of stormwater inlets, trash, debris, and sediment have a tendency to collect at the inlets and cause clogging. This reduces the inflow capacity of the inlets. Lower inflow capacity at the inlets causes the stormwater system to become backed up prematurely. For example, if a stormwater system were designed for a 10-year rainfall event and the inlets became partially clogged, then the stormwater system could become backed up during storms of lower return periods, such as from an 8- or 5-year rainfall event. Therefore, the result of a partially clogged inlet is that the stormwater will drain at a lower flow rate into the pipe network and may cause a backup of stormwater flow into the streets during a less severe rainfall event than that for which the system was designed.

Sources of clogging may include trash that is not properly disposed of prior to a storm, sediments already in the streets or washed off of parks, lawns, construction sites, etc., or leaves that fall in autumn and are not bagged prior to a storm. Small storms can

contribute to the clogging effect by carrying this material to the inlets. High intensity storms can also be a major contributor to clogging because the high flow rates can transport large volumes of trash, debris, and sediment to the inlets. Additionally, inlets can become increasingly clogged over the duration of a storm. This is especially true when the duration of a storm is several hours or more, allowing time for trash, debris, and sediment to accumulate at the inlets. However, for the following simulations it was assumed that the clogging reduced the inflow capacity by 50 percent and remained constant throughout the storm.

The effect of clogging was assessed under various conditions using the SWMM model. Because SWMM does not allow the specification of the flow characteristics of the inlet itself, this was accomplished by reducing the size of the pipe to which the clogged inlet drains such that the flow capacity became half of the original design capacity. For example, pipe C16 was originally designed to carry 12.2 cfs of flow, which required a diameter of 2 ft. To represent the half-clogged inlet condition, the capacity of the pipe was treated as half of the original 12.2 cfs, or 6.1 cfs. Therefore, the size of the pipe was reduced to a required diameter of 1.25 ft. This method of simulating clogging was used only for primary inlets, which are inlets at the upstream end of a pipe network whose only inflow is direct runoff from a subcatchment, not from other pipes or street channels. The same method of simulating clogging described here could also be used to model constricted flow in aging pipes throughout the system due to interior build up.

For this example drainage system, the two primary inlets were modeled as being half-clogged. The model was simulated under this condition for the 10-, 100-, and 200-yr storms. The results of these simulations are shown in Figure 3-32 to Figure 3-34. At the

bottom right of each of the figures is a map of the system being modeled. Highlighted in red are the inlets that are being represented as clogged. Highlighted in blue are the pipes for which the capacity was reduced by half in the SWMM model to represent the half-clogged inlet that drains into it. Additionally, each figure includes some reference depths to clearly indicate the severity of the overflow of stormwater in the streets. The three reference depths are the crown of the street, the height of the curb, and the edge of the sidewalk, at elevations of 0.35, 0.58, and 0.63 ft (4.2, 7.0, and 7.6 in.) respectively.

When a stormwater pipe network is designed for a 10-yr storm, significant clogging of inlets can cause flow to back up onto the streets that immediately surround the inlet (see Figure 3-32). In other words, the outlet capacity of a system that was designed to pass the 10-yr storm is reduced such that it cannot pass a 10-yr storm without overflow. Therefore, any flow depth in the street channels shown in Figure 3-32 suggests the degree of reduced capacity of the pipe system due to the clogging. Although the flow depths only reached about 2 inches for street channels C41 and C42, this can begin to be

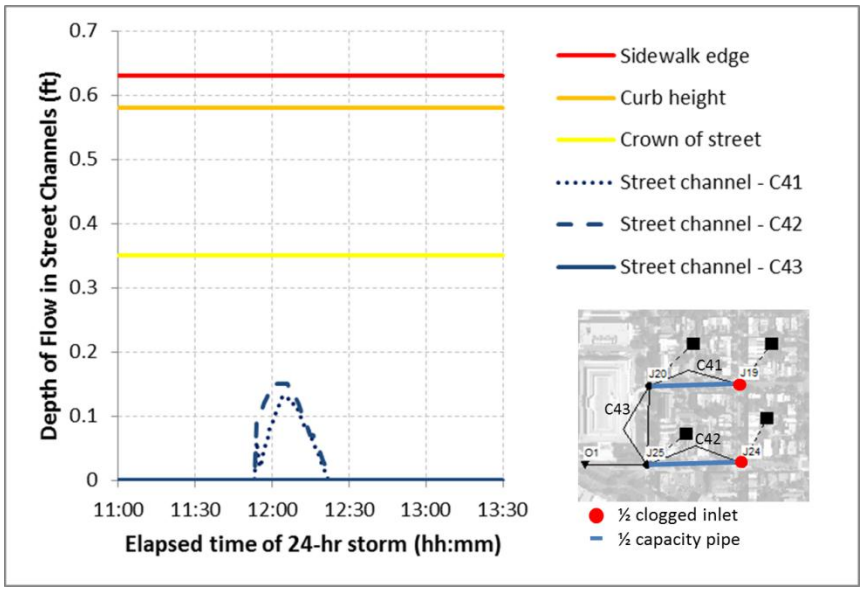

Figure 3-32. Flow depths in street channels (C41, C42, and C43) for a 10-yr storm when primary inlets J19 and J24 are half-clogged.

problematic for transportation. More importantly, this suggests that expected problems associated with larger storms would indubitably be intensified if any inlets were significantly clogged when such a storm struck. The results also suggest that without proper maintenance and frequent cleaning of inlets, when the design storm does occur, significant backup and accumulation of water in the streets is possible.

Even before flow depths reach the crown of the street, traffic is jeopardized but direct economic damages are not likely to occur. Public safety could be a concern if roads are not officially closed and people attempt to drive through flooded streets. When the flow depths reach the height of the curb (7 inches in DC) the same concerns exist, though they can be more significant in terms of public safety. This would be sufficient depth to lift and move cars parked along the streets, potentially causing some direct economic damages as well. When the flow depth surpasses the edge of the sidewalk, private property begins to be inundated. This is when economic damages accumulate very rapidly. Public safety also becomes a major concern.

Figure 3-33 indicates that the street channel flow depths increased substantially from the 10-yr storm to the 100-yr storm. During the peak of the 100-yr storm, street channel C43 experienced flow depths that exceeded the edge of the sidewalk. Again, this is when significant direct economic damages begin to occur, in addition to public safety issues. The flow depths in street channels C42 and C43 reached well above the sidewalk edge for the 200-yr storm (see Figure 3-34). Under such rainfall magnitudes and flow depths, significant damages to surrounding buildings and the contents in the lower levels of those buildings could occur. While simulations of the 100- and 200-yr storms without any clogging also resulted in flooding above the sidewalk edge, the depth of flooding and

potential economic damages were larger when the primary inlets were clogged, as was expected. This also indicates that flood depths that would cause significant damages would be reached sooner and for shorter return period storms if the primary inlets are allowed to partially clog.

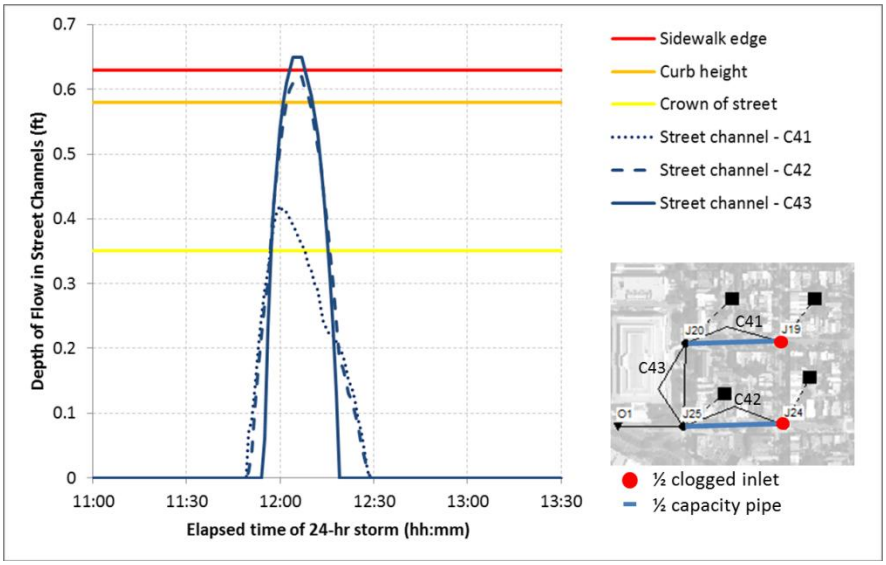

Figure 3-33. Flow depths in street channels (C41, C42, and C43) for a 100-yr storm when primary inlets J19 and J24 are half-clogged.

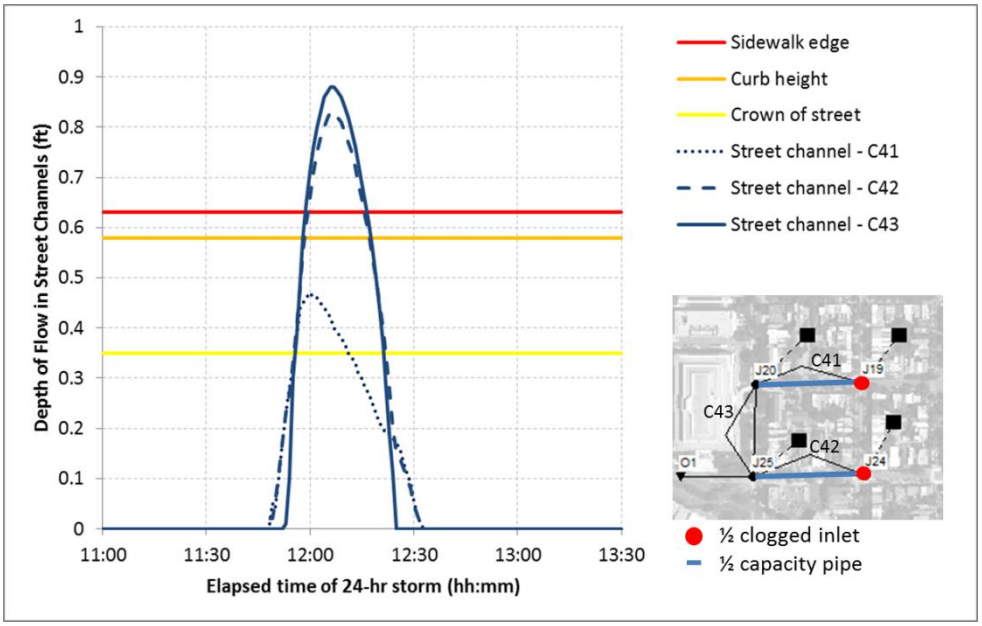

Figure 3-34. Flow depths in street channels (C41, C42, and C43) for a 200-yr storm when primary inlets J19 and J24 are half-clogged.

While the effect of clogged inlets appears to be localized, it is likely that if one inlet is significantly clogged in an area, that others are as well. Therefore, it may be useful to simulate all inlets as being partially clogged. Limitations of SWMM make it difficult to isolate and control the inflow patterns of inlets. One possible method of accomplishing this would be to add an additional pipe and street channel to which each subcatchment would immediately drain. This pipe and street channel would not be able to have any pipes or street channels connected to their upstream end. The pipe portion could be reduced in size to represent the reduced inflow capacity. The lengths of these segments would need to be user defined as very short, so as not to alter the drainage network significantly. Any excess flow that could not be carried by the constricted pipe (clogged inlet) would flow along the street channel to the next inlet where it would enter the main system. This method could be used to model partially clogged inlets for a selected region of a watershed, or for the entire system.

3.5 SUMMARY

The steps of setting up a dual-drainage model in SWMM require careful attention to ensure the modeling effort is successful and provides meaningful results. All assumptions should be clearly stated and justified. As much data and detailed information as possible that pertains to a specific study site should be obtained. This will serve to minimize the number of assumptions required, resulting in a more realistic model. Models developed for different sites, or by different developers, will be somewhat distinct. Therefore, sensitivity analyses performed will be specific to the model and conditions for which they were developed. This means that sensitivity analyses from one model may not be transferable to another model. The setup of the

model and determination of input sensitivities and requirements must be performed with care as they provide the foundation for a pluvial flood risk analysis.

CHAPTER 4

PLUVIAL FLOOD DAMAGE ESTIMATION

4.1 INTRODUCTION

When studying the effects of potential flooding, it is useful to discuss the effects in terms of monetary consequences. This increases the ability for people, especially decision makers, to understand the potential severity of a flood scenario. The actions that are justifiable to protect against 10 inches of potential flooding on a given street may not be clear if that is the only information available. However, if that same 10 inches of street flooding is linked to $100,000 in damages, then decision making ability is enhanced. Benefit-cost ratios could be used to determine the mitigation actions that are economically justifiable. Therefore, a method is needed to adequately translate depth of flooding into economic damages. This has traditionally been accomplished using depth-damage curves.

Depth-damage curves have been the basis of flood damage estimates for many years (White 1964; Penning-Roswell and Chatterton 1977; and Scawthorn et al. 2006). These curves directly relate depth of flooding for a particular type of structure to the percentage of the total value of the structure that would be damaged. The following includes a discussion of the depth-damage curve selection process and their appropriate use.

Examples are used to demonstrate the estimation of damages of an individual building, a city block, or a full microwatershed.

4.2 DEPTH-DAMAGE CURVE SELECTION

The specific characteristics of depth-damage curves obviously have a significant bearing on the estimates of total damages of any pluvial flood scenario. The total damages factor heavily into the determination of overall pluvial flood risk. Therefore, the depth damage curve selection process is important to any pluvial flood risk study.

Many depth-damage curves have been developed for various purposes and levels of specificity. This study will draw from the over 900 depth-damage curves developed by the US Army Corps of Engineers (USACE) and utilized by FEMA's HAZUS-MH software (Scawthorn et al. 2006). The advantage of using these depth-damage curves is that distinct curves are available for very specific categories of buildings, e.g., single-family, two-story residential with no basement, or commercial entertainment/recreation. They also provide flexibility because they relate flood depth to the percent of total value likely to be damaged. Therefore, some regional differences can be accounted for in the additional input of building and content values of the study site. The disadvantage of using these curves is that they are generally based on national averages for each building type. If depth-damage curves that more specifically reflect the local construction styles or other influential patterns of a study region are available, they may be preferable and be able to provide more accurate damage estimates.

The selection of the depth-damage curves will depend largely on intended use. For example, only one specific curve will be needed to predict damages to one specific building. However, when estimating the damages along a city block, or within a

microwatershed, several curves may be needed to accurately represent the variation in building type. If the variation is not significant (e.g., the buildings along a block are all townhouses with basements and most are three stories but some are two stories), then a single depth-damage curve may be able to adequately represent an entire block or watershed.

Specific information about a study site is needed to make a selection of a damage curve. This example study site covers four square city blocks of primarily residential townhomes. Figure 4-1 depicts the study site as displayed in SWMM with a flow depth scale and also shows townhomes that are mostly homogeneous across the site. The displayed flow depths are the result of a simulation of a 200-yr, 24-hr storm that will be used in the damage estimate examples to follow.

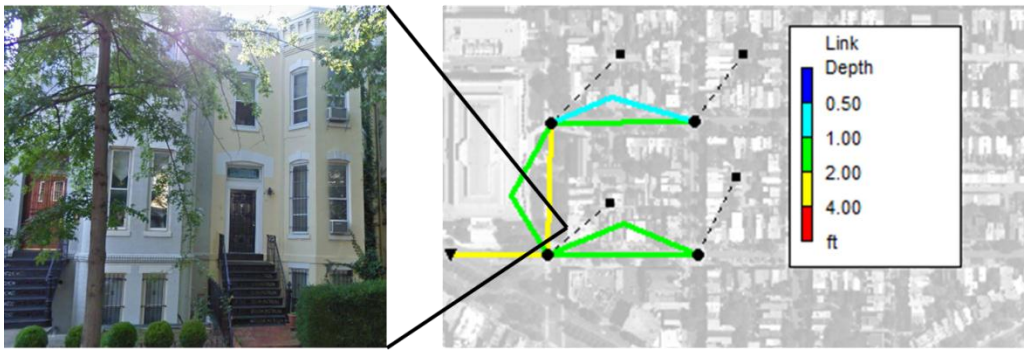

Figure 4-1. Example study site flow depths during the peak of a 200-yr, 24-hr storm and typical residential townhomes of the site.

The depth-damage curves selected for the damage estimate examples are shown in Figure 4-2. These curves were selected because they are representative of typical 3-story, single-family, residential buildings with basements, such as those depicted in Figure 4-1. A distinct depth-damage curve for the building and contents is needed for a complete damage estimate and both were drawn from the HAZUS-MH catalogue of

depth-damage curves. The information accessed from HAZUS-MH was in tabular form of 1-ft increments (Scott 2011). To make damage estimates from flood depth increments smaller than 1-ft, equations were fitted to the tabular data. Due to the complexity of the shape of each curve, it was determined that acceptable accuracy could be achieved only by separating the tabular data into areas of similar trends and using a composite model.

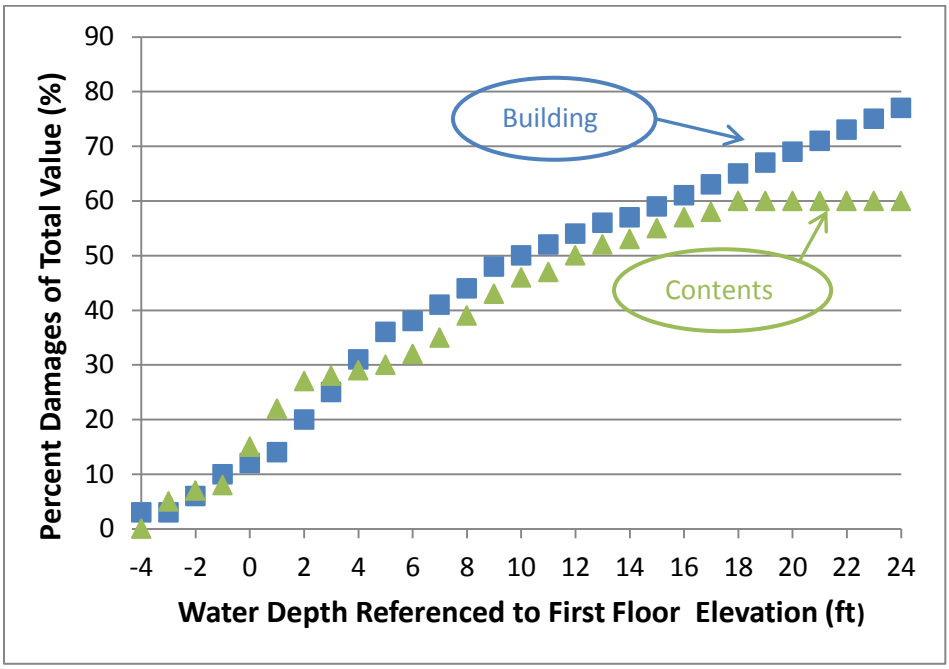

Figure 4-2. Depth-damage curves for 3-story, single-family, residential buildings with basements obtained from HAZUS-MH.

A composite model is one that represents different portions of the data using different functional forms. The process of constructing a composite model requires only a few more steps than the process of constructing a single-function model. First, the locations where the curve will be divided needed to be determined. Whenever possible, this decision should be based on some physical transition in the variable being predicted. In this case, for example, the division locations were at 0- and 8-ft, indicative of the presumable elevations of the first and second floors of this type of building. Second, a

model structure for each segment had to be selected. Third, constraints needed to be placed on the segments of the model to enforce continuity at the division locations. Finally, least-squares fitting must be accomplished while satisfying the imposed constraints and maintaining rationality. Adhering to these steps produced the following composite models for the building and contents depth-damage curves,

$$B = \begin{cases} e^{0.3465(d+4)} & for \ -4 \le d \le 0 \quad (4.1a) \\ \frac{50.432}{1+e^{-0.388(d-3)}} & for \ \ 0 \le d \le 8 \quad (4.1b) \\ 15.868d^{0.4916} & for \ \ 8 \le d \le 24 \quad (4.1c) \end{cases}$$

$$C = \begin{cases} 2.051\sin\big(1.645(d+4)\big) + 3.599(d+4) & for \ -4 \le d \le 0 \quad (4.2a) \\ -4.09\sin(16d) + 3.3105d + 15 & for \ \ 0 \le d \le 8 \quad (4.2b) \\ \frac{45.2}{1+e^{-0.335(d-8)}} + 14.87 & for \ \ 8 \le d \le 24 \quad (4.2c) \end{cases}$$

where B and C are the percentages of the total value damaged of the building and the contents, respectively, and *d* is the depth (ft) of flooding measured with respect to the first floor elevation. The arguments for the sine functions used in Equations 4.2a and 4.2b are in radians. Figure 4-3 shows these equations fitted to the original HAZUS-MH depth-damage curves and Table 4-1 and Table 4-2 provide a summary of the goodness-of-fit statistics of the component models and the full composite models. The models all show good fitting, with high correlation coefficients and relatively low S_e/S_y values, though the full composite models show the lowest S_e/S_y values.

Table 4-1. Summary of goodness-of-fit statistics for each component of the composite models for the building and contents depth-damage curves.

Building			
Statistic	**Section 1**	**Section 2**	**Section 3**
n	5	9	17
R	0.9673	0.9902	0.9986
R^2	0.9356	0.9805	0.9972
S_e (damage %)	1.1312	1.0290	0.8183
S_y (damage %)	4.0866	11.8004	9.9028
S_e/S_y	0.2768	0.0872	0.0826

Contents			
Statistic	**Section 1**	**Section 2**	**Section 3**
n	5	9	17
R	0.9607	0.9558	0.9298
R^2	0.9229	0.9136	0.8645
S_e (damage %)	0.6077	1.4689	1.0888
S_y (damage %)	5.4314	7.0198	6.8819
S_e/S_y	0.1118	0.2093	0.1582

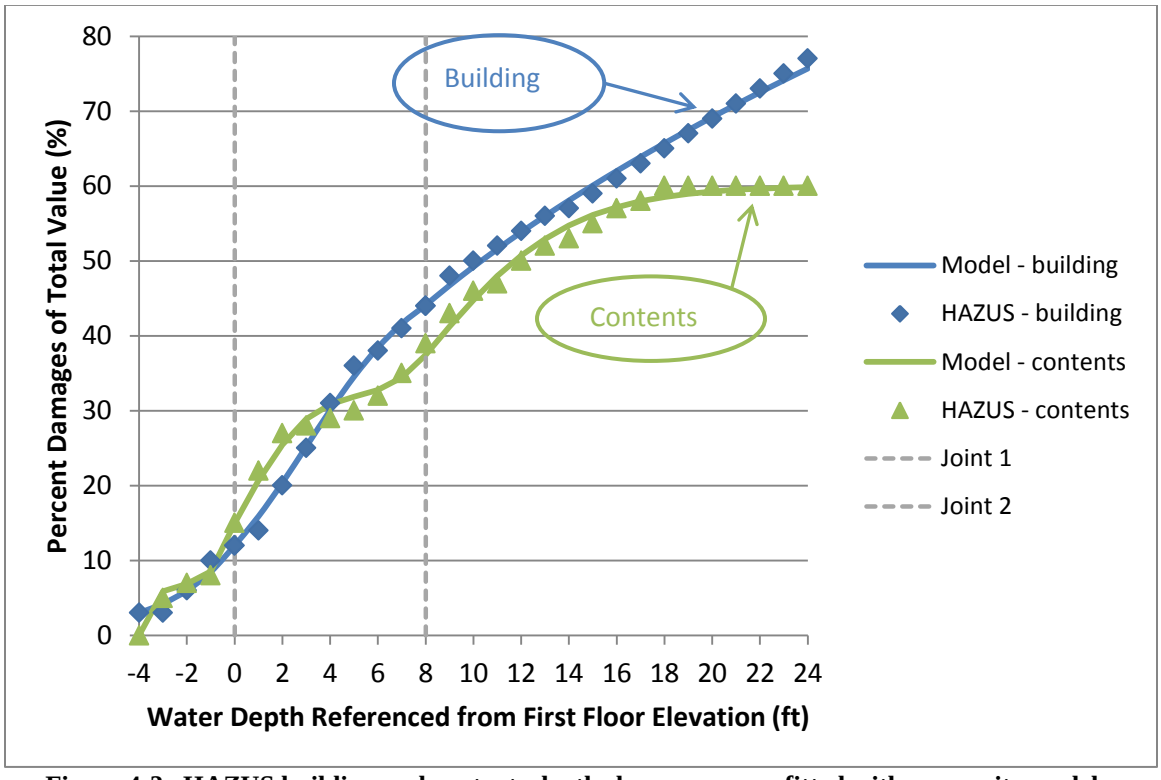

Figure 4-3. HAZUS building and contents depth-damage curves fitted with composite models.

Table 4-2. Summary of goodness-of-fit statistics for full composite models of the building and contents depth-damage curves.

Statistic	Building	Contents
n	29	29
R	0.9843	0.9639
R^2	0.9688	0.9291
S_e (damage %)	0.8878	1.0828
S_y (damage %)	23.6941	19.5081
S_e/S_y	0.0375	0.0555

The total value of buildings must be known or estimated in order for a depth-damage curve to produce a dollar amount. These values can be estimated from property assessments or local median prices. Typically, after the value of a building has been determined, the total value of the contents is estimated using a direct building-to-contents value ratio. The USACE (1992) found from the results of numerous surveys that for the region covered by their North Atlantic Division, of which Washington, DC, is a part, this ratio ranged from 0.50 to 0.72 for residential buildings. For this study, a building-to-contents ratio of 0.60 was used.

4.3 ESTIMATION OF DAMAGES

Economic damages caused by pluvial flooding can be estimated at several different scales. This section discusses the process of estimating damages for an individual property, a city block, and a full microwatershed. It should be noted that smaller scale damage estimates will have a higher level of uncertainty (Merz et al. 2010). That is, a high level of precision should not be expected when estimating damages of an individual property because of uncertainties of many of the model inputs. Additionally, non-residential properties introduce more uncertainty due to more variation in the value of the building and contents. However, a rough estimate of damages to an individual property

can still be useful in informing property owners of the approximate risks to which they are subject and for which they should prepare. Such an estimate is even more useful when considered in the context of damage estimates along the same block and over the associated microwatershed. Together these damage estimates would be able to communicate pluvial flood risk more effectively to a property owner than they could separately.

4.3.1 Individual Property Damages

Estimates of pluvial flood damages to individual properties can be useful in determining the actions that property owners should take to protect their property. If property owners were to have a dollar value of potential pluvial flood damages to their specific property presented to them, they may be more willing to invest in flood risk reduction strategies that would help protect themselves, and at the same time, their community. This would be especially valuable in areas of considerable flood risk in which people do not currently take action to help mitigate potential flood damages. It should be remembered, however, that of the three scales of pluvial flood damage estimates discussed here, a damage estimate of an individual property carries the largest uncertainty. Therefore, a damage estimate of an individual property should only be considered a rough estimate.

The property shown in Figure 4-1 was used to provide an example of the method used to estimate pluvial flood damages of an individual property. First, flood depths along the street channel where the property is located are needed for the return period storm and conditions of interest. The flood depths were obtained from a previous simulation of the model shown in Figure 4-1 using the 200-yr, 24-hr storm. Along

street channel C43 (where the selected property is located), the average longitudinal depth at the time of peak depth was 1.25-ft. This depth was the result of using vertical boundaries at the edge of the sidewalk. However, the building that was analyzed, as well as the other buildings along the same street, is set back a distance from the sidewalk. Therefore, the width of the cross-section of the street channel needed to be adjusted to reflect the setback distance.

An accurate determination of a new cross-section of the street channel that includes the distance the buildings are set back from the sidewalk is important because it directly influences the flood depth. A measurement tool was utilized in GIS to measure the distance from the edge of the building footprints on one side of street channel C43 to the edge of the building footprints on the other side. For this street channel, the average total width was determined to be about 90-ft. Therefore, 20 additional feet were added to either side of the already 50-ft wide street channel to make a total of 90-ft wide (see Figure 4-4). The same 0.5 percent slope used from the top of the curb to the edge of the sidewalk was used, providing a constant cross-sectional slope from the curb to the edge of the building. The new cross-section would be able to convey the same volume of

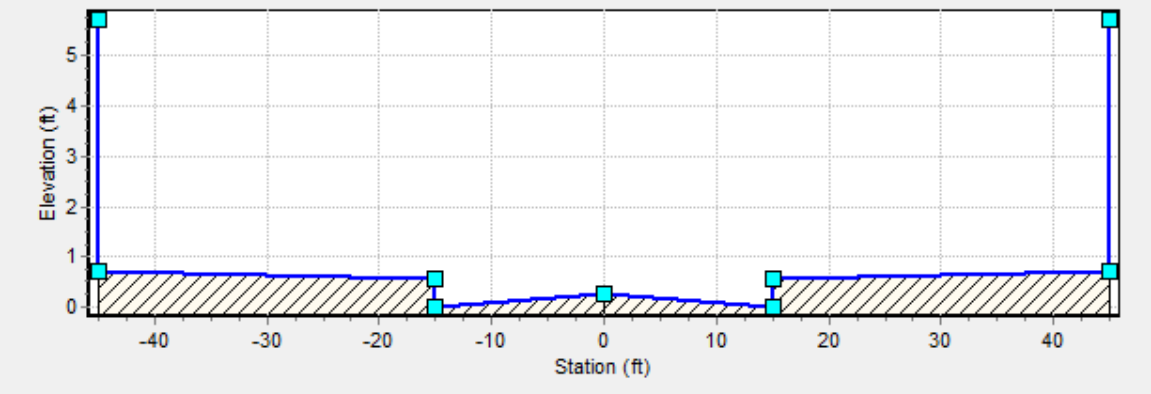

Figure 4-4. Cross-section for street channel C43 (3rd St NE, Washington, DC) adjusted to reflect building setback distance.

water at a lower depth. The model was simulated with the new cross-section, and the average peak depth along street channel C43 changed from 1.25 to 1.01-ft. The results of the latter simulation were used in the damage estimation because they more accurately reflect local conditions.

Next, the flood depth at the specific location of the building of interest along the street channel needed to be determined. The 1.01-ft depth previously cited represented the average depth along the street channel. However, the depth is not constant along the channel (see Figure 4-5). Therefore, the depth at each end of the street channel and the length were used to determine the slope of the depth as 0.0026. The distance of the building from the downstream end of the street channel was estimated using GIS to be 80-ft. Using this method, the depth in the street channel at the location of the building was estimated as 1.30-ft. However, cross-sectional geometry of the street channel allows 0.73-ft of flow depth before the water reaches the edge of the building. Therefore, the final flood depth that was input to the depth-damage functions was 0.57-ft. This depth was used with the tax assessed value of the building ($428,510) to produce the final damage estimate of about $25,000. The main inputs and results are summarized in Table 4-3.

Table 4-3. Summary of significant inputs and results of the damage estimate for a 200-yr rainfall event for a selected individual property with a flood depth of 0.57ft in Washington, DC.

Criterion	Building	Contents
Damage (%)	3.659	3.724
Value ($)	428,510	257,106
Damage ($)	15,681	9,574
Total Damage ($)	25,255	

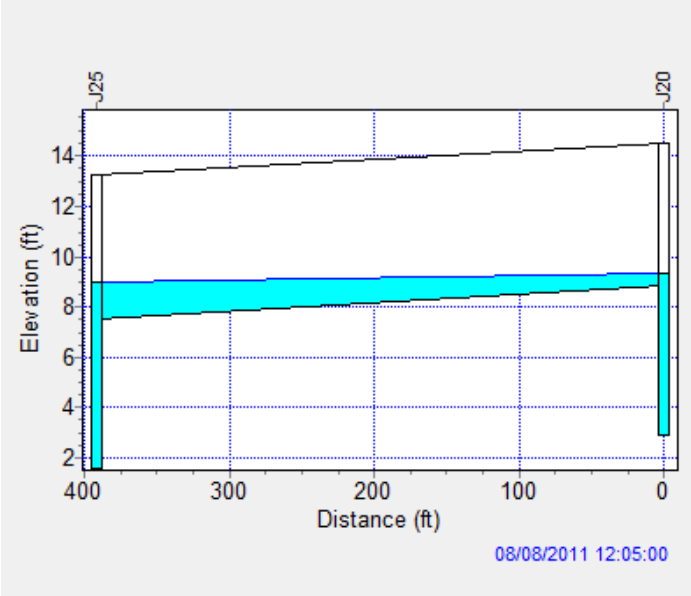

Figure 4-5. Flood depth profile along street channel C43, from inlet J20 to J25, for 200-yr, 24-hr storm with adjusted street channel cross-section.

4.3.2 City Block Damages

Estimating pluvial flood damages along a city block can provide valuable information to local authorities and decision makers. Such estimates can assist in pinpointing specific streets that most urgently need site assessments of drainage system performance and potential upgrades. Damage estimates obtained from a pluvial flood analysis can serve as justification for such upgrades and assist in gathering support for initiatives to that end.

The process for estimating pluvial flood damages along a city block is similar to that of estimating pluvial flood damages for an individual building. The major difference is that the steps must be repeated for each building along the block and the damage estimates of each individual building summed to produce an estimate for the entire block. In order to demonstrate this process, the same study site, modeling conditions, and simulation results were used. The city block along which the individual building from

the previous analysis was located was examined in this case. Because the street along this same block served as the boundary of the study site, only the side of the street within the study site was analyzed.

The same process used to estimate damages of a single property was again used here, only it was repeated for each building along the block. In cases where individual building values are not available, using an average value for a particular building type may be suitable. Often more than one type of building exists along a block. In this case, an apartment building and a church were located along the block being analyzed. For the most accurate analysis, separate depth-damage curves should be selected and composite models fitted for each different building type. However, it is sufficient for this example to use the same depth-damage curves introduced previously for the entire block. Under these conditions, it was estimated that the overall damages to the city block would be approximately $430,000. A summary of the significant inputs and results of the damage estimate for the city block are given in Table 4-4. More detailed calculations of each building along the block are provided in Appendix A.

Table 4-4. Summary of significant inputs and results of the damage estimate for a 200-yr rainfall event for a selected city block with an average flood depth of 0.49ft in Washington, DC.

Criterion	Building	Contents
Average Damage (%)	3.562	3.221
Total Value ($)	7,615,620	4,569,372
Total Damage ($)	274,194	155,740
Total Damage ($)	429,934	

4.3.3 Microwatershed Damages

Estimating damages on the level of the microwatershed can provide another layer of valuable information for local authorities and decision makers. This type of damage

estimate can inform local leaders of appropriate levels of investment to protect against flood damages in specific regions of their jurisdictions or evaluate the capacity of major drainage infrastructure. The same process used for the previous damage estimates was used again in this case, but was expanded to cover the full microwatershed.

The relative simplicity of the example microwatershed led to a relatively simple microwatershed damage estimate process. Under the same conditions as the previous analysis, only two streets in the microwatershed experienced flooding. Therefore, the same analysis that was performed on the city block level was repeated for the second flooded street to provide a full microwatershed damage estimate in the range of $771,000. A summary of the significant inputs and results of the damage estimate of the full microwatershed are given in Table 4-5. More detailed calculations of each flooded building within the microwatershed are provided in Appendix A.

Table 4-5. Summary of significant inputs and results of the damage estimate for a 200-yr rainfall event for a selected microwatershed in Washington, DC.

Criterion	Building	Contents
Average Damage (%)	3.480	2.744
Total Value ($)	14,366,569	8,619,941
Total Damage ($)	508,617	262,847
Total Damage ($)	771,464	

4.4 SUMMARY

The processes of estimating damages at each level (individual building, city block, and microwatershed) are essentially the same. The main differences are in the computational steps required. The examples shown demonstrated that even with relatively shallow flood depths, significant damages can accumulate. The damage estimates at each level are best used together to inform property owners and local

officials of the potential consequences of a significant pluvial flood event. Table 4-6 provides a summary of the damages estimated at three levels of analysis.

Table 4-6. Summary of damage estimates for three levels of analysis.

Level of analysis	Overall damage estimate ($)	Number of buildings flooded
Individual building	25,000	1
City block	430,000	8
Microwatershed	771,000	20

CHAPTER 5

PLUVIAL FLOOD RISK ESTIMATION

5.1 FLOOD FREQUENCY ANALYSES

While flood depths and damages can be estimated at discrete return periods using individual model simulations, estimating the severity of these consequences at any return period requires a flood frequency analysis. A flood frequency analysis uses sample data, often measured flood magnitudes, to develop a population that is a more systematic representation of flooding than that provided by the sample points. A flood frequency analysis can be useful for multiple purposes. It can provide greater confidence in the planning of projects with various design return periods and can provide a stronger argument for adjusting community policies and initiatives that would be implemented over various time periods. In a broad sense, a flood frequency analysis provides greater accuracy of interpolation between, and extrapolation beyond, known flood magnitudes and exceedence probabilities.

The purpose of a flood frequency analysis is to fit an assumed population model with a set of measured flood magnitudes. Flood frequency analyses are often performed at stream gages where the flowrate is the characteristic being predicted. However, variables other than flowrate, such as flow depth or even expected damages, can be analyzed in the same manner. In this case, the flow depth along street channel C43 was analyzed for the

2-, 10-, 100-, and 200-yr storms with the condition that the inlets were partially clogged. The resulting flow depths used for the flood frequency analyses are given in Table 5-1. For this study, it was assumed that the n-year rainfall event generates the n-year flood.

Table 5-1. Various return period flood depths along street channel C43 which were used in flood frequency analyses.

Return period (yrs)	Flood depth (ft)
2	0.30
10	0.80
100	1.57
200	1.83

The process for performing a flood frequency analysis can be summarized as follows:

1. Assume a probability density function for the population (normal, log-normal, log-Pearson III, etc.).
2. Compute moments from sample (mean, standard deviation, skew).
3. Construct a frequency curve to represent the population by equating the sample moments and the parameters for the assumed density function.
4. Plot sample points and assess goodness-of-fit.

5.1.1 Assume a Probability Density Function

The method for selecting a probability density function to represent the population should be based on knowledge about the type of data that is being analyzed. For example, probability density functions commonly used in hydrology are the normal, log-normal, and log-Pearson III distributions (McCuen 2005). Flood characteristics can usually be best described by the log-Pearson III distribution (USGS 1982). For this

demonstration, both the log-normal and log-Pearson III distributions will be tested in order to provide a comparison.

5.1.2 Estimate Population Parameters from Known Flood Magnitudes

In some cases, sample flood magnitudes are not available, but magnitudes of the 2-, 10-, and 100-yr floods are known. These flood estimates can be used to estimate the log-normal and log-Pearson III parameters. The Interagency Advisory Committee on Water Data (1982) issued Bulletin 17B that contains the following equations for computing the moments of a log-Pearson III distribution from estimates of flood magnitudes for the 2-yr, 10-yr, and 100-yr events (e.g., $Q_{0.5}$, $Q_{0.1}$, $Q_{0.01}$, respectively):

$$G_s = -2.50 + 3.12\frac{Log(Q_{0.01}/Q_{0.10})}{Log(Q_{0.10}/Q_{0.50})} \tag{5.1}$$

$$S_s = \frac{Log(Q_{0.01}/Q_{0.50})}{K_{0.01} - K_{0.50}} \tag{5.2}$$

$$\bar{X}_s = Log(Q_{0.50}) - K_{0.50}(S_s) \tag{5.3}$$

where G_s, S_s, and X_s are the standardized skew coefficient, log-standard deviation, and log-mean, respectively; $Q_{0.01}$, $Q_{0.10}$, and $Q_{0.50}$ are the magnitudes for the 100-, 10-, and 2-yr return periods, respectively; and $K_{0.01}$ and $K_{0.50}$ are the frequency factors for the 100- and 2-yr return periods. For the log-normal distribution the skew need not be computed because it is by definition zero. Also, the K-values are the same as z-values when the skew is zero, which is the case with the log-normal distribution. K-values can be found

for a various probabilities and skew coefficients in the K-table (USGS 1982). A skew coefficient may be positive or negative, but is generally rounded to the nearest tenth when using the K-table.

5.1.3 Construct a Frequency Curve

Using the sample moments computed in the previous step, a frequency curve representing the assumed population can now be constructed. The equation for the curve is in the form,

$$X = \bar{X}_s + KS_s \tag{5.4}$$

where X is the predicted magnitude (flowrate, flow depth, etc.) and K is the frequency factor which is dependent on the return period and skew coefficient (McCuen 2005). Using numerous exceedence probabilities, estimated X values can be determined and plotted on probability paper to give an accurate representation of the underlying frequency curve. It should be noted that the larger the absolute value of the skew coefficient, the greater the curvature of the frequency curve. This requires more X values will need to be computed to get an accurate representation of the frequency curve. As the log-normal distribution has a skew of zero, it will plot as a straight line, and as such, requires only two points to be plotted. However, for the purpose of comparison, values were computed for all the same return periods that were used to develop the log-Pearson III curve. A summary of these computations is given in Table 5-2. These results were then plotted on probability paper. Then the data from the SWMM simulations of the 2-,

10-, 100-, and 200-yr rainfall events were plotted and the goodness-of-fit for each model was evaluated (see Figure 5-1).

Table 5-2. Flood frequency curve calculations for log-normal and log-Pearson III distributions based on flood depth of a selected property within the watershed.

Log-normal (mean = -0.523, st.dev. = 0.309, skew = 0)				
Return Period (yrs)	**1-P**	**Probability of exceedence**	**K**	**Log(depth)**
2	0.500	0.500	0.00000	-0.5229
5	0.800	0.200	0.84162	-0.2628
10	0.900	0.100	1.28155	-0.1269
25	0.960	0.040	1.75069	0.0180
50	0.980	0.020	2.05375	0.1117
100	0.990	0.010	2.32635	0.1959
200	0.995	0.005	2.57583	0.2730
Log-Pearson III (mean = -0.547, st.dev. = 0.366, skew = -0.355)				
Return Period (yrs)	**1-P**	**Probability of exceedence**	**K**	**Log(depth)**
2	0.500	0.500	0.06651	-0.5229
5	0.800	0.200	0.85508	-0.2341
10	0.900	0.100	1.23114	-0.0964
25	0.960	0.040	1.60574	0.0408
50	0.980	0.020	1.83361	0.1242
100	0.990	0.010	2.02933	0.1959
200	0.995	0.005	2.20029	0.2585

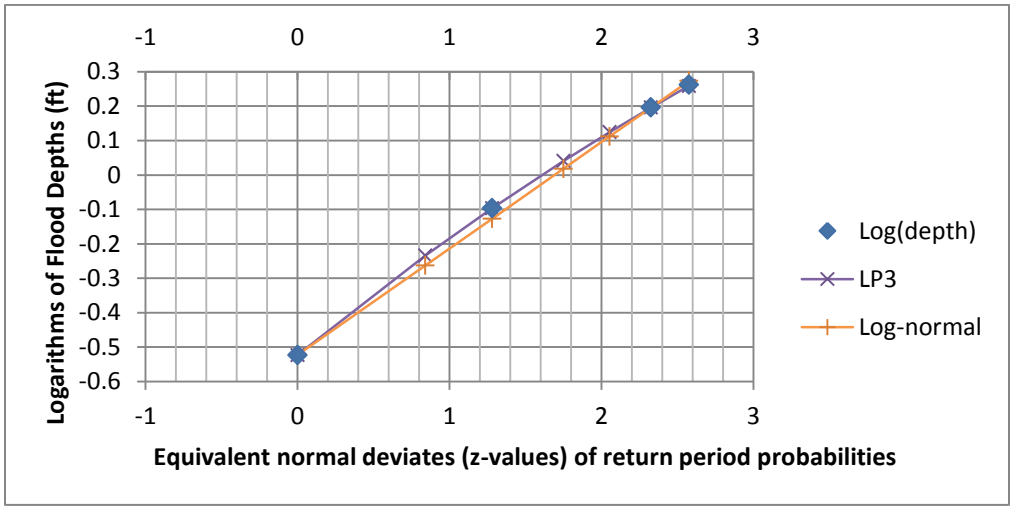

Figure 5-1. Comparison of log-normal and log-Pearson III distribution curves fitted to flood depths of a selected property within the watershed.

An analysis of residuals was then conducted to more specifically compare the ability of the log-normal and log-Pearson III distributions to fit predicted flood depths. The statistics calculated based on the results of using each type of distribution are given in Table 5-3. Both graphical and statistical analyses reveal excellent goodness-of-fit for both the log-normal and log-Pearson III distribution models. However, the predicted depths of flooding of the log-normal model were not as accurate with large return periods as with the log-Pearson III model. For the 200-yr return period the log-normal distribution overpredicted the depth of flooding by 0.045 ft (0.54 in.) while the log-Pearson distribution underpredicted the depth of flooding by 0.017 ft (0.20 in.). These differences represented relative errors of 2.45% and -0.90%, respectively. The lack of curvature (skew) in the log-normal distribution suggests that any degree of extrapolation beyond the 200-yr return period would bring ever increasing inaccuracy. Also, the sum of the errors squared was 0.005 for the log-normal distribution as compared with 0.0003 for the log-Pearson III distribution. Therefore, even though both distributions provide a

Table 5-3. Summary of errors using the log-normal and log-Pearson III distributions to predict flood depths along street channel C43 for various return periods.

Log-normal					
Return Period (yrs)	Predicted depth (ft)	Actual depth (ft)	Error	Relative error	Error squared
2	0.300	0.300	0.000	0.00%	0.000000
10	0.747	0.800	-0.053	-6.68%	0.002852
100	1.570	1.570	0.000	0.00%	0.000000
200	1.875	1.830	0.045	2.45%	0.002018
Log-Pearson III					
Return Period (yrs)	Predicted depth (ft)	Actual depth (ft)	Error	Relative error	Error squared
2	0.300	0.300	0.000	0.00%	0.000000
10	0.801	0.800	0.001	0.12%	0.000001
100	1.570	1.570	0.000	0.00%	0.000000
200	1.813	1.830	-0.017	-0.90%	0.000274

good fit to the data, the log-Pearson III distribution provides a slightly better fit and would also be better suited to make estimates of flood depth for return periods of greater than 200 years.

5.1.4 Flood Frequency Curve for Flood Damages

The same process described above for developing frequency curves that relate various return period rainfall events to flood depths can also be used to develop frequency curves that relate various return period rainfall events directly to estimated damages. This type of frequency curve can be especially useful for planning purposes by providing a comprehensive view of pluvial flood risk. Flood frequency curves for flood damages of any spatial scale can be developed, as long as reliable damage estimates can be provided as inputs.

A flood frequency analysis that relates flood damages to various return periods was performed to provide an improved understanding of the overall pluvial flood risk at the site location. Flood damage estimates for various return periods were needed to perform the analysis. These estimates were determined using the flood depths from Table 5-1 and the depth-damage curves described by Equations 4.1 and 4.2 (see Table 5-4). It should be noted that, when using Equations 5.1 to 5.3 to calculate the parameters of the log-normal or log-Pearson III distribution of damages, the damages associated with the 2-yr return period must be greater than zero to avoid numerical errors. However, the rainfall volume of the 2-yr storm is generally too small to produce any pluvial flooding, and therefore, any damage. Therefore, in order to both avoid numerical errors and reasonably represent damage estimates for return periods that do not produce any damage, a near-

zero damage estimate (e.g., $1) should be used. Additionally, the value ($428,510) of the individual building that was analyzed previously was used again here to provide the basis of the damage estimates.

Table 5-4. Damage estimates of a selected building within the watershed for various return periods.

Return period (yrs)	Estimated damages ($)
2	0
10	14,425
100	30,150
200	34,122

A flood frequency curve was constructed using the estimated damages in Table 5-4 for both the log-normal and log-Pearson III distribution in order to determine which distribution better represents flood damage trends. A comparison of the results clearly indicates that the log-Pearson III distribution better describes the distribution of flood damage estimates (see Figure 5-2). Therefore, the log-Pearson III distribution was used. Finally, the logarithms were converted back into dollar values to produce the final curve (see Figure 5-3). This curve can be described by

$$X = 10^{1.323+K*3.189} \tag{5.5}$$

In which X is the real dollar value of damage estimate ($) and K is a frequency factor which is dependent on the return period and skew coefficient. In this case the skew coefficient was -1.962. Equation 5.5 can be used to predict damages to the selected building for rainfall events of any return period.

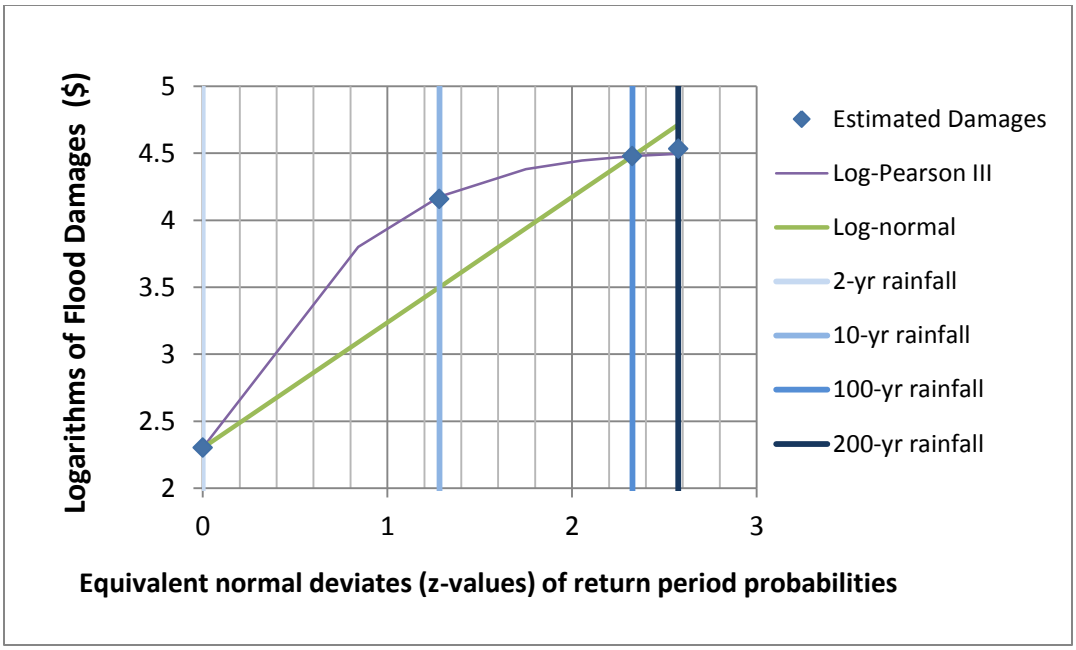

Figure 5-2. Flood frequency curves plotted of logarithmic scale for log-normal and log-Pearson III distributions.

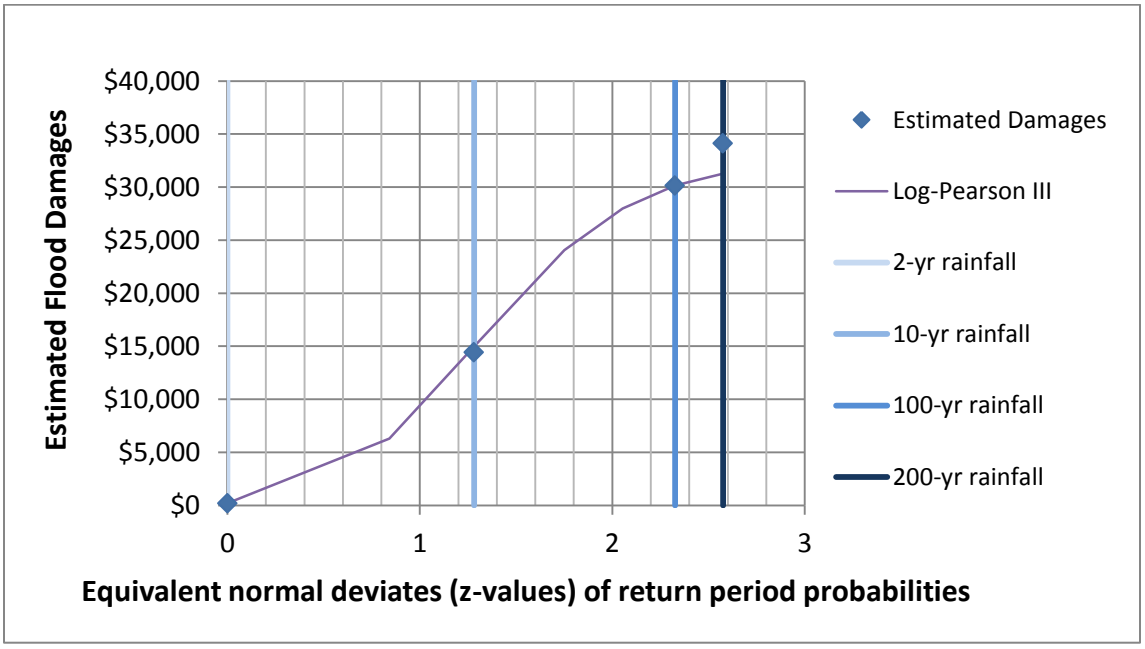

Figure 5-3. Final flood frequency curve using log-Pearson III distribution with logarithms converted back to dollar values.

CHAPTER 6

CASE STUDY – CAPITOL HILL SEWERSHED

6.1 INTRODUCTION

A case study of an existing location was used to show that the processes explained in the previous chapters can provide reasonable results. Many of the inputs in the previous examples were assumed values or synthetic data and were applied to a simplified and very small-scale site. This allowed the effects of each individual input on the behavior of the model to be closely evaluated. Alternatively, this case study will show how the process developed in the previous chapters can be applied to a real site, using actual data, and provide realistic results. While some input values still needed to be estimated, actual data were used whenever available. The end product of this case study was an estimate of the pluvial flood risk of an actual site.

6.2 SITE SELECTION

In any modeling scenario, one of the earliest and sometimes difficult questions to answer is, What is the extent of the site being modeled? After a general location is selected, the specific boundary surrounding that location must be determined. Two different types of boundaries could be used for pluvial flood modeling: a watershed boundary or a sewershed boundary. These two terms often have similar physical boundaries, even though they have somewhat different definitions.

A watershed can be defined as the area over which rainfall will drain to a specific point, or outlet. Because water runs downhill to the outlet, accurate topographic data of an appropriate resolution is required to determine the extent of a watershed. The smaller the scale of the watershed, the higher resolution of elevation data is required. Defining the boundaries of an urban watershed often requires even higher resolutions than for a natural watershed because of the many unnatural contours and obstructions to flow. The highest resolution elevation data available for Washington, DC, is 1m. For urban watersheds on the scale of a few hundred acres or less this resolution may not be sufficient to accurately delineate the boundaries of a watershed.

Another challenge in delineating small urban watersheds is that the outlet point is generally inland, or not along an existing stream channel. Several methods exist within a GIS framework to delineate a watershed based upon elevation data and a selected outlet point. However, these methods work best when the outlet point lies on an existing stream channel. Using ArcHydro, an extension of the ArcGIS software, to delineate a watershed with an outlet that does not lie on a stream channel can produce meaningless results. Therefore, the location of the outlet is an important factor in delineating the boundary of a watershed. If the outlet does not lie along a stream channel or the resolution of elevation data is insufficient, it may be better to use a sewershed boundary instead.

A sewershed is the area that a sewer pipe network drains to a specific outlet pipe. While this may be a somewhat different area than the corresponding watershed, the two areas are generally similar, particularly in a gravity flow pipe network (one without pumps or turbines). Pipes are required to be laid at certain depths below the surface elevation but generally maintain the same slope as the surface. In some cases pipes are

used to transport runoff from one watershed to another. However, for this case study it was assumed that the boundaries of the watershed and sewershed are closely aligned. This assumption allows delineation of the sewershed to be used to define the extent of the study area.

Delineating a sewershed requires knowledge of the pipe layout and some of the surface characteristics, such as slope, elevation, and flow direction. Some jurisdictions have sewershed boundaries delineated and available, probably through the local agency in charge of stormwater management. The sewershed boundaries for most sections of Washington, DC, are available in a shapefile format from the District's GIS database. If this type of data is not available, it may be necessary to manually delineate a sewershed. The sewershed selected is shown in Figure 6-1. A sewershed was intentionally selected

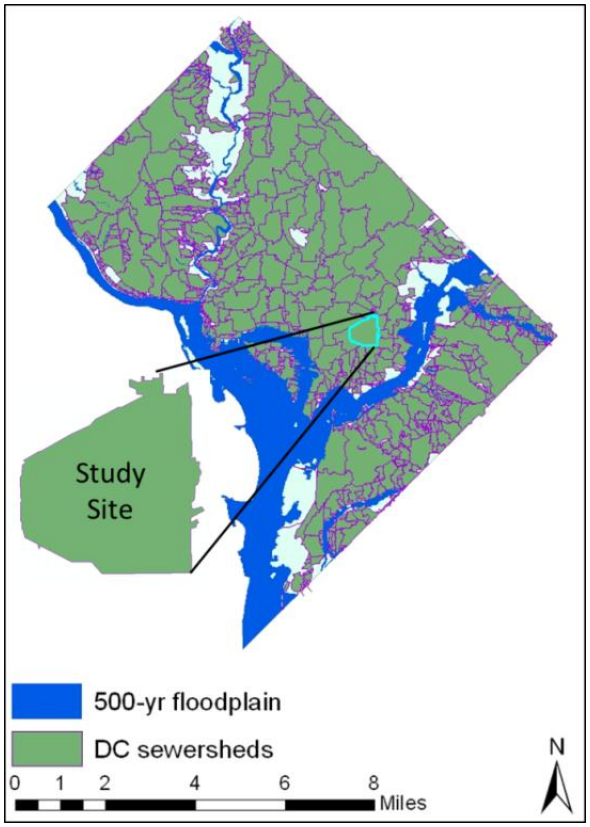

Figure 6-1. Delineated sewersheds in Washington, DC, with selected study site highlighted. FEMA's 500-yr floodplain is also shown.

that was outside the designated floodplains to evaluate flood risk in a location that is not influenced by any existing water bodies. Also, this sewershed covers part of Capitol Hill, which has relatively high elevations for Washington, DC. Therefore, the selected sewershed does not have any upstream sewersheds draining into it. These factors were desirable to provide a contrast with the floodplains and low elevation sections of the city to emphasize that flood risk, to some degree, exists everywhere.

6.3 SITE SPECIFIC DATA

Once the boundary of the study site was determined, data specific to the area within that boundary needed to be gathered. Two types of elevation data were retrieved from the Office of the Chief Technology Officer (OCTO)'s GIS repository: a 1-m resolution raster shapefile obtained using LiDAR and a shapefile with 2-ft elevation contours (OCTO 2011). The same GIS repository provided shapefiles of impervious area, soil types, zoning, buildings, property lots, and a high resolution orthographic image. The property lots shapefile also contained tax assessed property values of both the land and building(s) associated with each property lot. This information was important when estimating damages from various return period storms. Finally, a shapefile from DC Water provided the storm sewer pipe layout and details, which became the central element of the model setup. These shapefiles needed to be clipped to the extent of the study site to be utilized. Also, DDOT specifications for roadway design were followed when specifying the street channel cross-sections. The quality and completeness of the datasets used should be considered when selecting data sources. Using the highest quality data available for the inputs will provide the highest level of accuracy in the model results.

6.4 MODELING THE PIPE NETWORK

Following the procedure described in Chapter 3, an image of the study site was imported into SWMM to be used as a backdrop and drawing aid. The image was exported from GIS and contained an orthophoto of the site, along with the pipe layout, the locations of catchbasins, and the 2-ft elevation contours (see Figure 6-2). Using this backdrop image, and making sure that SWMM's Auto-length setting was on, the pipes were drawn to match the image and the characteristics of the pipes were obtained from the DC Water shapefile data table.

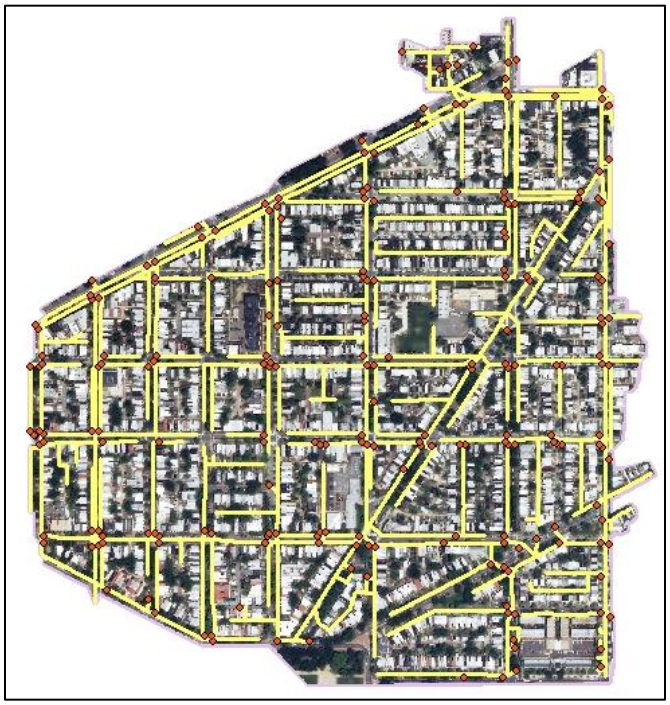

Figure 6-2. Exported GIS image to be imported as SWMM backdrop. Pipe segments are in yellow and catchbasins are in red.

The DC Water stormsewer shapefile provided the details of the stormsewer system used to layout the pipe network in SWMM; however, the data set was incomplete. The data table that supports the shapefile contained the height, width, upstream invert

elevation, downstream invert elevation, and slope of each pipe segment, though some or all of this data was missing for several pipes. In some cases, pipe segments were eliminated if deemed unimportant to the functioning of the model. In other cases, if a pipe segment was critical to the overall network but was missing some data, the missing data was inferred from other surrounding pipes and supporting data. For example, if a pipe segment did not include a downstream elevation and other pipes were connected to the same node, the downstream elevation of one of the other pipes would be used to define the elevation of the node. If other pipes with elevation information were not connected to the same node, then the elevation was interpolated between two surrounding nodes with known elevations using the 2-ft elevation contours as a guide. The 2-ft elevation contours and the LiDAR elevations were also useful in determining the ends of the pipe segment that were upstream and downstream in cases where it was not obvious.

After all of the pipes were laid out according to DC Water's shapefile, subcatchments were created to cover the full area of the sewershed. Both the size of the subcatchments and the node to which each subcatchment drains were determined using the geometry of the pipe network and the elevation contours as guides. Once the subcatchments were completed, the rainfall distributions previously determined for the 2-, 10-, 100-, and 200-yr storms were imported so that simulations could be made. Without the street channels added to the model, these simulations were made only to highlight and correct any errors or issues in the model. At this stage, the model contained 479 pipe segments and 259 subcatchments, as shown in Figure 6-3. Also indicated in Figure 6-3 are the invert elevations at each node and the slopes of the pipes segments.

6.5 MODELING THE STREET CHANNELS

Modeling the street channels was the final step in developing a fully-functional dual drainage model of the sewershed. This was accomplished as described in Chapter 3. The street channels are shown as two angled line segments in order to visually distinguish them from the pipes that are already in place in the model. The street channel lengths were manually input to match the lengths of the pipe

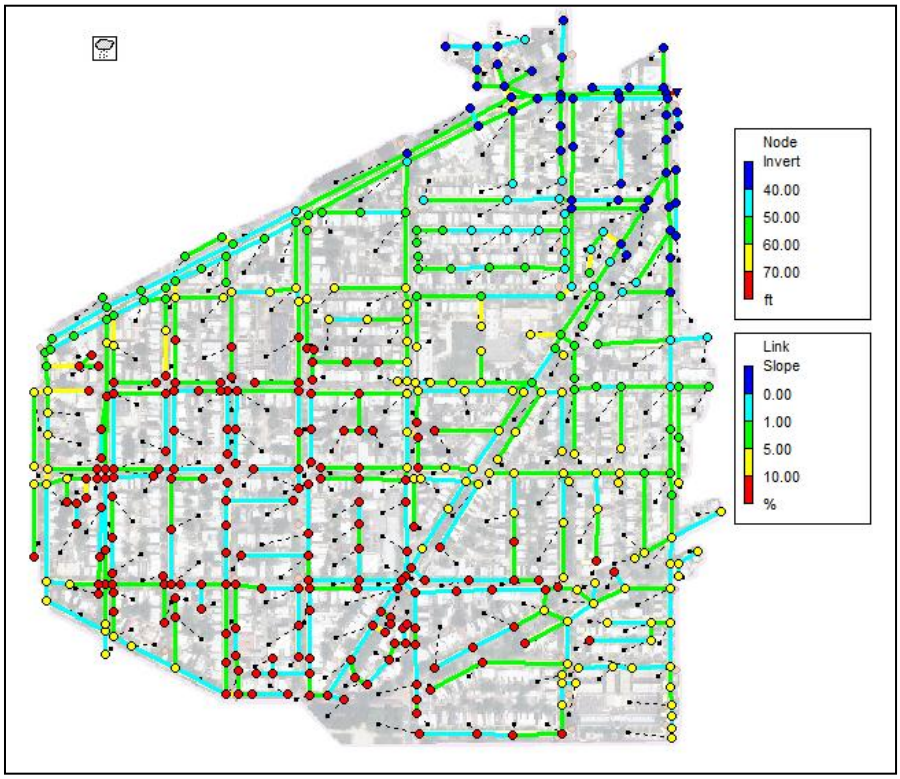

Figure 6-3. Capitol Hill sewershed SWMM model layout with pipes and subcatchments.

segments that shared a path. The street channels were connected to the pipe network at inlets at street intersections. Street channels that represent alleys were not modeled. The final layout of the model of this sewershed, with both the pipe network and the street channels included, is shown in Figure 6-4.

Street channel cross-sections were based upon DDOT design standards (DDOT 2009). Several street cross-sections were used to represent different road types. For example, the sewershed is primarily residential and consists of one- and two-way residential streets. These two road types have different design criteria, according to DDOT, and therefore, were modeled using different widths and overall cross-sections. This is important because the width and cross-section of a street channel has a significant bearing on the volume of runoff that it can convey before overtopping. Again, an artificial barrier was placed at the edge of the sidewalk of each street channel in order to more easily keep track of the runoff volumes and flow depths along the length of the street channels.

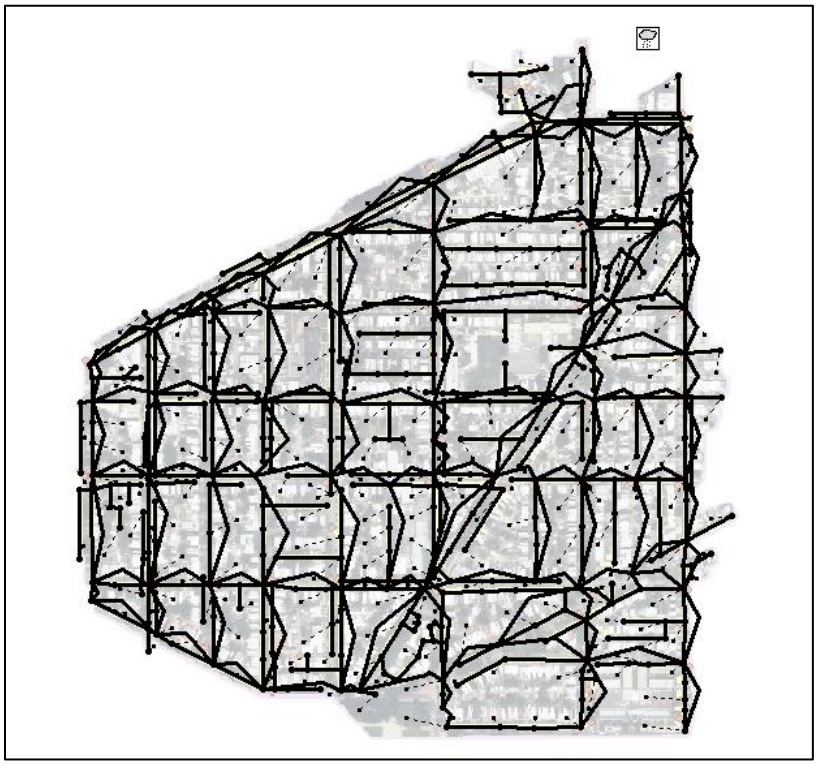

Figure 6-4. Capitol Hill sewershed SWMM model layout with pipes, subcatchments, and street channels included.

Once model was working properly, simulations for storms of various return periods were made in order to assess the flood depths and damages. Once the spatial extent of flooding was observed, the flooded street channels were analyzed more closely. Buildings are often set back some distance from the sidewalk. Therefore, for the flooded street channels the distance from the edge of a building footprint on one side of the street to a building footprint on the opposite side of the street was measured. The average width was used as the new width of the street channel cross section. This was done so the reported flood depths from SWMM simulations would more accurately represent the actual depth of water that reaches the buildings.

6.6 SIMULATION RESULTS

Simulations were made for storms of several return periods in order to understand the performance of the drainage system under conditions of varying risk levels. Many of the input parameters were treated as constant across the sewershed and for each return period (see Table 6-1). Most of these parameter values were selected from the sensitivity analyses performed in Chapter 3. The percent imperviousness value was determined from a raster dataset of imperviousness analyzed in GIS. The roughness coefficient of impervious areas was changed from 0.011 to 0.015 because several other impervious surfaces with higher roughness coefficients than smooth asphalt exist in the sewershed, e.g., brick sidewalks. Using the input parameters in Table 6-1, simulations of the 2-, 10-, 100-, and 200-yr storms were made. The results of these simulations provided the necessary data to perform several flood frequency analyses. Analyses were performed for the estimated flood depths and flood damages at multiple spatial scales.

Table 6-1. Summary of input parameters that remained constant across the sewershed and for each return period.

Parameter	Value
Initial infiltration rate (in./hr)	3.00
Final infiltration rate (in./hr)	0.13
Decay constant (hr^{-1})	5
Imperviousness (%)	64
Depression storage, impervious (in.)	0.05
Depression storage, pervious (in.)	0.05
Overland flow width (ft)	50
Roughness coefficient, impervious	0.015
Roughness coefficient, pervious	0.150
Roughness coefficient, pipes	0.013
Roughness coefficient, street channels	0.015

Flood frequency analyses that were based on flood depths of various return periods were performed. First, predicted flood depths at an individual building were analyzed. The selected building was in the middle of the block nearest to the outlet pipe of the sewershed. SWMM records the average depth along a conduit at each timestep. In order to find the maximum depth at a specific location along a street channel, additional calculations were necessary. In this case the selected building was 145ft from the downstream end of the 240-ft street channel. The maximum depth along the street channel for the 2-yr storm occurred 12 hours and 5 minutes into the 24-hr storm. At the same time during the storm, the depths at the upstream and downstream inlets were 0.37 and 0.98-ft, respectively. From these depths, the slope of the depth along the street channel was determined to be 0.0025ft/ft. The depth at the downstream end, the distance of the building from the downstream end, and the slope of the depth along the channel were then used to determine that the maximum depth at the location of the selected building during the 2-yr storm was 0.611ft. This depth was able to be contained within the actual street and did not reach the footprint of the building at 0.72ft. This process was

repeated for each building along each flooded street channel in order to produce accurate damage estimates.

Flood frequency analyses of flood depths can provide important information to individual property owners and community leaders alike. In some situations, a knowledge of potential flood depths and their associated probabilities of occurrence is all that is wanted. Property owners will generally have a more detailed understanding of their property and its contents than any model can predict. Therefore, if time permits, it may be more accurate for a property owner to determine expected damages directly from flood depths. The same can be true on the community level. The results of flood frequency analyses of flood depths at the location of the building previously selected and the maximum average depths along the same block as the selected building are shown in Figure 6-5 and Figure 6-6. These analyses show that the log-Pearson III distribution provides good estimates of flood depths.

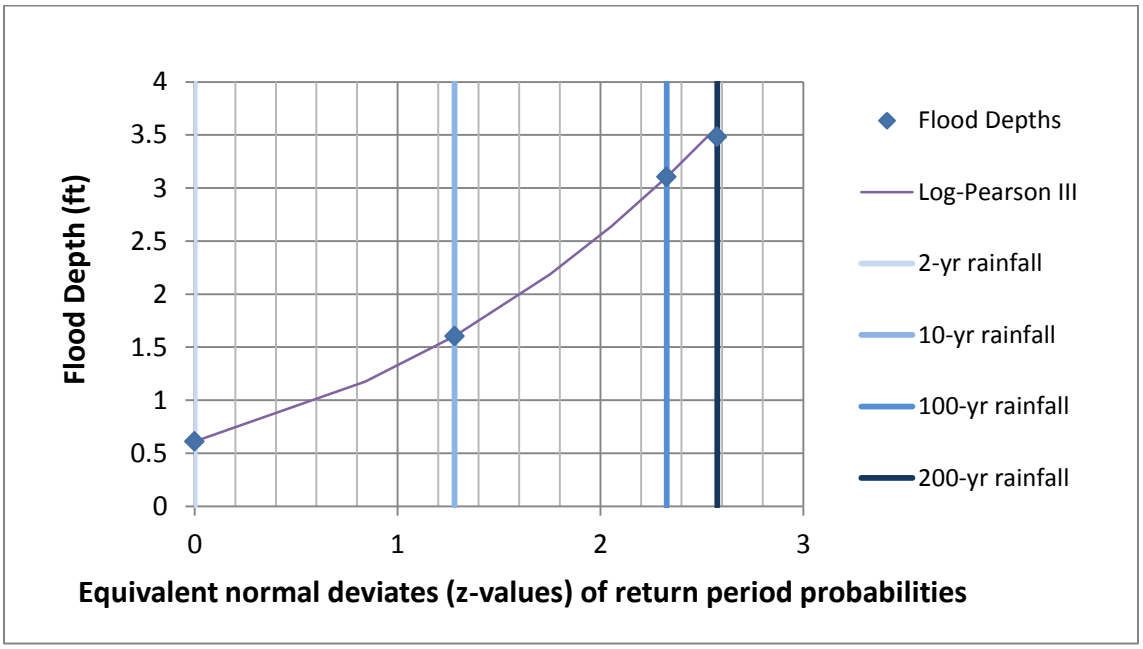

Figure 6-5. Flood frequency analysis of flood depths of a selected building in the sewershed. The parameters of the log-Pearson III distribution were -0.2375, 0.3595, and -0.36 for the mean, standard deviation, and skew coefficient, respectively.

Flood frequency analyses were also performed for the estimated damages of various return periods. An analysis was conducted at the individual building, city block, and full sewershed spatial scales, with the results of these analyses are represented in Figure 6-7, Figure 6-8, and Figure 6-9, respectively. Each spatial scale of analysis revealed very similar trends. It is clear that the damage estimates do not follow a log-Pearson III distribution as closely as the flood depths. This makes sense because of factors such as the street channel cross-sections and the selected depth-damage curves that provide a non-linear, intermediate influence on the estimated damages when the return period is changed. However, the log-Pearson III distribution does appear to be able to capture the overall trends of the damage estimates and would provide reasonable estimates of damages directly from the return period.

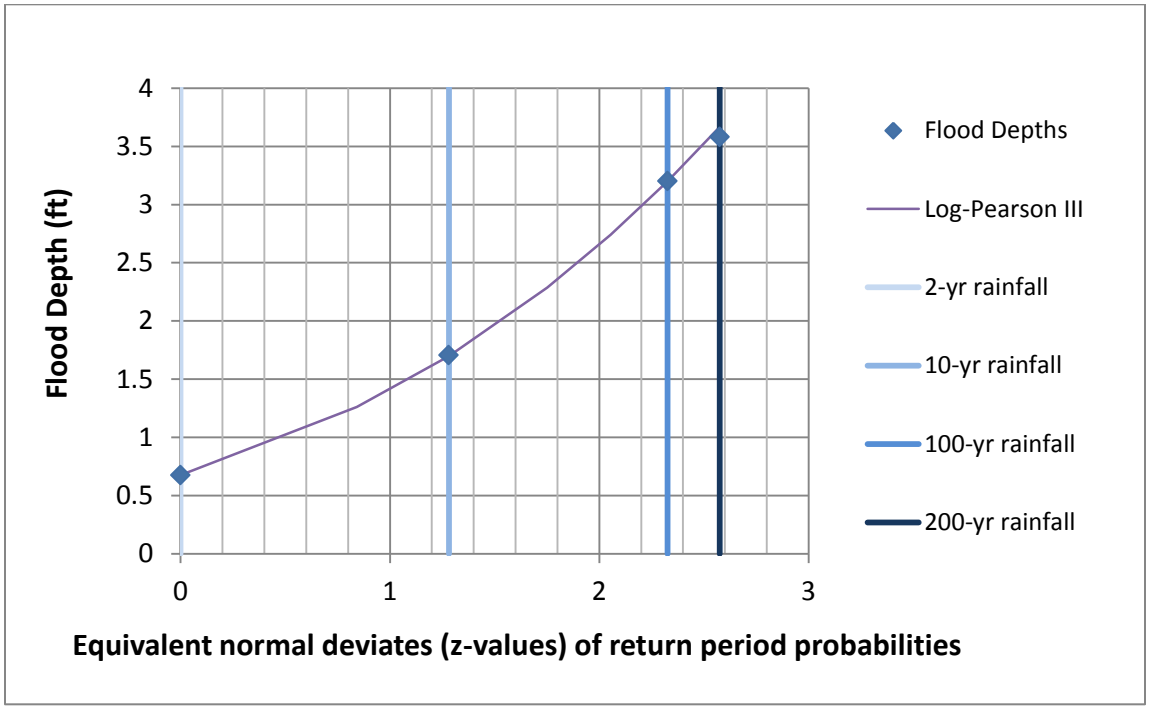

Figure 6-6. Flood frequency analysis of peak average flood depths along the street channel of the selected building. The parameters of the log-Pearson III distribution were -0.1936, 0.3443, and -0.38 for the mean, standard deviation, and skew coefficient, respectively.

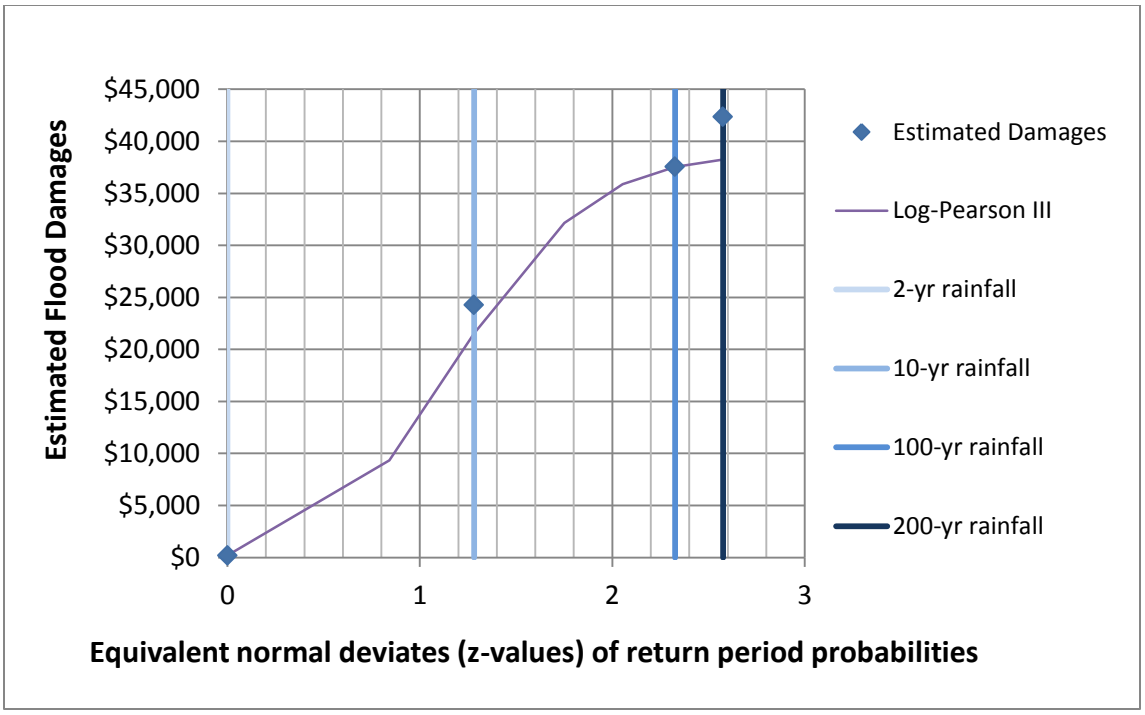

Figure 6-7. Flood frequency analysis of estimated damages of the selected building. The parameters of the log-Pearson III distribution were 0.9962, 3.9540, and -2.22 for the mean, standard deviation, and skew coefficient, respectively.

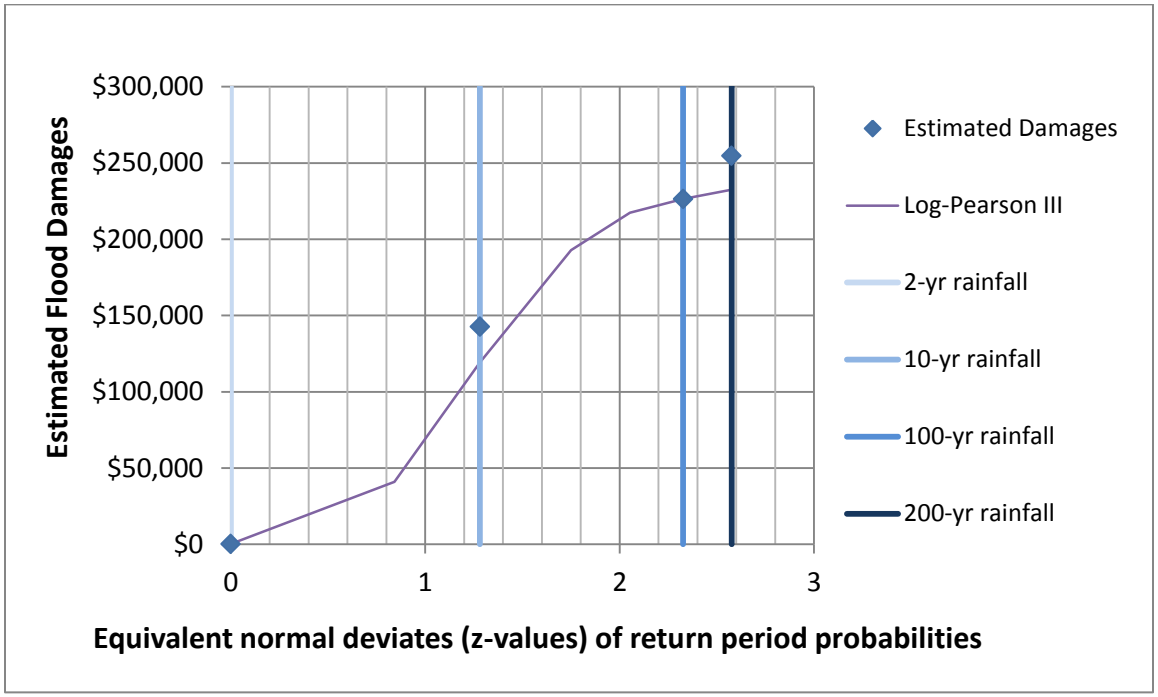

Figure 6-8. Flood frequency analysis of estimated damages of the block on which the selected building is located. The parameters of the log-Pearson III distribution were 0.3213, 5.8057, and -2.28 for the mean, standard deviation, and skew coefficient, respectively.

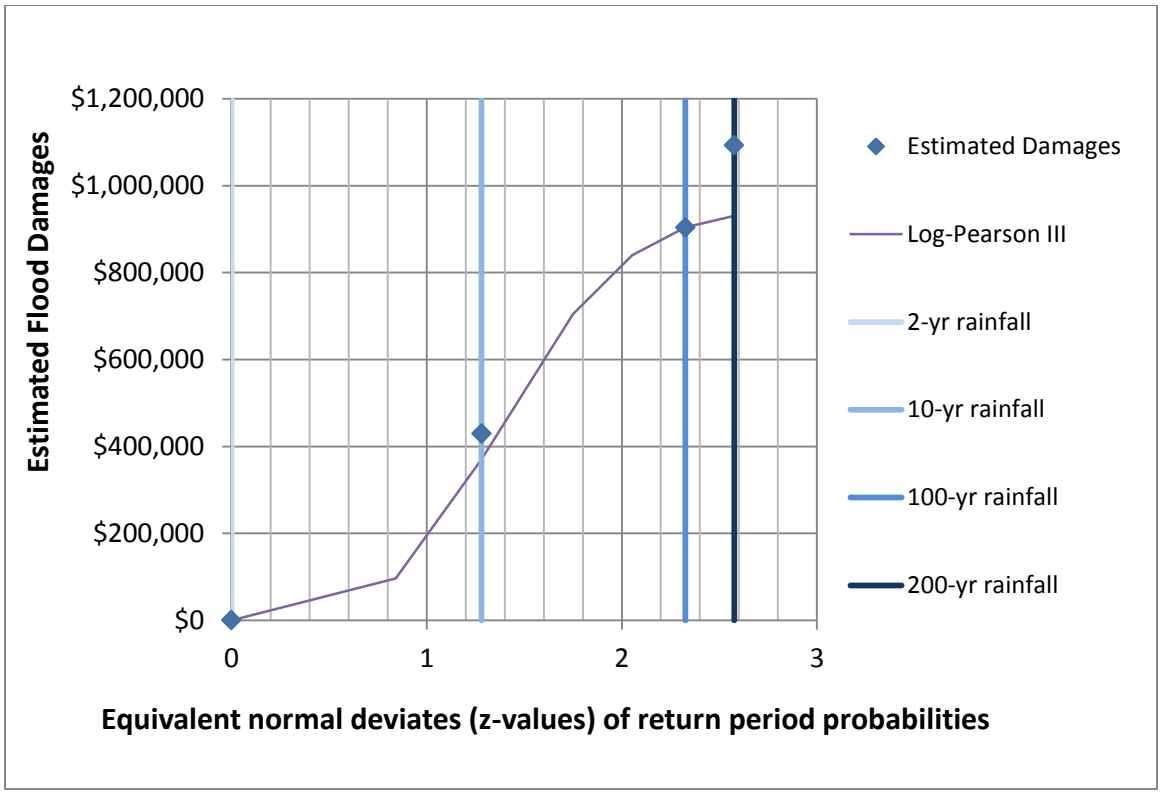

Figure 6-9. Flood frequency analysis of estimated damages of the full sewershed. The parameters of the log-Pearson III distribution were 0.2033, 6.3567, and -2.19 for the mean, standard deviation, and skew coefficient, respectively.

The errors and relative errors of the log-Pearson III distributions fitted to the damage estimates can help to assess the reasonability of the predictions the distribution functions provide. A summary of these errors are provided in Table 6-2. While the magnitudes of some of the errors are very large (e.g. $162,236), the relative errors never reach above 20 percent of the original damage estimate. Considering the degree of uncertainty involved in flood damage estimates, and depending on the intended use of the damage estimate, a margin of error of 20 percent may be acceptable. A negative bias is also evident. This indicates consistent underprediction. In other words, this distribution function produces conservative predictions. The negative bias could be a result of the nonlinearity of the depth-damage functions.

Table 6-2. Errors and relative errors of log-Pearson III distribution functions and estimated damages for various return periods of each spatial scale.

Spatial Scale	Return Period	LP3 Damages ($)	Estimated Damages ($)	Error ($)	Relative Error (%)
Building	2-yr	200	200	0	0
	10-yr	21,547	24,270	-2,724	-0.12641
	100-yr	37,547	37,547	0	0
	200-yr	38,237	42,360	-4,123	-0.10784
Block	2-yr	200	200	0	0
	10-yr	119,170	142,593	-23,423	-0.19655
	100-yr	226,381	226,381	0	0
	200-yr	232,515	254,751	-22,236	-0.09563
Sewershed	2-yr	200	200	0	0
	10-yr	370,162	429,548	-59,386	-0.16043
	100-yr	903,968	903,968	0	0
	200-yr	930,822	1,093,059	-162,236	-0.17429

It can be concluded from this case study that pluvial flood damages can be significant even in small urban watersheds. The predicted damages for the relatively small sewershed of 215 acres for the 100- and 200-yr rainfall events were $904,000 and $1,093,000, respectively. It was also shown that predictions of pluvial flood depths and damages can be effectively made at several spatial scales. Log-Pearson III distribution functions were able to describe the flood depths very well and the estimated damages reasonably well.

CHAPTER 7

CONCLUSIONS

The goal of this research was to develop a procedure for modeling pluvial flooding scenarios in small urban watersheds and estimate the resulting damages. The procedure for developing the model using SWMM, with the aide of GIS tools and datasets, was discussed in Chapter 3. The procedure was intended to be applicable to any location and a wide user base. Possible resources where site specific data may be found were discussed; however, many other sources of data could be used. This is true particularly outside of the U.S. Once sufficient supporting data are gathered, then the model setup process that was used herein may be followed to develop a SWMM model that represents the drainage system of interest.

Also within Chapter 3, a series of sensitivity analyses was conducted on a sample watershed in order to better understand the response of the system to changes in various input parameters. The results of these analyses suggested high sensitivities for the watershed slope, percent imperviousness, overland flow width, impervious area roughness coefficient, pipe roughness coefficient, and low sensitivities for the infiltration parameters, depression storage, pervious area roughness coefficient, and street channel coefficients. These results provided a clear indication of which input parameters require a higher level of accuracy in order for the model to deliver the most accurate pluvial

flood depths. Sensitivity analyses such as those in Chapter 3 may need to be remade for other locations of different land covers.

After having obtained pluvial flood depths from simulations of the SWMM model, Chapter 4 described the pluvial flood damage estimation process. This process required the use of depth-damage curves. In this case, depth-damage curves were extracted from FEMA's HAZUS-MH software and used to predict damages to each building and the contents therein, based upon the flood depth at the location of the building. It was shown that damages could be reasonably estimated for several spatial scales: for an individual building, a city block, or the full microwatershed. Damage estimates for each of these spatial scales for the 13.32-acre sample microwatershed for a 200-yr, 24-hr rainfall event came out to be $25,255, $429,934, and $771,464, respectively. It should be noted that for smaller spatial scales, the degree of uncertainty in the estimates increases. However, these results emphasized how quickly pluvial flood damages can accumulate in highly urban areas.

Using flood depths and damage estimates that result from various return period rainfall events, the process of performing flood frequency analyses was discussed in Chapter 5. It was shown that log-Pearson III distribution functions provide a better fit to the flood depth and flood damage results than the log-normal distribution. Log-Pearson III distribution functions fit the flood depth results almost exactly. They also fit the damage estimate results reasonably well with the largest relative error reaching 20 percent. The log-Pearson III analyses use equations of the form,

$$X = 10^{\bar{X}_S + KS_S} \tag{7.1}$$

where X is the logarithm of the predicted magnitude (either flood depth or estimated damages), $\bar{X}_s$ is the mean value, S_s is the standard deviation, and K is the frequency factor which is dependent on the return period and skew coefficient. Flood frequency analyses simplify all of the previous results into a concise equation that can predict pluvial flood depths or damages for the modeled site for any return period. Flood frequency analyses can be performed on any spatial scale for which flood depths or damages are available. The resulting equations can significantly aid in communicating pluvial flood risk to local leaders, decision-makers, and citizens.

Using all of the processes described in the previous chapters, a case study of a 215-acre sewershed in the Capitol Hill neighborhood of Washington, DC, was discussed in Chapter 6. Accessibility to high quality input data was an ongoing concern. For some inputs, average values needed to be used and/or assumptions needed to be made. The results of this case study primarily agreed with expectations. One unexpected result was the relatively high value of damages ($429,548) over the full sewershed that resulted from the 10-yr rainfall event. This indicated that the existing stormsewer network would not pass the 10-yr rainfall event. Considering the age of the development in this location (much of it dating back to the 1800s), the stormsewer network may have been designed for the 10-yr event given knowledge at that time and under potential risk at that time but is not adequate any longer. This could be a result of dramatic changes in local conditions, such as land cover, since the pipe network was originally installed. The 100- and 200-yr rainfall events resulted in damage estimates over the sewershed of $903,968 and $1,093,059, respectively.

Similar to the results of Chapter 4, the results of the case study in Chapter 6 indicated that pluvial flooding can potentially have significant consequences. This was learned by experience when pluvial flooding caused over $10 million in damages in the Federal Triangle area of Washington, DC, in 2006. Even still, few resources have been allocated to the study pluvial flood risk specifically. The results of this research should help to ensure that discussions and research centered on flood risk do not overlook the component of pluvial flood risk.

The case study site was specifically selected as an area that was not adjacent to a water body and was situated at a relatively high elevation to show that, if significant pluvial flooding can occur in such a location, it can occur virtually anywhere. This conclusion will help to strengthen the NFIP by encouraging more people, even those who do not live within FEMA's 100-yr floodplain boundary, to purchase flood insurance as a protection against potential pluvial flooding. Additionally, the simple equations that result from flood frequency analyses of both flood depth and estimated damages will help improve public outreach and communication efforts. This means that more people will be able to understand the degree of pluvial flood risk that they face, as individuals and communities, and will be able to make more informed decisions about how to best manage those risks.

While data used in this research was drawn from reliable sources, there remain data quality issues that should be further analyzed. For example, when drawing on the tax assessed values of the buildings within the study site, information was unavailable for a small number of buildings. In order to fill the data gaps, the average value of the buildings along the same block was used. A specific analysis of the influence of using

incomplete datasets, and different methods of filling in data gaps, on the output of the overall model would be useful to better understand one of the sources of uncertainty in the modeling process. Additionally, even when working with complete datasets, errors or inaccuracies often exist. A full analysis of model sensitivity to the quality of input data would be valuable to the SWMM user.

This research and modeling process could be built upon and improved by testing it with a case study of a previous event of isolated pluvial flooding. A possible example would be the 2006 Federal Triangle flooding in Washington, DC. This type of study would help to further verify the value and accuracy of this modeling process, while allowing any necessary calibration to be made.

APPENDIX

APPENDIX A

Table A-1. Ordinates the central two hours of the NRCS 24-hr Type II rainfall with 2-minute time increments for various return periods. Depths for all return periods are reported in inches.

Duration (min)	Duration (hrs)	Cumulative Depths	Incremental Depths	2-yr	10-yr	100-yr	200-yr
660	11.0000	0.2330	0.00240	0.67057	1.17642	2.00613	2.28923
662	11.0333	0.2356	0.00256	0.67794	1.18934	2.02817	2.31438
664	11.0667	0.2382	0.00266	0.68560	1.20277	2.05107	2.34051
666	11.1000	0.2410	0.00278	0.69360	1.21681	2.07501	2.36783
668	11.1333	0.2438	0.00284	0.70177	1.23115	2.09946	2.39573
670	11.1667	0.2468	0.00299	0.71038	1.24624	2.12521	2.42510
672	11.2000	0.2500	0.00317	0.71950	1.26225	2.15250	2.45625
674	11.2333	0.2535	0.00349	0.72954	1.27987	2.18255	2.49054
676	11.2667	0.2572	0.00368	0.74014	1.29845	2.21423	2.52670
678	11.3000	0.2610	0.00383	0.75116	1.31779	2.24721	2.56433
680	11.3333	0.2649	0.00389	0.76235	1.33743	2.28070	2.60254
682	11.3667	0.2689	0.00400	0.77387	1.35763	2.31514	2.64184
684	11.4000	0.2730	0.00411	0.78569	1.37838	2.35053	2.68223
686	11.4333	0.2772	0.00417	0.79770	1.39943	2.38643	2.72320
688	11.4667	0.2815	0.00432	0.81013	1.42124	2.42363	2.76564
690	11.5000	0.2860	0.00451	0.82311	1.44401	2.46246	2.80995
692	11.5333	0.2896	0.00364	0.83358	1.46239	2.49380	2.84571
694	11.5667	0.2944	0.00472	0.84717	1.48622	2.53444	2.89209
696	11.6000	0.3010	0.00664	0.86628	1.51975	2.59161	2.95733
698	11.6333	0.3112	0.01021	0.89566	1.57130	2.67952	3.05764
700	11.6667	0.3245	0.01325	0.93380	1.63820	2.79360	3.18782
702	11.7000	0.3410	0.01654	0.98140	1.72171	2.93601	3.35033
704	11.7333	0.3581	0.01709	1.03058	1.80800	3.08315	3.51823
706	11.7667	0.3813	0.02316	1.09724	1.92493	3.28256	3.74578
708	11.8000	0.4130	0.03175	1.18861	2.08524	3.55593	4.05773
710	11.8333	0.4688	0.05580	1.34921	2.36697	4.03637	4.60596
712	11.8667	0.5285	0.05973	1.52111	2.66855	4.55064	5.19281
714	11.9000	0.5850	0.05647	1.68363	2.95367	5.03685	5.74763
716	11.9333	0.6194	0.03442	1.78269	3.12745	5.33321	6.08580
718	11.9667	0.6449	0.02549	1.85605	3.25615	5.55268	6.33624
720	12.0000	0.6630	0.01809	1.90811	3.34749	5.70843	6.51398
722	12.0333	0.6752	0.01215	1.94308	3.40883	5.81304	6.63335
724	12.0667	0.6830	0.00781	1.96556	3.44827	5.88029	6.71008

726	12.1000	0.6880	0.00504	1.98006	3.47371	5.92368	6.75960
728	12.1333	0.6934	0.00544	1.99572	3.50118	5.97052	6.81305
730	12.1667	0.6980	0.00456	2.00884	3.52420	6.00978	6.85785
732	12.2000	0.7020	0.00400	2.02036	3.54440	6.04422	6.89715
734	12.2333	0.7062	0.00417	2.03236	3.56545	6.08012	6.93812
736	12.2667	0.7102	0.00399	2.04384	3.58560	6.11448	6.97732
738	12.3000	0.7140	0.00384	2.05489	3.60499	6.14754	7.01505
740	12.3333	0.7178	0.00378	2.06577	3.62407	6.18009	7.05219
742	12.3667	0.7214	0.00366	2.07630	3.64255	6.21160	7.08815
744	12.4000	0.7250	0.00356	2.08655	3.66053	6.24225	7.12313
746	12.4333	0.7284	0.00344	2.09645	3.67789	6.27187	7.15692
748	12.4667	0.7318	0.00334	2.10606	3.69476	6.30063	7.18974
750	12.5000	0.7350	0.00322	2.11533	3.71102	6.32835	7.22138
752	12.5333	0.7381	0.00311	2.12428	3.72672	6.35513	7.25193
754	12.5667	0.7411	0.00300	2.13291	3.74186	6.38096	7.28141
756	12.6000	0.7440	0.00289	2.14123	3.75646	6.40584	7.30980
758	12.6333	0.7468	0.00276	2.14918	3.77039	6.42960	7.33692
760	12.6667	0.7494	0.00266	2.15683	3.78382	6.45251	7.36305
762	12.7000	0.7520	0.00258	2.16426	3.79685	6.47472	7.38840
764	12.7333	0.7545	0.00254	2.17157	3.80967	6.49659	7.41336
766	12.7667	0.7570	0.00247	2.17867	3.82214	6.51786	7.43762
768	12.8000	0.7594	0.00239	2.18555	3.83421	6.53843	7.46111
770	12.8333	0.7617	0.00227	2.19209	3.84567	6.55798	7.48341
772	12.8667	0.7639	0.00219	2.19839	3.85673	6.57683	7.50492
774	12.9000	0.7660	0.00214	2.20455	3.86753	6.59526	7.52595
776	12.9333	0.7681	0.00211	2.21062	3.87819	6.61343	7.54668
778	12.9667	0.7702	0.00207	2.21658	3.88864	6.63125	7.56702
780	13.0000	0.7722	0.00202	2.22239	3.89884	6.64864	7.58687

Table A-2. Damage estimates of each flooded building along 3rd St and Independence Avenue during a 200-yr rainfall events from Chapter 4 analysis.

3rd St						
Building values ($)	**Contents values ($)**	**Building damages (%)**	**Contents Damage (%)**	**Building Damages ($)**	**Contents Damages ($)**	**Total damages**
681,980	409,188	3.9310	4.7739	26,808	19,534	$ 46,343
3,793,260	2,275,956	3.6593	3.7236	138,808	84,748	$ 223,555
590,590	354,354	3.6105	3.5041	21,323	12,417	$ 33,740
345,810	207,486	3.5624	3.2781	12,319	6,802	$ 19,121
389,230	233,538	3.5149	3.0461	13,681	7,114	$ 20,795
303,410	182,046	3.4680	2.8084	10,522	5,113	$ 15,635
428,510	257,106	3.4217	2.5654	14,663	6,596	$ 21,258
1,082,830	649,698	3.3311	2.0652	36,070	13,418	$ 49,488
7,615,620	4,569,372	3.5624	3.2206	274,194	155,740	**$ 429,934**

Independence Ave						
Building values ($)	**Contents values ($)**	**Building damages (%)**	**Contents Damage (%)**	**Building Damages ($)**	**Contents Damages ($)**	**Total damages**
1,082,830	649,698	3.9310	4.7739	42,566	31,016	$ 73,582
606,900	364,140	3.8137	4.3557	23,145	15,861	$ 39,006
569,720	341,832	3.6999	3.8989	21,079	13,328	$ 34,407
413,660	248,196	3.6100	3.5016	14,933	8,691	$ 23,624
625,230	375,138	3.5222	3.0826	22,022	11,564	$ 33,586
562,579	337,547	3.4562	2.7471	19,444	9,273	$ 28,717
343,070	205,842	3.3404	2.1181	11,460	4,360	$ 15,820
374,060	224,436	3.2778	1.7568	12,261	3,943	$ 16,204
370,830	222,498	3.2163	1.3888	11,927	3,090	$ 15,017
732,330	439,398	3.1560	1.0154	23,112	4,461	$ 27,574
529,230	317,538	3.0676	0.4483	16,235	1,424	$ 17,658
540,510	324,306	3.0044	0.0297	16,239	96	$ 16,336
6,750,949	4,050,569	3.4246	2.4264	234,423	107,106	**$ 341,529**

REFERENCES

Akan, A. O. (1985). Kinematic-Wave Method for Peak Runoff Estimates. *Journal of Transportation Engineering* ASCE. **111**:419-425.

American Concrete Pipe Association (ACPA) (1974). Design Manual: Concrete Pipe. Arlington, VA.

ASCE (1982). Gravity Sanitary Sewer Design and Construction, ASCE Manual of Practice No. 60, New York, NY.

ASCE (1992). Design & Construction of Urban Stormwater Management Systems, New York, NY.

Barber, C. P. and Shortridge, A. (2005). Lidar Elevation Data for Surface Hydrologic Modeling: Resolution and Representation Issues. *Cartography and Geographic Information Science* **32**:401-410.

Behera, P. K. (2011). Personal Communication. Associate Professor of Civil Engineering, University of the District of Columbia.

Butler, S. S. (1977). Overland-Flow Travel Time Versus Reynolds-Number. *Journal of Hydrology* **32**:175-182.

Chin, D. A. (2006). Water-Resources Engineering: Second Edition. Prentice Hall. Upper Saddle River, NJ.

District of Columbia Department of Transportation (DDOT) (2009). Design and Engineering Manual. U. S. Department of Transportation, Federal Highway Administration, Washington, DC.

Du, J. K., Xie, H., Hu, Y. J., Xu, Y. P., and Xu, C. Y. (2009). Development and testing of a new storm runoff routing approach based on time variant spatially distributed travel time method. *Journal of Hydrology* **369**:44-54.

Dutta, D., Herath, S., and Musiakec, K. (2003). A mathematical model for flood loss estimation. *Journal of Hydrology* **277**:24-49.

Freni, G., La Loggia, G., and Notaro, V. (2010). Uncertainty in urban flood damage assessment due to urban drainage modelling and depth-damage curve estimation. *Water Science and Technology* **61**:2979-2993.

Ghosh, I. and Hellweger, F. L. (2012). Effects of Spatial Resolution in Urban Hydrologic Simulations. *Journal of Hydrologic Engineering* **17**:129-137.

Jain, M. K., Kothyari, U. C., and Raju, K. G. R. (2004). A GIS based distributed rainfall-runoff model. *Journal of Hydrology* **299**:107-135.

Jonkman, S. N., Bockarjova, M., Kok, M. and Bernardini, P. (2008). Integrated hydrodynamic and economic modelling of flood damage in the Netherlands. *Ecological Economics* **66**:77-90.

Kalin, L., Govindaraju, R. S., and Hantush, M. M. (2003). Effect of geomorphologic resolution on modeling of runoff hydrograph and sedimentograph over small watersheds. *Journal of Hydrology* **276**:89-111.

McCuen, R. H., Johnson, P. A., and Ragan, R. M. (2002). Highway Hydrology: Hydraulic Design, Series Number 2, Second Edition. Federal Highway Administration. Washington, DC.

McCuen, R. H. (2005). Hydrologic Analysis and Design: 3rd ed. Prentice Hall. Upper Saddle River, NJ.

Melesse, A. M. and Shih, S. F. (2002). Spatially distributed storm runoff depth estimation using Landsat images and GIS. *Computers and Electronics in Agriculture* **37**:173-183.

Merz, B., Kreibich, H., Thieken, A. and Schmidtke, R. (2004). Estimation uncertainty of direct monetary flood damage to buildings. *Natural Hazards and Earth System Sciences* **4**:153-163.

Myers, T. G. (2002). Modeling laminar sheet flow over rough surfaces. *Water Resources Research* **38**:1230-1241.

National Oceanic and Atmospheric Administration (NOAA) (2012). http://hdsc.nws.noaa.gov/hdsc/pfds/index.html. Accessed on 17 July 2011.

DC Office of the Chief Technology Officer (OCTO) (2011). http://data.dc.gov. Accessed on 14 Jan 2012.

Olivera, F. and Maidment, D. (1999). Geographic information systems (GIS)-based spatially distributed model for runoff routing. *Water Resources Research* **35**:1155-1164.

Penning-Roswell, E. C. and Chatterton, J. B. (1977). The benefits of flood alleviation – A manual of assessment techniques (Blue Manuals). Gower Technical Press.

Rawls, W. J., Brakensiek, D. L., and Saxton, K. E. (1982). Estimation of Soil-Water Properties. *Transactions of the ASAE* **25**:1316-1328.

Scawthorn, C., Flores, P., Blais, N., Seligson, H., Tate, E. Chang, S., Mifflin, E., Thomas, W., Murphy, J., Jones, C., and M. Lawrence (2006). HAZUS-MH Flood Loss Estimation Methodology – II: Damage and Loss Assessment. *Nat. Hazards Rev*. **7**:72-82.

Scott, M. (2011). Personal Communication. Faculty, Department of Geography, Salisbury University.

Smith, D. I. (1994). Flood Damage Estimation - A Review of Urban Stage-Damage Curves and Loss Functions. *Water SA* **20**:231-238.

Stephenson, D. (1981). Stormwater Hydrology and Drainage. Elsevier Scientific Publishing Company. New York, NY.

U. S. Geological Survey (USGS) (1982). Guidelines for Determining Flood Flow Frequency. Bulletin #17B of the Hydrology Subcommittee. Interagency Advisory Committee on Water Data. Reston, VA.

U. S. Geographical Survey (USGS) (2006). http://ned.usgs.gov/#. Accessed on 23 Aug 2011.

U. S. Army Corps of Engineers (USACE) (1992). Catalog of Residential Depth-Damage Functions Used by the Army Corps of Engineers is Flood Damage Estimation. Institute for Water Resources, Washington, DC.

U. S. Army Corps of Engineers (USACE) (2003). http://corpsnedmanuals.us/-FloodDamageReduction/FDRID022DamageDpthRel.asp. Accessed on 10 Aug 2011.

U. S. Army Corps of Engineers (USACE) (2008). HEC-FDA Flood Damage Reduction Analysis: User's Manual: Version 1.2.4. USACE, Institute of Water Resources, Hydrologic Engineering Center. Davis, CA.

U. S. Environmental Protection Agency (EPA) (2004). Storm Water Management Model: User's Manual: Version 5.0. EPA, Water Supply and Water Resources Division, National Risk Management Research Laboratory. Cincinatti, OH.

U. S. Environmental Protection Agency (EPA) (2009). Storm Water Management Model: Applications Manual. EPA, Water Supply and Water Resources Division, National Risk Management Research Laboratory. Cincinatti, OH.

Wanielista, M., Kersten, R., and Eaglin, R. (1997). Hydrology: Water Quantity and Quality Control. John Wiley & Sons, Inc. Hoboken, NJ.

White, G. F. (1964). Choice of Adjustment to Floods. University of Chicago, Department of Geography. Research Paper No. 93. Chicago, IL.

Wong, T. S. W. and Chen, C. N. (1997). Time of Concentration Formula for Sheet Flow of Varying Flow Regime. *Journal of Hydrologic Engineering* **2**:136-139.

Woods, R. and M. Sivapalan (1999). A synthesis of space-time variability in storm response: Rainfall, runoff generation, and routing. *Water Resources Research* **35**:2469-2485.